Treball de Fi de Màster

Màster Universitari en Enginyeria Industrial

Implementation of DC/DC converters in hybrid LCC-VSC HVDC grids

Autor: Josep Arévalo Soler

Director: Ricard Ferrer San José

Convocatòria: Juny 2019

Escola Tècnica Superior
d'Enginyeria Industrial de Barcelona

Abstract

This Master Thesis presents the modelling, control and simulation of a hybrid multi-terminal High Voltage Direct Current (HVDC) grid. This network is composed by two point-to-point lines linked by a DC/DC converter. One point-to-point line is based on Line-Commutated Converters (LCC) and the other one is based on Voltage Source Converters (VSC), modeled as Modular Multilevel Converters (MMC). These two technologies are the most used ones in HVDC. The DC/DC converters chosen to analyze the multi-terminal grid are the Front-to-Front MMC and the DC-MMC.

In order to achieve the final multi-terminal HVDC grid, the basics of both HVDC technologies are studied. It also includes the modelling, control and simulation of two point-to-point lines. One for LCC technology and the other one for VSC technology. The principles of DC/DC converters are also studied, including the modelling and control of a Front-to-Front MMC converter and a DC-MMC converter.

Finally, simulations of the multi-terminal grid are performed with Matlab Simulink in different scenarios, including four cases for each DC/DC converter. In these different cases the DC/DC converter is placed regulating the DC voltage or controlling the power flow in the different point-to-point links.

Contents

List of Figures

List of Tables

Chapter 1

Introduction

1.1 Research Background

During the development of the current electric network, AC (Alternating Current) system has been the preferred method for power transmission. However, High-Voltage Direct Current (HVDC) is winning popularity in some applications such as long-distance transport of electrical energy and submarine and underground cable transmission [1]. Since the middle of the twentieth century, more than 200 high-voltage DC projects have been commissioned, and this is expected to grew up fast as the development of the voltage source converters (VSC) opens this technology to new projects such as the connection to weak islanded grids. An example of this could be the connection of offshore wind power plants. However, VSCs have higher switching losses and construction costs compared to the conventional HVDC transmission based on Line Commuted Converters (LCC).

With pros and cons for both HVDC technologies (LCC and VSC) it is logic to foresee that a future HVDC grid will be based on both technologies. And, as the quantity of DC grids is expected to grow up, it will be necessary to find an element able to interconnect these different technologies in order to create a similar grid as the existing one in AC. A possible solution is DC/DC converters, which can act as transformers do in the existing grid but can also provide new features. Is then necessary to conduct a study on the operation and control of these new DC/DC converters in a hybrid LCC-VSC HVDC transmission system.

This thesis, analyzes the basic of both HVDC technologies, LCC and VSC. Point-to-point systems of both technologies are first studied and the controls necessary for its operation are designed. Two DC/DC converters are also studied and two different control structures are proposed in order to establish a good performance of these new kind of converters. The converters chosen are the Front-to-Front MMC converter and the DC-MMC converter. Finally, a multiterminal HVDC grid composed with two Point-to-Point links, one of each HVDC technology, linked with a DC/DC converter is simulated in order to validate the proposed controllers.

1.2 Research Questions

Design and operational conditions for DC/DC converters can be found in the literature. However, the implementation of these converters in a hybrid LCC-VSC HVDC grid is not studied

in detail. The aim of this thesis is to provide a solid background for the future study of these DC/DC converters in a mixed LCC-VSC grid, specially for the Front-to-Front converter and the DC-MMC converter.

1.3 Objectives

The main objective of this thesis consists on the design and implementation of a multi-terminal HVDC grid model composed by LCC and VSC point-to-point lines interconnected by two different DC/DC converter. This objective involves 11 intermediate goals:

- To understand the theoretical background of LCC HVDC lines.
- To design the control system for an appropriate operation of a LCC transmission line.
- To model and analyze a point-to-point LCC transmission system.
- To understand the theoretical background of VSC HVDC lines.
- To design the control system for an appropriate operation of a VSC transmission line.
- To model and analyze a point-to-point VSC transmission system.
- To understand the theoretical background of DC/DC converters.
- To design the control system for a Front-to-Front MMC converter.
- To design the control system for a DC-MMC converter.
- To model and analyze a multi-terminal HVDC grid interconnected by a Front-to-Front converter.
- To model and analyze a multi-terminal HVDC grid interconnected by a DC-MMC converter.

1.4 Related Publications

During the development of this thesis, the author has been involved in a publication as a co-author, which has already been submitted:

- Marc Cheah-Mane, **Josep Arevalo-Soler**, Eduardo Prieto-Araujo and Oriol Gomis-Bellmunt. Operation and control design of a DC Modular Multilevel Converter for HVDC grids. In *IEEE Transactions on Power Delivery*. (Under review)

1.5 Thesis Outline

The thesis is organized as follows:

- Chapter 2 introduces the basics of HVDC.
- Chapter 3 presents the basics of LCC systems. Includes the design of the converters controls and a model of a point-to-point LCC transmission system.
- Chapter 4 analyzes the fundamentals of VSC systems. Propose the design of MMC converters for power and voltage regulation. It also includes a model of a point-to-point VSC transmission system.
- Chapter 5 introduces two different DC/DC converters, and two control strategies are proposed for the Front-to-Front MMC converter and for the DC-MMC converter. A discussion on the interconnection of different kind of grids with these converters is also included.
- Chapter 6 validates the proposed controls and models in a multi-terminal HVDC grid in different scenarios.

Chapter 2

High-Voltage Direct Current

2.1 Introduction to HVDC

High-Voltage Direct Current (HVDC) is a technology less extended compared with High-Voltage Alternating Current (HVAC) for power transfer. However, in the last 50 years this kind of systems has gained interest and nowadays there are more than 200 HVDC systems. Its main applications are the interconnection of non-synchronous networks, long-distance transport of electrical energy, and submarine and underground cable transmission [1].

One of the most discussed issues for this technology is knowing when HVDC is cheaper compared to the classic AC transmission lines. Figure 2.1 shows the cost of installing a new HVDC system compared with the cost of installing the same system in HVAC. As is reflected in Figure 2.1, in the case of HVDC the initial investment is higher due to the installation of converters. However, as the distance of this line increases, the benefits of HVDC can reduce the cost of the transmission line until a breaking distance where HVDC starts to be more beneficial. This distance is not an standard, but to fix some limits it is said that for submarine cables is between 40-70 km and for overhead lines is in the range of 600-800 km [2].

Aside from cost matters, there are other benefits of using HVDC. These are listed below [3]:

- Lower transmission losses over long distances.
- Makes possible the interconnection with submarine and underground cables over long distances without the need of reactive power compensation.
- Connection of asynchronous grids.
- Full control of power flow.
- Black start capability.
- Smaller footprint compared with AC overhead lines.
- HVDC magnetic fields are negligible compared with AC lines.

There are basically two kind of systems for HVDC applications based on the type of converter used to transform the electric wave from AC to DC. The most common ones are based on

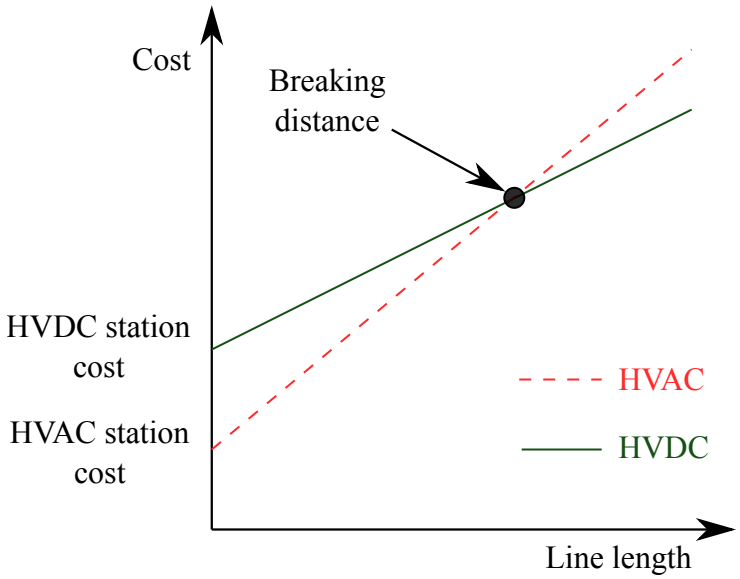

Figure 2.1: HVDC vs HVAC transmission cost

line commutated converters (LCC) which use thyristors. The second one, which is newer, is based upon voltage source converters (VSC) using faster power electronics switches such as the IGBT [1].

2.2 Configuration of Point-to-Point Connections

There are two basic configurations for HVDC systems, symmetric and asymmetric monopole, where the last one can be extended to a bipolar configuration [4]. These basic configurations are shown in Figure 2.2.

- Asymmetric monopolar configuration: This grounding scheme can be provided with metallic return or without it. However, for environmental aspects the majority of them have this metallic return. During normal operation the voltage of the metallic return conductor is near-zero while the positive pole is equal to the nominal voltage.
- Symmetric monopolar configuration: During normal operation the voltage of the converter is divided at each pole as half the nominal voltage. Is it possible to have a neutral point by means of large impedances [4].
- Bipolar configuration: This layout presents two converters, one for each pole. These converters are linked by two conductors, one of positive polarity and the other one with negative polarity. If a failure occurs in one pole, the system can continue operating with one pole as a monopolar configuration.
- Back to Back: It is the configuration used for the interconnection of two asynchronous AC networks. This, locates the rectifier and the inverter at the same place without a DC transmission line between the converters.

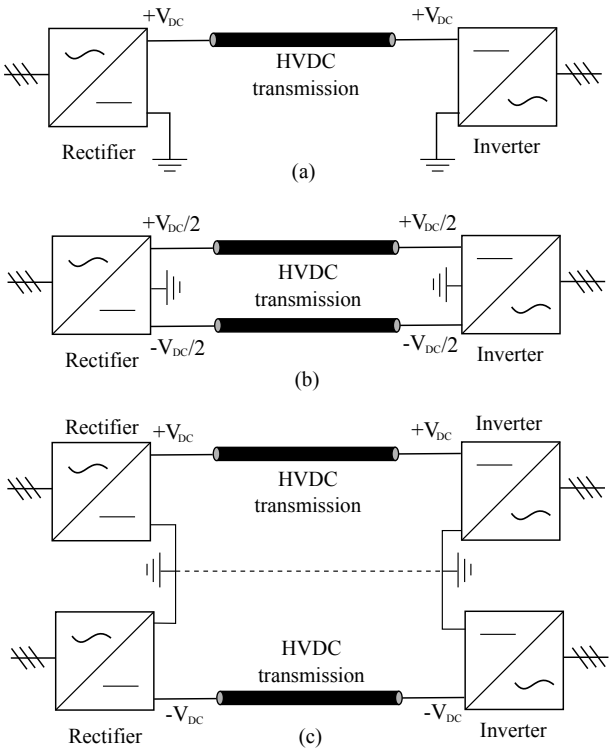

Figure 2.2: Base configurations options for point-to-point HVDC connections. (a) Asymmetric monopole. (b) Symmetric monopole. (c) Bipolar configuration

2.3 Multi-terminal HVDC System

Although nowadays most of the operative HVDC grids are connected as a point-to-point configuration, multi-terminal HVDC grids are expected to grew up. The increasing production of energy in renewables needs a feasible solution to achieve a suitable relation between the energy demand and its supply, and this can be achieved with these multi-terminal HVDC grids.

There are different possible multi-terminal HVDC configurations and different topologies are possible [1].

A first possible topology can consists in a DC bus with several tappings. This configuration lies on a main DC line where different converters are connected to it in order to extract power from the main line. This is not really a grid as it does not offers redundancy [1]. This topology is shown in Figure 2.3.

A second possible configuration is to have a grid of DC lines, where power have different paths to flow and the different converters are connected between them. This kind of grid is more flexible but may need additional devices such can be DC/DC converters to control the power flow. This is also known as a meshed DC grid, shown in Figure 2.4.

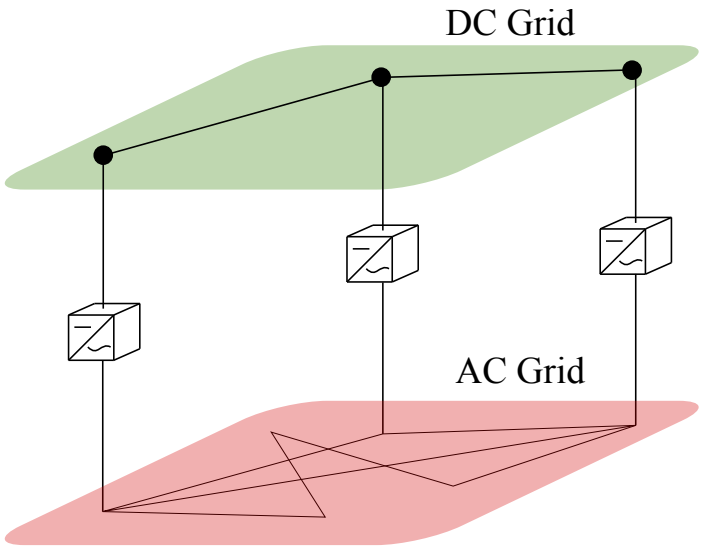

Figure 2.3: DC bus with tappings

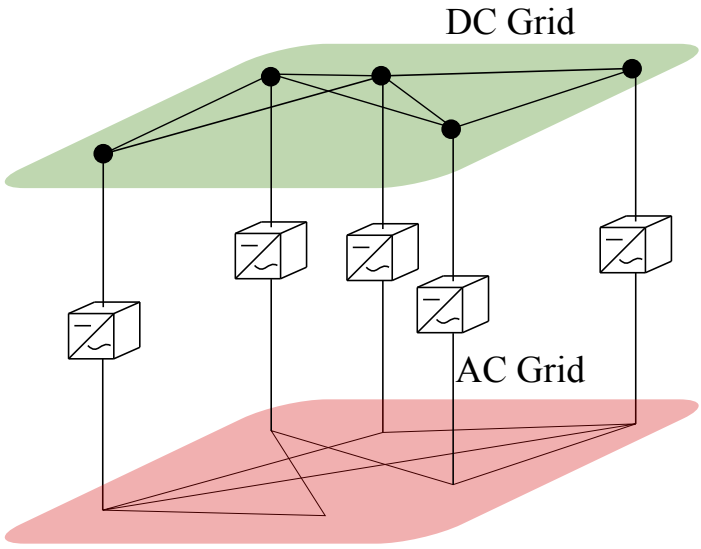

Figure 2.4: Meshed DC grid

Chapter 3

LCC-HVDC System

3.1 Introduction to LCC-HVDC Systems

LCC-HVDC systems have been proven to be technologically and economically superior to a classic AC power transmission in more than 150 point-to-point connexions worldwide [5].

A typical configuration for an LCC-HVDC system is depicted in Figure 3.1. The converter connecting the AC system to the DC system is the inverter and the converter connecting the DC system to the AC network is the rectifier.

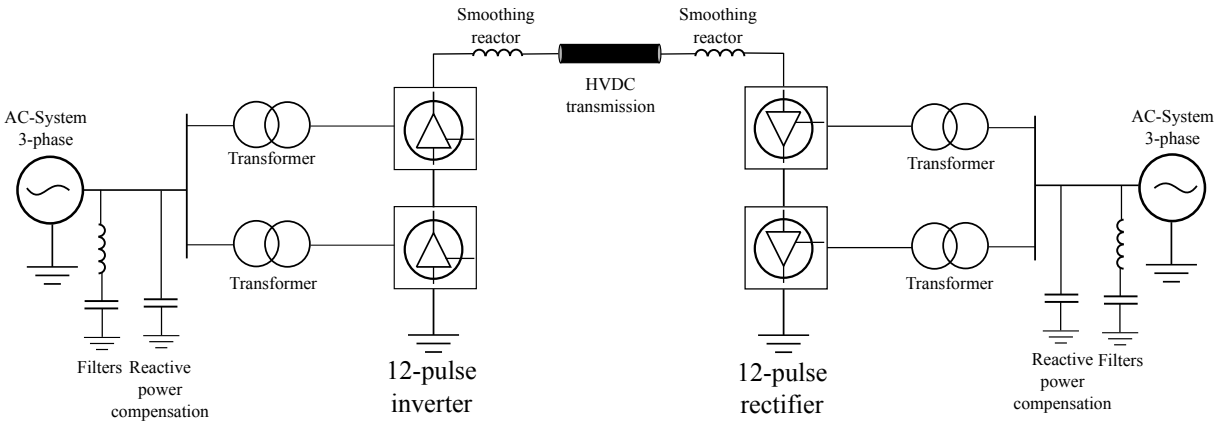

Figure 3.1: LCC-HVDC System

As shown in Figure 3.1 each terminal includes the following equipment:

- Converters: One or more six-pulse bridges (usually more than one in order to reduce harmonics). These bridges are connected in series forming a 12-pulse or 24-pulse configuration. These converters are based on thyristors.
- Transformers: Designed to operate with high harmonics and to deal with AC and DC components.
- Filters: It is necessary to install filters in order to mitigate the commutation ripple. A typical 12-pulse configuration will need filters for the 11th, 13th, 23rd and 25th harmonics on the AC side.

- Smoothing reactors: These are connected in the DC side and are calculated considering DC faults, the possibility of commutation failure and the dynamic stability of the system.
- Reactive power compensation: The operation of an LCC converter requires about a 60% of the power rating as reactive power [2] this can be compensated using filter banks and/or capacitor banks.

3.2 LCC Converters: Introduction

The basic operation of an LCC converter consists on sending a signal to the thyristors in order to fire them. This signal is calculated with the fire angle. This angle is measured from the instant of two phase voltage intersection till the moment when the thyristor is fired. The fired thyristor will stop conducting when the current crosses zero. Controlling this angle it is possible to achieve different DC voltage levels.

The layout of this converter is sketched in Figure 3.2.

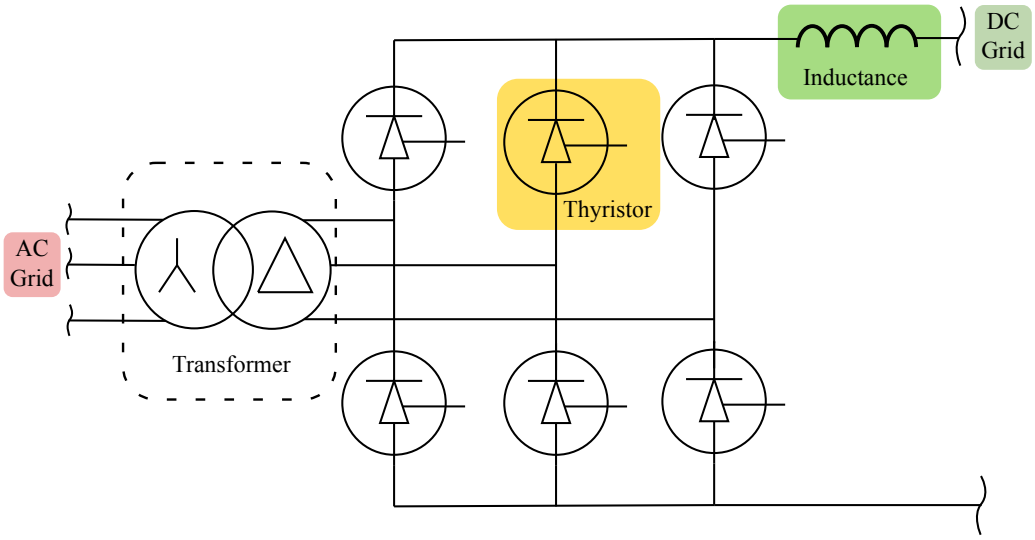

Figure 3.2: Six-pulse LCC converter with a transformer

3.3 LCC Converters: Modeling

A simplified model has been used to simulate this converter. This model divides the AC and DC parts in two different circuits. However, both parts are still in connection.

Starting with the DC part of this model, it is seen that for rectifier and inverter, the equations that regulate the voltage level are the following ones:

$$V_{DC,r} = \frac{3\sqrt{2}}{\pi} V_{LL} \cos\alpha - \frac{3}{\pi} I_{DC} \omega L_t \tag{3.1}$$

$$V_{DC,i} = \frac{3\sqrt{2}}{\pi} V_{LL} \cos\gamma + \frac{3}{\pi} I_{DC} \omega L_t \tag{3.2}$$

As can be seen in Equations 3.1 and 3.2 the DC voltage level depends on the firing angle of both converters Rectifier (α) and Inverter (γ). Thus, it is possible to model this part as a controllable voltage source, that will depend on these firing angles [2].

The AC circuit of the model ensures the power balance between the AC and the DC part. This part is modelled as a controllable current source [2]. There are two magnitudes to fix in this current source, the amplitude and phase of its current. As there is only one equation to satisfy (active power balance), it is necessary to make a simplification. One possible simplification explained in [2] is to consider this angle as the converter's firing angle. Finally, the reference for the current source can be calculated in terms of the Park transformation (Appendix A). In order to apply this transformation it is necessary to obtain the angle of the AC grid, which can be obtained with a Phase-Locked Loop (PLL) (Appendix B):

Equations 3.3 and 3.4 are the ones used to obtain the necessary AC current to ensure the power balance.

$$i_q = \frac{2}{3}\left(\frac{v_q P - v_d Q}{v_q^2 + v_d^2}\right) \tag{3.3}$$

$$i_d = \frac{2}{3}\left(\frac{v_d P + v_q Q}{v_q^2 + v_d^2}\right) \tag{3.4}$$

Applying these currents the active power balance is ensured as well as the reactive power consumed by the converter.

The final model of this converter is sketched in Figure 3.3. Where I_l^{abc} can be obtained applying the inverse of the Park Transformation to Equations 3.3 and 3.4.

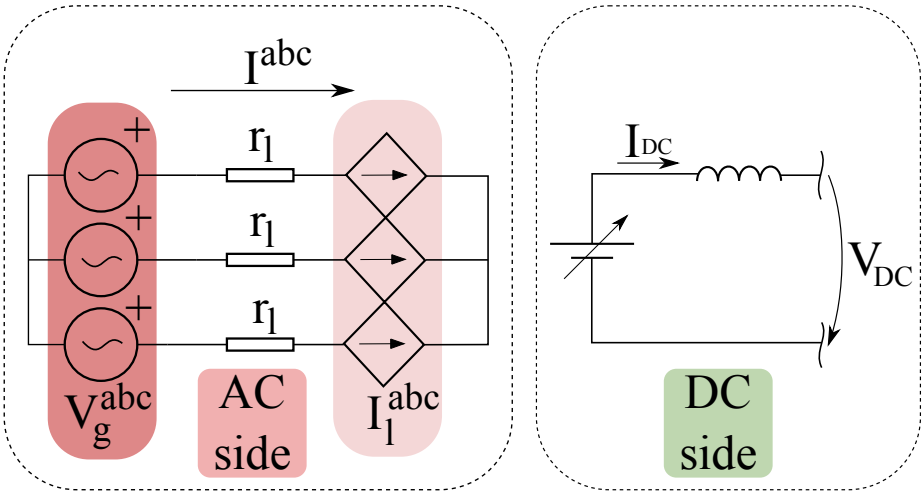

Figure 3.3: LCC converter model

3.4 LCC Converters: Control

The HVDC link formed by the inverter and rectifier can be expressed in terms of the rectifier and inverter voltages, $V_{DC,r}$ and $V_{DC,i}$ respectively, as [2]:

$$I_{DC} = \frac{V_{DC,r} - V_{DC,i}}{R_{DC}} \tag{3.5}$$

where R_{DC} is the total DC-side resistance and I_{DC} is the current flowing through the HVDC link. This current can be controlled using the rectifier or the inverter DC voltage but it its more common to be controlled by the rectifier due to the risk of commutation failure in the inverter [2].

A common way to design the control for this system is using a V-I curve as the one represented in Figure 3.4:

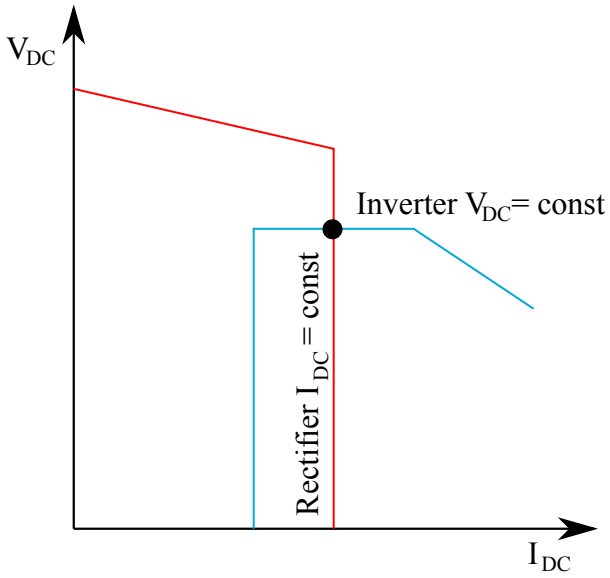

Figure 3.4: LCC point-to-point operation curve

To ensure that the system is working on the desired working point a PI controller can be used to control the I_{DC} current and $V_{DC,r}$ or $V_{DC,i}$ voltages. The structures for these controllers are represented in Figure 3.5.

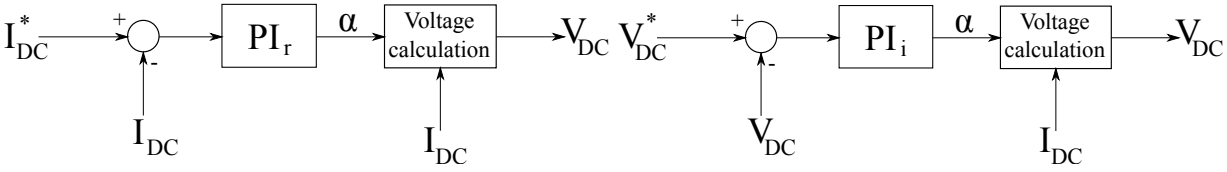

(a) Rectifier control (b) Inverter Control

Figure 3.5: LCC control modes

The parameters chosen for the rectifier are:

$$PI_r = K_{p,r} + \frac{K_{i,r}}{s} \tag{3.6}$$

$$\begin{cases} K_{p,r} = 9 \cdot 10^{-5} \\ K_{i,r} = 2 \cdot 10^{-3} \end{cases} \tag{3.7}$$

Table 3.1: System parameters for the LCC Point-to-Point case study

Magnitudes	Symbol	Value	Units
AC frequency	f_{AC}	50	Hz
AC Grid Voltage (Line to Line)	V_{AC}	50	kV
AC Grid resistance	R_{AC}	0.01	Ω
DC Grid voltage	V_{DC}	600	kV
DC cable capacitance	C_{DC}	19.06	μC
DC cable inductance	L_{DC}	0.2122	H
DC cable resistance	R_{DC}	0.950	Ω
Smoothing inductance	L_{smooth}	0.2	H

In the case of the inverter these parameters are:

$$PI_i = K_{p,i} + \frac{K_{i,i}}{s} \tag{3.8}$$

$$\begin{cases} K_{p,i} = 1 \cdot 10^{-4} \\ K_{i,i} = 2 \cdot 10^{-3} \end{cases} \tag{3.9}$$

3.5 LCC-HVDC Point-to-Point Simulation Results

A bipolar LCC-HVDC link has been modeled with MATLAB Simulink. The DC link has been modeled using a T-equivalent model of a 100 km DC cable. The system parameters are listed in Table 3.1.

Figures 3.6a and 3.6b shows the DC link response to a power reference set-point change at time 2 s. Figure 3.6a shows the active and reactive power consume in the LCC rectifier, and Figure 3.6b, shows the active and reactive power consume on the inverter side. Figure 3.7a shows the DC current in the rectifier side, and Figure 3.7b shows the current flowing in the inverter side. Figure 3.8a shows how the inverter is able to maintain the DC voltage in the desired point (500 kV). Figures 3.9 and 3.10 shows the response in the rectifier and inverter AC sides. Finally, Figure 3.8b shows the converters firing angles.

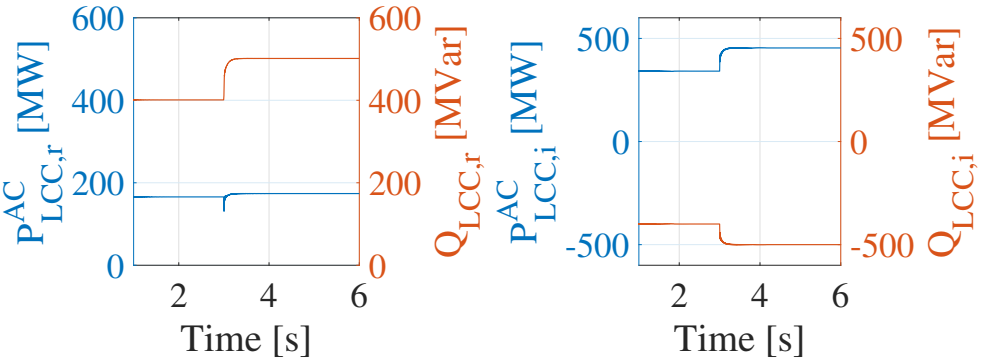

(a) Active and reactive power at the rectifier side

(b) Active and reactive power at the inverter side

Figure 3.6: Active and reactive power flowing in the system

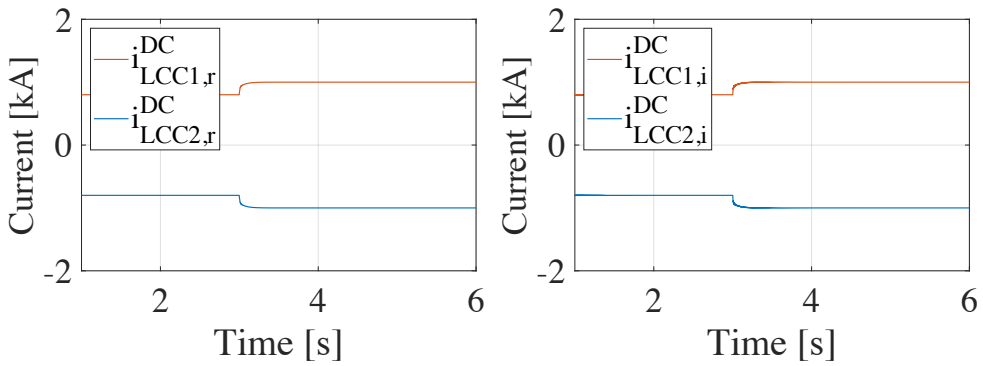

(a) DC currents at the rectifier side

(b) DC currents at the inverter side

Figure 3.7: DC currents flowing in the system

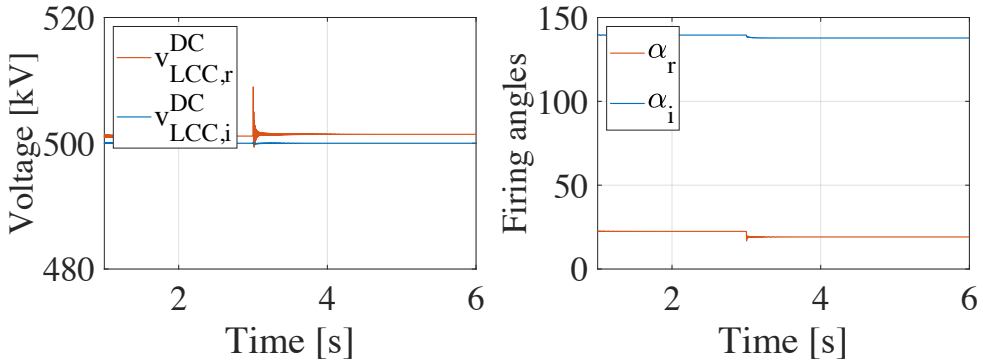

(a) DC voltages at the rectifier and inverter side

(b) Converters firing angles

Figure 3.8: DC voltages and firing angles

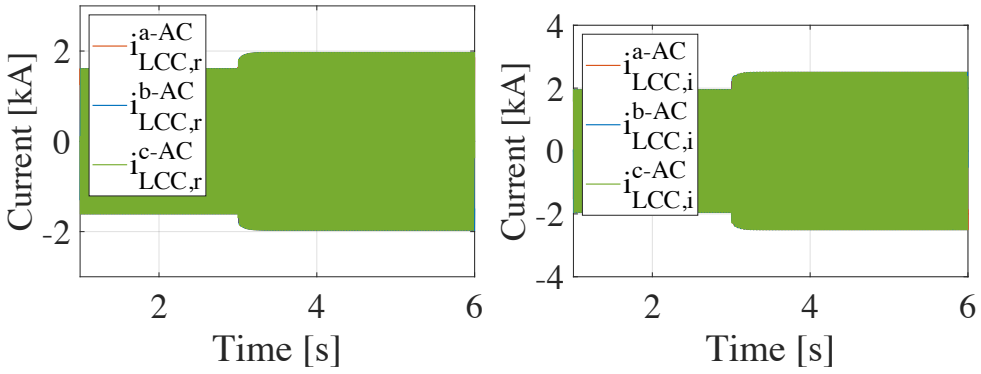

(a) AC rectifier current (b) AC inverter current

Figure 3.9: AC side currents

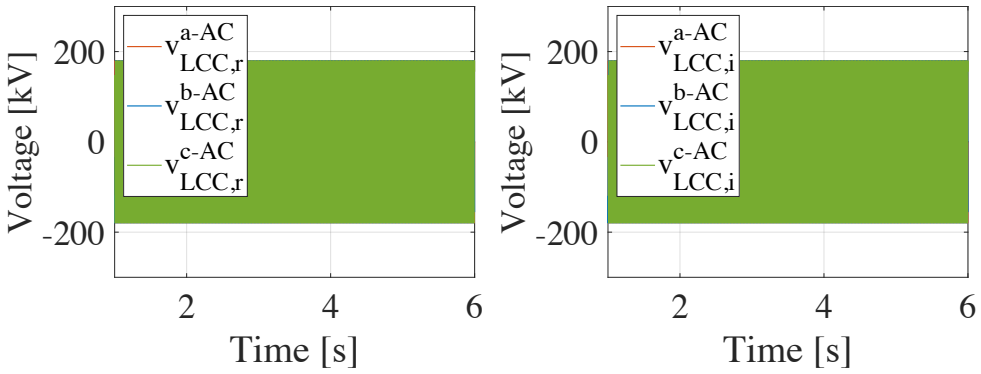

(a) AC rectifier voltage (b) AC inverter voltage

Figure 3.10: AC side voltages

Chapter 4

VSC-HVDC Systems

4.1 Introduction to VSC-HVDC System

Voltage Source Converters (VSC) are typically based on insulated-gate bipolar transistors (IGBT), this technology presents some advantages compared with the use of thyristors. The main difference is the possibility to control the switching on and off of these transistors by control actions. This allows the application of high-frequency (over 1 kHz [2]) modulation techniques such as PWM which permits the reduction of filters [6]. The use of this kind of modulation permits the control of the active and reactive power independently because it can create any phase and/or amplitude by changing the PWM pattern [7]. This can be achived because the switch it on/off of these transistors are both controlled.

The first demonstration of this technology for DC power transmission was commissioned in Hellsjön, Sweden in 1997 with a line of 3 MW ±10 kV. Since then more than 30 VSC lines are in operation worldwide [8].

A basic schematic representation of a VSC-HVDC system is depicted in Figure 4.1.

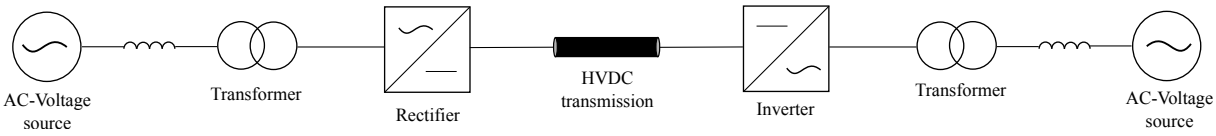

Figure 4.1: VSC-HVDC System

The first generation of VSC-HVDC links was constructed as a Two-level Sinusoidal Pulse Width Modulation (SPWM), which was the main topology during the period between 1996 and 2006 [2]. However, the state-of-the-art of this technology is currently the multilevel VSCs, known as Multilevel Modular Converters (MMC). The main advantage on the use of MMC converters is lower power losses and harmonics compared with the Two-level converters. On the other hand, this technology requires a larger number of switches.

4.2 Modular Multilevel Converters: Introduction

An MMC converter consists of various sub-modules (SM) make by IGBTs and capacitors. These can be half-bridge SM or full-bridge SM. Figure 4.2 represents a sketched representation of these

configurations. The first one can only apply positive voltages while the second one can apply both, positive and negative voltages. These SM can be controlled individually to insert its capacitor in series or to bypass it [9], emulating a controllable voltage source, being possible to control the current flowing inside the converter.

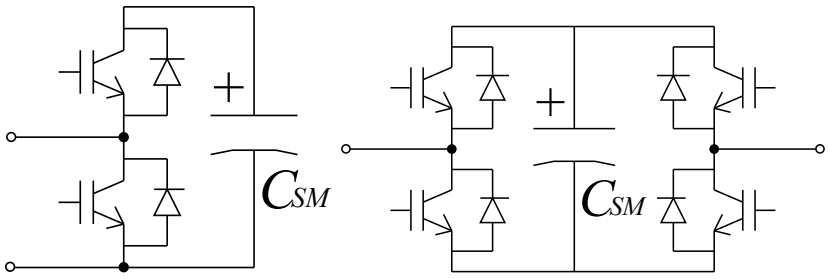

(a) Half-bridge sub-module (b) Full-bride sub-module

Figure 4.2: Sub-modules topologies

The MMC, Figure 4.3, can be represented by the following circuit equations per each phase j ($j = a,b,c$):

$$V_u^{DC} - v_u^j - v_g^j = R_a i_u^j + L_a \frac{di_u^j}{dt} + R_s i_s^j + L_s \frac{di_s^j}{dt} \tag{4.1}$$

$$-V_l^{DC} + v_u^j - v_g^j = -R_a i_u^j - L_a \frac{di_u^j}{dt} + R_s i_s^j + L_s \frac{di_s^j}{dt} \tag{4.2}$$

where v_u^j and v_l^j are the voltages applied by the upper and lower arms, i_u^j and i_l^j are the currents through the upper and lower arms, i_s^j is the current through the phase reactors, R_a and L_a are the resistance and inductance of the arm reactors and R_s and L_s are the resistance and inductance of the phase reactors.

4.3 Modular Multilevel Converters: Modeling

MMCs for HVDC applications use hundreds of sub-modules, therefore a detailed model for an MMC would include several switching elements, resulting in long time simulations. For this reason, an averaged model has been used in this thesis. In particular, the Arm-Level Averaged (ALA) [10] model is the one chosen. In this type of modeling, each converter arm (N sub-modules) is approximated by a controlled voltage source, a controlled current source and an averaged capacitor simulating the whole arm capacitance. Figure 4.4 shows the model used.

This model is able to reflect the dynamics of the AC and DC sides, the only ignored aspects are PWM dynamics and capacitor voltage unbalance in the same arm [10].

4.4 Modular Multilevel Converters: Control

To control this converter a decoupled system is used. To obtain this system the following variables and parameters are defined:

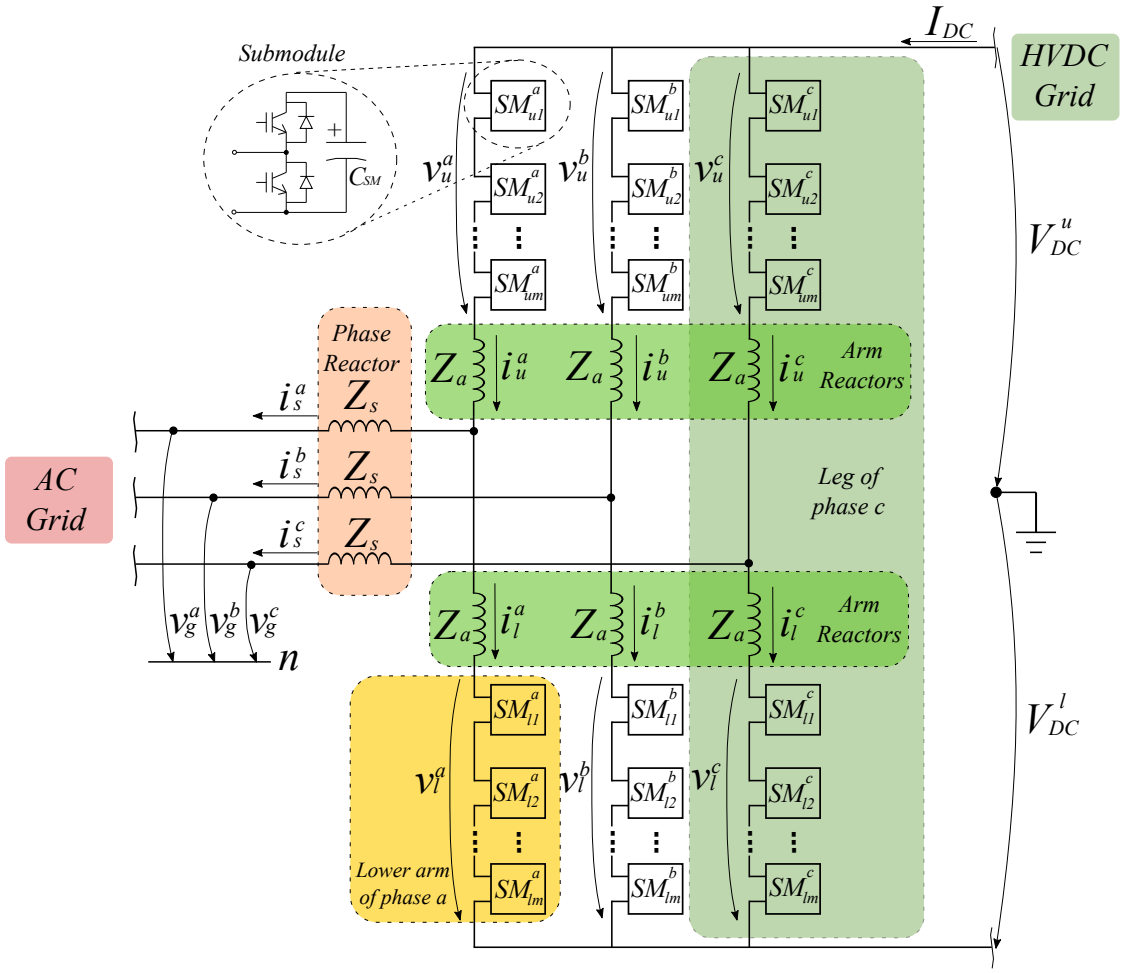

Figure 4.3: MMC complete scheme

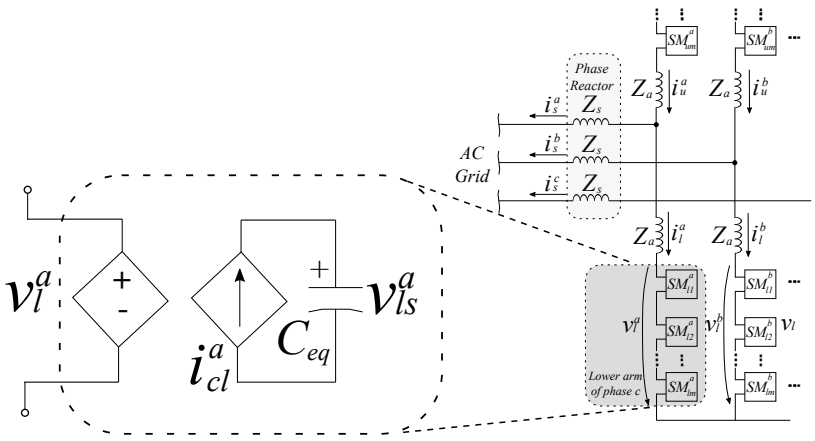

Figure 4.4: Arm-Level Averaged (ALA) model

$$\begin{cases} v^j_{diff} & = \frac{1}{2}(-v^j_u + v^j_l) \\ v^j_{sum} & = v^j_u + v^j_l \\ i^j_{sum} & = \frac{1}{2}(i^j_u + i^j_l) \\ R & = R_s + \frac{R_a}{2} \\ L & = L_s + \frac{L_a}{2} \end{cases} \text{ and } \begin{cases} v^j_u & = -v^j_{diff} + \frac{1}{2}v^j_{sum} \\ v^j_l & = v^j_{diff} + \frac{1}{2}v^j_{sum} \\ i^j_u & = \frac{1}{2}i^j_s + i^j_{sum} \\ i^j_l & = -\frac{1}{2}i^j_s + i^j_{sum} \end{cases} \tag{4.3}$$

Adding and subtracting Equations 4.1 and 4.2 and using the variables defined below 4.3, leads to the following equations per each phase j ($j = a,b,c$):

$$v^j_{diff} - v^j_g = Ri^j_s + L\frac{di^j_s}{dt} \tag{4.4}$$

$$v^j_{sum} - (V^{DC}_u + V^{DC}_l) = -2R_a i^j_{sum} - 2L_a\frac{di^j_{sum}}{dt} \tag{4.5}$$

The control of this converter consists of three differentiated control systems:

- Grid current control: This control is related with Equation 4.4. Is in charge of the active and reactive power reference control in one mode. It is also possible to regulates the DC voltage and the reactive power in a second mode.
- Energy control: This control ensures the stability of the converter energies stored in the different SM.
- Inner current control. This control is related with Equation 4.5 and controls the I_{sum} current which is the output of the Energy control.

A general scheme for an active power and reactive power control is represented in Figure 4.5a and Figure 4.5b represents the control scheme in the case of DC voltage regulation mode.

4.4.1 Grid Current Control

The AC current exchanged with the AC grid can be controlled using Equation 4.4. In fact, I_s is the current flowing to the AC network.

Applying the Park Transformation, with the AC grid angle obtained from a PLL to the studied system, it is possible to transform the references into constant signals, simplifying the controllers needed for this converter. In this new reference the q stands for the active power while d refers to the the reactive power.

Applying the Park transformation to Equation 4.4 and taking into account that for a three-wire systems $i_0 = 0$ [11], the AC system can be expressed as:

$$\begin{bmatrix} v^q_{diff} \\ v^d_{diff} \end{bmatrix} - \begin{bmatrix} v^q_g \\ v^d_g \end{bmatrix} = \begin{bmatrix} R & -L\omega_e \\ L\omega_e & R \end{bmatrix} \begin{bmatrix} i^q_s \\ i^d_s \end{bmatrix} + \begin{bmatrix} L & 0 \\ 0 & L \end{bmatrix} \frac{d}{dt} \begin{bmatrix} i^q_s \\ i^d_s \end{bmatrix} \tag{4.6}$$

As can be seen in Equation 4.6 the q and d components are coupled, these can be decoupled introducing new variables which are defined as follows:

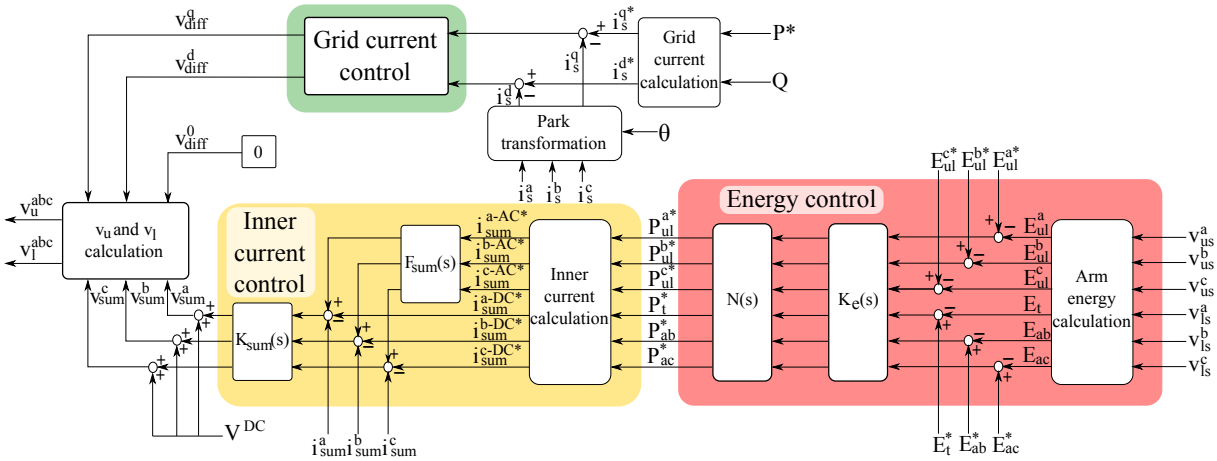

(a) MMC control scheme for power flow control

(b) MMC control scheme for DC voltage regulation

Figure 4.5: MMC control schemes modes

$$\begin{bmatrix} \hat{v}^q_{diff} \\ \hat{v}^d_{diff} \end{bmatrix} = \begin{bmatrix} v^q_g - L\omega i^d_s - v^q_{diff} \\ L\omega i^q_s - v^d_{diff} \end{bmatrix} \tag{4.7}$$

Where $\hat{v}^q_{diff}$ and $\hat{v}^d_{diff}$ are the outputs of the current controllers and v^q_{diff} and v^d_{diff} are the voltages to be applied by the converter.

Using these new variables, and applying the Laplace transformation the transfer functions between these currents and the new variables are the following ones:

$$\frac{i^q_s(s)}{\hat{v}^q_{diff}(s)} = \frac{1}{Ls + R} \tag{4.8}$$

$$\frac{i^d_s(s)}{\hat{v}^d_{diff}(s)} = \frac{1}{Ls + R} \tag{4.9}$$

Using the Internal Model Control technique [12] the PI controller necessary to control these currents presents the following constants:

$$PI_{MMC} = K_{ps,MMC} + \frac{K_{is,MMC}}{s} \tag{4.10}$$

$$\begin{cases} K_{ps,MMC} = \frac{L}{\tau} \\ K_{is,MMC} = \frac{R}{\tau} \end{cases} \tag{4.11}$$

Figure 4.6 represents the current control scheme.

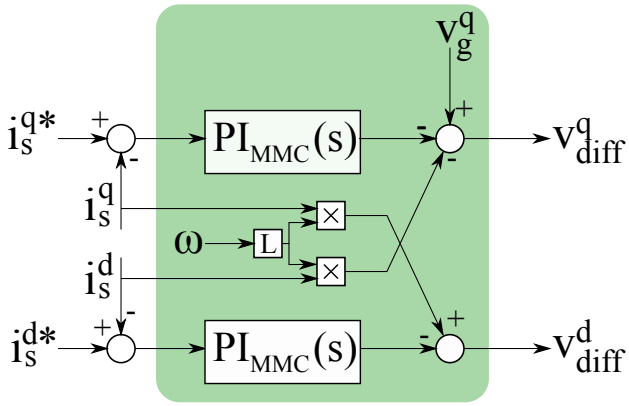

Figure 4.6: Grid Current Control

The references for i_q and i_d can be calculated as:

$$i^{q*}_s = \frac{2}{3}\frac{P^*}{v^q_g} \tag{4.12}$$

$$i^{d*}_s = \frac{2}{3}\frac{Q^*}{v^q_g} \tag{4.13}$$

4.4.2 Voltage Control

The DC voltage loop regulates the voltage at the DC side. The output of this controller is the reference i_s^q for the grid current control. This control is implemented as a PI. This is designed considering the cable equivalent capacitance (C) seen by the converter [13]. The constants of this PI can be calculated as:

$$PI_{V_{DC}-MMC} = K_{p,V_{DC}-MMC} + \frac{K_{i,V_{DC}-MMC}}{s} \tag{4.14}$$

$$K_{p,V_{DC}-MMC} = \frac{1}{2}\xi\omega_n C \tag{4.15}$$

$$K_{i,V_{DC}-MMC} = \frac{1}{4}\omega_n^2 C \tag{4.16}$$

The chosen values for ξ and ω_n are 0.707 and $2\pi(1/15\tau)$, respectively [13].

4.4.3 Energy Control

As mentioned before, this control is needed to ensure the internal energy balance. The different energies that have to be controlled in order to ensure the desired performance for this converter are:

1. Total Converter's Energy: E_t:
2. Energy between Legs: E_{ab} and E_{ac}
3. Energy between Arms: E_{ul}^a, E_{ul}^b and E_{ul}^c

In order to ensure the converter stability, energy differences between legs and between upper and lowers arms must be regulated to zero while the total energy of the converter must be regulated to constant value, which can be calculated as [9]:

$$E_t^* = 6\frac{1}{2}\frac{C_{module}}{N_{arm}}(V_{module})^2 \tag{4.17}$$

where V_{module} is the nominal voltage of each sub-module.

As these energies have components in the AC frequency ω and 2ω, a Noch filter is used to eliminate this ripple in order to avoid that the controller attempts to compensate these oscillations. The Noch filter used to cancel these frequencies is of the form:

$$N_{\omega_n}(s) = \frac{s^2 + w_n^2}{1 + \frac{2w_n}{Q} + w_n^2} \tag{4.18}$$

Where w_n is the AC frequency to be avoided and Q is the quality factor of the filter. The Bode diagram of this filter is shown in Figure 4.7.

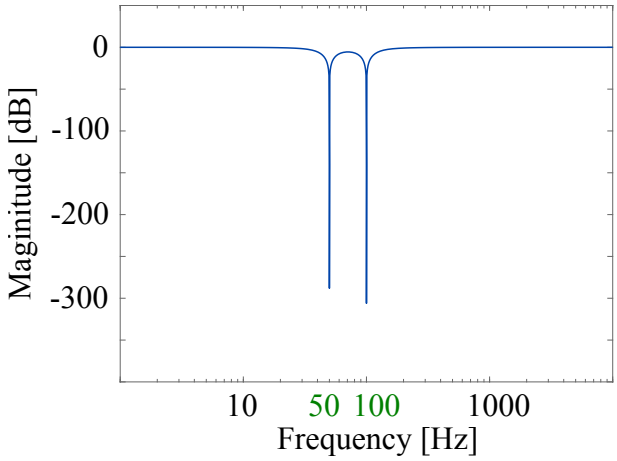

Figure 4.7: Noch filter Bode diagram

These filtered variables are controlled using a PI which can be designed considering a disturbance rejection problem through a loop shaping strategy [9]. The restriction applied to this control is the following one:

- Settling time off 1 second after a power disturbance equal to the nominal power.

Then, the parameters for this controller are set to:

$$K_{e-MMC}(s) = K_{p,e-MMC} + \frac{K_{i,e-MMC}}{s} \tag{4.19}$$

$$\begin{cases} K_{p,e-MMC} = 100 \\ K_{i,e-MMC} = 200 \end{cases} \tag{4.20}$$

4.4.4 Inner Current Control

The outputs of the energy control are different powers, these can be related with the I_{sum} current. The total energy, and the energy between legs can be compensated using the DC part of the I_{sum} current (I_{sum}^{DC}). While the energy difference between upper and lower arms can be canceled with the AC part of the I_{sum} current (I_{sum}^{AC}).

The reference calculation for I_{sum}^{DC} is obtained from the following system:

$$\begin{bmatrix} P_t \\ P_{a-b} \\ P_{a-c} \end{bmatrix} = V^{DC1} \begin{bmatrix} 1 & 1 & 1 \\ 1 & -1 & 0 \\ 1 & 0 & -1 \end{bmatrix} \begin{bmatrix} i_{sum}^{a-DC*} \\ i_{sum}^{b-DC*} \\ i_{sum}^{c-DC*} \end{bmatrix} \tag{4.21}$$

The module for the I_{sum}^{AC} can be calculated from the next relation:

$$I_{sum}^{j-AC*} = \frac{P_{ul}^{j-AC}}{v_g^q} \tag{4.22}$$

Then, the AC inner current references are expressed as:

$$i_{sum}^{j-AC*} = I_{sum}^{j-AC*} \cos(\theta + \phi_{isum}^{j}) \tag{4.23}$$

The angle for this current is a degree of freedom that can be used to optimize the power losses [9].

In order to control the DC and AC parts of this current the control structure chosen is a PI. For the AC reference, a pre-filter is used to compensate the deviation applied by the closed loop controller. This pre-filter is a lead compensator that corrects the gain M_t and phase M_p deviation at the grid frequency ω. Figure 4.8a shows the gain magnitude of the closed loop transfer function of the inner current regulation without the lead compensator. As can be seen it presents a deviation in 50 Hz. Figures 4.8b and 4.8c shows how adding the lead compensator this deviation is compensated at 50 Hz.

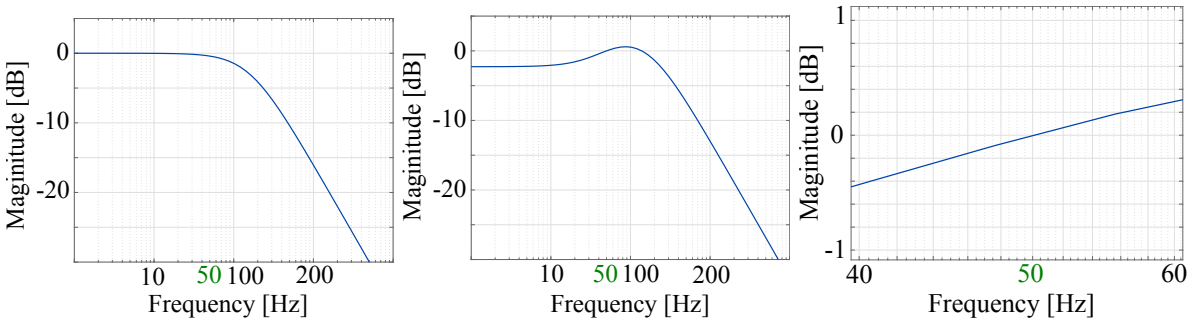

(a) Current regulation without lead compensator

(b) Current regulation with lead compensator

(c) Zoom in 50 Hz for current regulation with lead compensator

Figure 4.8: Bode diagram of closed loop transfer function for current regulation

The PI is calculated using the IMC method resulting the following controller:

$$K_{sum-MMC} = K_{p,sum-MMC} + \frac{K_{i,sum-MMC}}{s} \tag{4.24}$$

$$K_{p,sum-MMC} = \frac{2La}{\tau_{sum}} \tag{4.25}$$

$$K_{i,sum-MMC} = \frac{2Ra}{\tau_{sum}} \tag{4.26}$$

And for the lead compensator its parameters can be calculated as:

$$F_{sum-MMC}(s) = \alpha K_f \frac{s + \omega_1}{s + \omega_2}; \tag{4.27}$$

Table 4.1: System parameters for the VSC Point-to-Point case study

Magnitudes	Symbol	Value	Units
AC frequency	f_{AC}	50	Hz
AC Grid Voltage (Line to Line)	V_{AC}	50	kV
DC Grid voltage	V_{DC}	400	kV
DC cable capacitance	C_{DC}	57.18	μC
DC cable inductance	L_{DC}	0.3168	H
DC cable resistance	R_{DC}	1.425	Ω

$$\begin{cases} \alpha = \frac{1+M_p}{1-M_p} \\ \omega_1 = \omega/\sqrt{\alpha} \\ \omega_2 = \omega\sqrt{\alpha} \\ K_f = \frac{1}{M_t M_f} \\ M_f = \sqrt{\frac{1+M_p}{1-M_p}} \end{cases} \tag{4.28}$$

4.5 VSC-HVDC Point-to-Point Simulation Results

A symmetric monopole VSC-HVDC link has been modeled with MATLAB Simulink. The DC link has been modeled using a T-equivalent model of a 300 km DC cable. The rectifier is controlling the active and reactive power exchanged with the grid and the inverter is controlling the DC voltage and the reactive power. The system parameters are listed in Table 4.1.

Figure 4.10a shows the DC link response to a power reference set-point change at time 2 s. Figure 4.10b shows how the system response to a change in the reactive reference in the inverter at time 3 s an in the rectifier side at time 4 s. Figure 4.9a shows the DC current in the HVDC link during these different operation points and Figure 4.9b shows how the rectifier is able to maintain the DC voltage in the desired point (400 kV). Finally, Figure 4.11 shows AC current response in the rectifier and inverter sides.

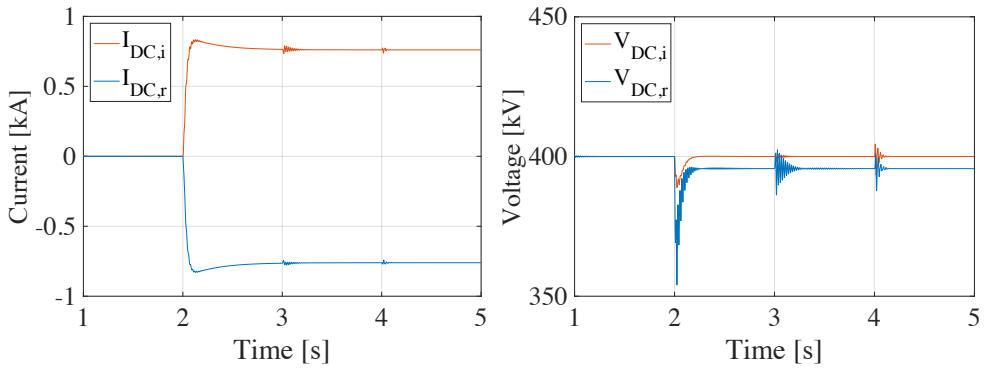

(a) DC current at the rectifier and inverter sides

(b) DC voltage at the rectifier and inverter sides

Figure 4.9: DC side currents and voltages

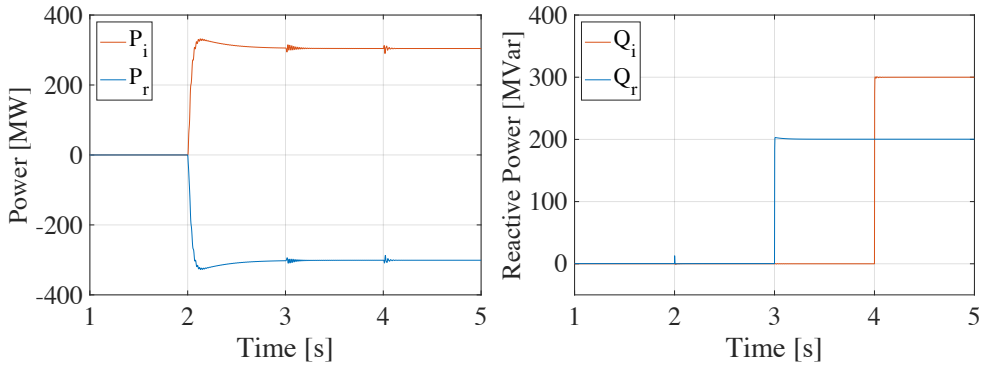

(a) Active power at the rectifier and inverter sides

(b) Reactive power at the rectifier and inverter sides

Figure 4.10: Active and reactive power flowing in the system

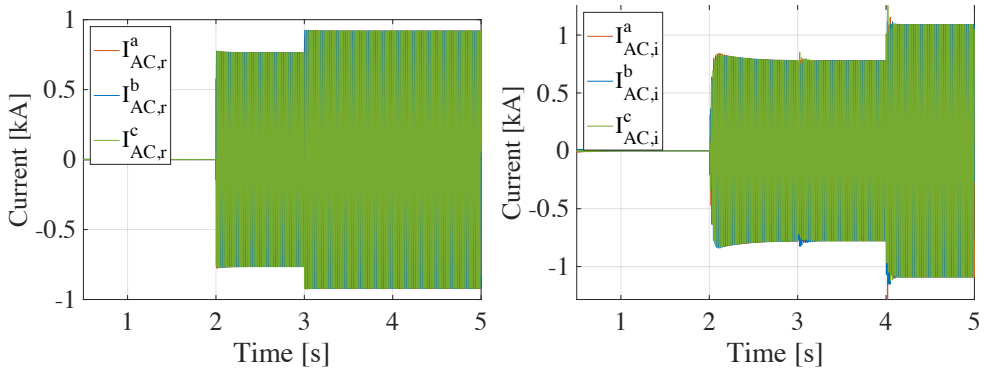

(a) AC rectifier current

(b) AC inverter current

Figure 4.11: AC side currents

Chapter 5

DC/DC Converters

5.1 Introduction to DC/DC Converters

The current HVDC grids include non-standardized point-to-point links. Each link has been developed independently and presents some differences such as [14]:

- Operating DC voltages: While AC grids have a standard for the nominal voltages, DC grids do not have such standards. The nominal voltage for this kind of grids can vary from ±100 kV to ±800 kV.
- HVDC grid configuration: As has been explained in Section 2.2 there are different possible configurations for a HVDC grid. It is necessary to have an element that could interconnect two links with different configurations.
- HVDC technology: As it is described in Chapters 3 and 4 there are two main technologies being in operation nowadays, LCC based and VSC based. DC/DC converters should be able to interconnect these two different technologies.

The function of these DC-DC converters interconnecting different HVDC grids is not only voltage stepping as the classic AC transformers do. These converters can also provide more services such as power flow, voltage regulation and fault isolation.

A classification for such converters can be found in [14] and is reflected in Figure 5.1.

The proposed classification has a first grouping dividing these converters in isolated and non-isolated:

- Isolated: This group presents galvanic isolation and the converters are based on a DC-AC-DC conversion where the galvanic separation is done on the AC bus by magnetic coupling, this can be done by an AC transformer or by coupled inductors [14]. Isolation is mainly needed for safety and grounding reasons being possible to interconnect DC grids with different grounding schemes.
- Non-isolated: These converters can be also divided based on the presence of a transformer, having then two sub-families: DC-Autotransformer converters and Transformerless. In

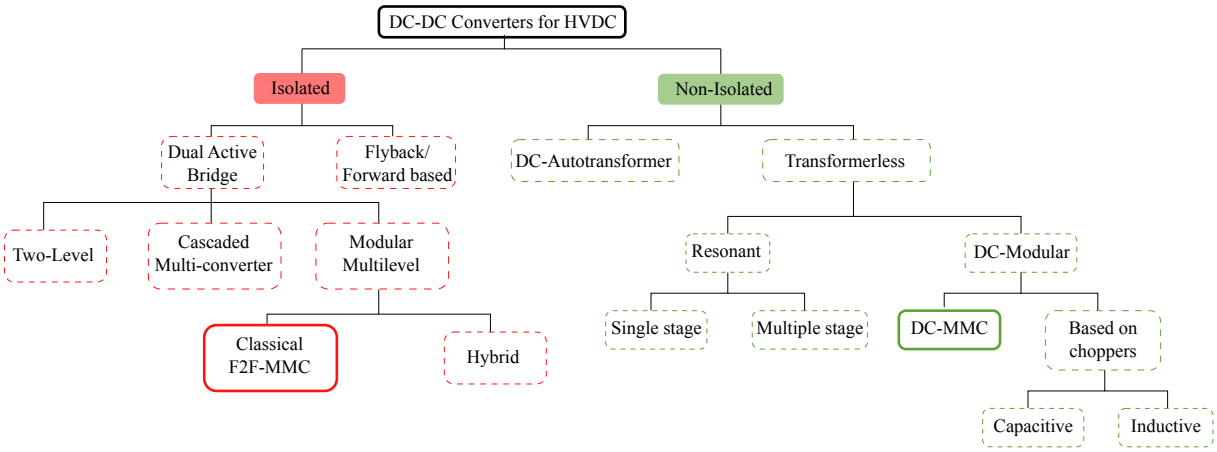

Figure 5.1: Classification for DC/DC converters for HVDC applications

both cases, the DC grids are not isolated by the converter, being more difficult the connection between grids with different grounding schemes.

This Thesis is focused in two of these different converters. The converters chosen for the analysis are the Classical F2F-MMC and the DC-MMC, choosing one for the isolated category and one for the non-isolated category.

5.2 Front-to-Front Modular Multilevel Converter

The strategy followed by this converter consists on coupling two converters. The first one converts form DC to an intermediate AC and then the second converter transforms the AC back to DC. These converters can be either two-level converter or Modular Multi-level Converters (MMC). In this case MMC has been chosen, because in general, MMC provides low switching rates, redundancy and increased reliability. A schematic of the converter is shown in Figure 5.2.

Between both converters it is possible to install a transformer. The main advantage of using a transformer is to isolate the DC grids, being able to connect two HVDC links that differ on the grounding. This transformer can have a voltage ratio equal to 1:1 or can be used to step up/down the voltage level.

The number of phases for each converter connected to the transformer should be the same. However, the sub-modules within these phases do not need to be equally charged. The sub-modules from the first converter do not need to be identical to the other converter being possible to have full bridge sub-modules in one converter and half-bridge sub-modules in the other one.

Another advantage of this converter is that its modularity makes possible to scale up to high voltage levels [15].

5.2.1 Front-to-Front Modular Multilevel Converter: Modeling

As this DC/DC converter is based on the classic AC/DC MMC converter the model that has been chosen is the same as the one presented in Section 4.3.

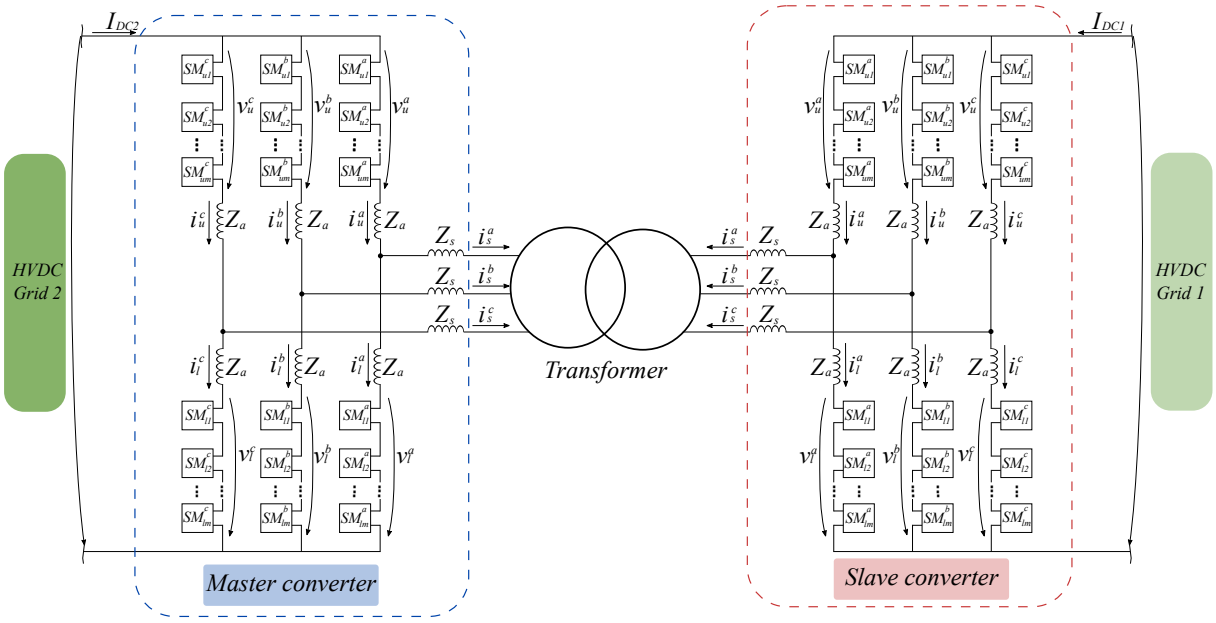

Figure 5.2: Front-to-Front Modular Multilevel Converter scheme

The transformer linking the AC sides of the converter is modeled as a series impedance as the transformer ratio is chosen as 1:1. It has to be noted then, that this model is not suitable for fault simulations because this series impedance will not reflect the transformer response, but as this thesis is not focused on fault studies, this model is considered appropriate.

5.2.2 Front-to-Front Modular Multilevel Converter: Control

The control structure for this converter is divided between the two converters. One converter has a master role over the DC link while the other one is forming the AC grid between the converters. If both converters attempted to regulate the DC side, the power flow or the DC voltage, the system would not be stable. The converter creating the AC grid is called the slave converter. The other one controlling the DC side is called the master converter. This last one is able to control the DC power flow or DC voltage level.

Slave converter control

The control strategy followed by the slave converter is the same as the one used in the AC/DC MMC explained in Section 4.4. The only difference is that the grid current control has been removed and replaced by a constant voltage reference which will generate the AC grid. This control can be left in open loop because the AC link is enclosed in the converter and it is not necessary to respect grid limitations. The energy control is the same one as for the AC/DC MMC and it is controlling all the energies to ensure the internal stability: the converter total energy, energy between legs and energy between upper and lower arms. A general scheme for this control is represented in Figure 5.3

Master converter DC power control

An efficient way to control the power flow in the F2F converter often proposed in the literature is the Phase-Shift control. Its main objective is to introduce a phase angle between the AC

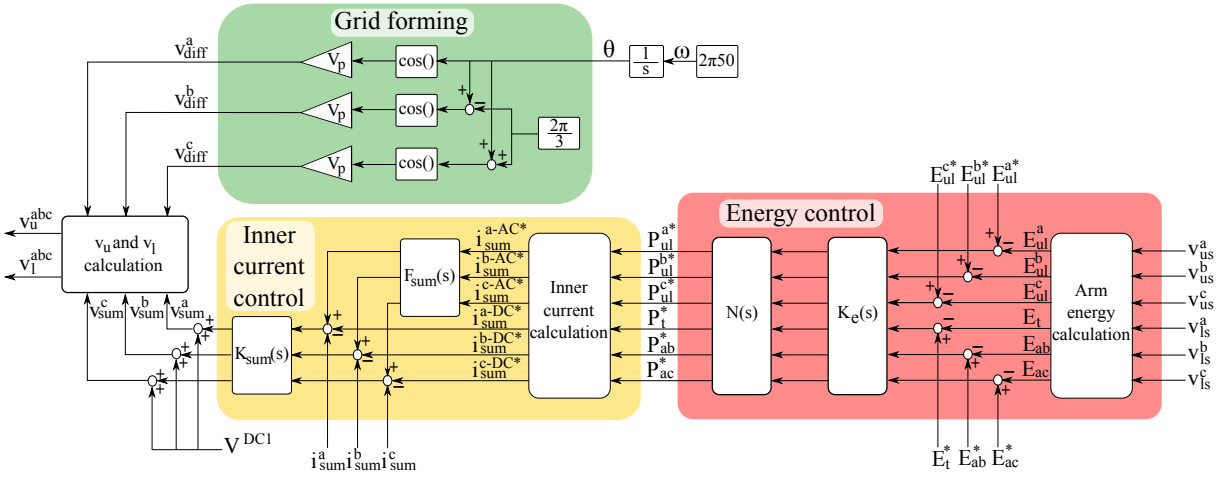

Figure 5.3: Front-to-Front Modular Multilevel Converter slave control

voltages created by both converters in the AC coupling in order to generate the power flow. This is a similar strategy as the one used in a DAB converter [16].

The AC link circuit equation, neglecting losses, can be written as:

$$P_{AC} = \frac{V_s V_m \sin\delta}{2\omega L} \tag{5.1}$$

where V_s and V_m is the amplitude of the voltages applied by the slave and master converters, δ is the angle difference between both voltages, ω is the angular frequency of the AC grid and L is the AC circuit inductance:

$$L = L_{transformer} + L_s \tag{5.2}$$

Thus, it is possible to control the power flow in terms of the angle difference δ. Furthermore, if the losses inside the converter are neglected is possible to replace P_{AC} for P_{DC} controlling then the power flowing to the DC grid.

The reactive power transmitted by the converters can be expressed as:

$$\begin{cases} Q_s = \frac{V_s V_m \cos\delta - V_s^2}{2\omega L} \\ Q_m = \frac{V_m^2 - V_s V_m \cos\delta}{2\omega L} \end{cases} \tag{5.3}$$

where Q_s is the reactive power transmitted by the slave converter and Q_m is the reactive power transmitted by the master converter. Having similar AC voltage amplitudes and low phase shift δ ensures a low transmission of reactive power. On the other hand, in order to transmit active power it is necessary to ensure enough phase shift. In general low δ is desired to ensure low power losses.

The active power control is possible with a PI. To tune this controller the symmetrical criteria calculations presented in [16] are used. Defining the following constants for this controller:

$$PI_{ps} = K_{p,ps} + \frac{K_{i,ps}}{s} \tag{5.4}$$

$$K_{p,ps} = \frac{T_n}{T_i} \tag{5.5}$$

$$K_{i,ps} = \frac{1}{T_i} \tag{5.6}$$

where

$$T_n = 4T_p, T_i = 8\frac{K_{cm}}{T_1}T_p^2, T_1 = \frac{C}{N} \tag{5.7}$$

are time constants defined according to the control circuit. T_p is the sum of all the time delays in the circuit and K_{cm} represents the gain between the current command and the output signal, set to one.

The complete control scheme for the master converter is represented in Figure 5.4.

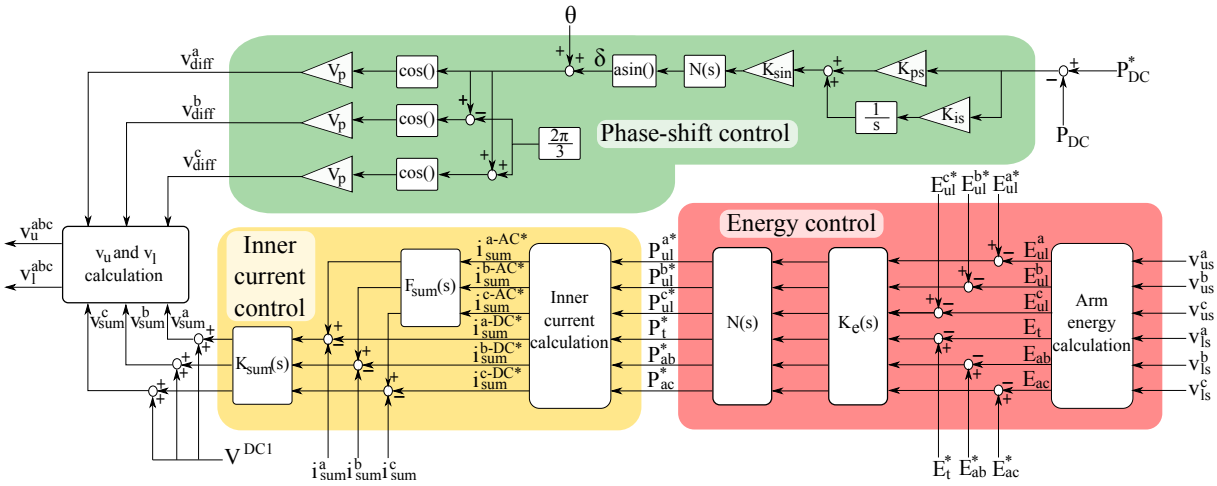

Figure 5.4: Front-to-Front Modular Multilevel Converter master power flow control

Master converter DC voltage regulation

The DC voltage control chosen for this converter is the cross control presented in [13] for an AC/DC MMC. This control has been adapted for the F2F converter combining it with the phase shift control presented in the previous master control. The final structure for this control consists on cascade the DC voltage loop with the DC inner current loop (i_{sum}^{DC}). Finally, the total energy control is cascaded with the phase shift control. The other energies and current loops are the same as the previous control. This new control scheme is shown in Figure 5.5.

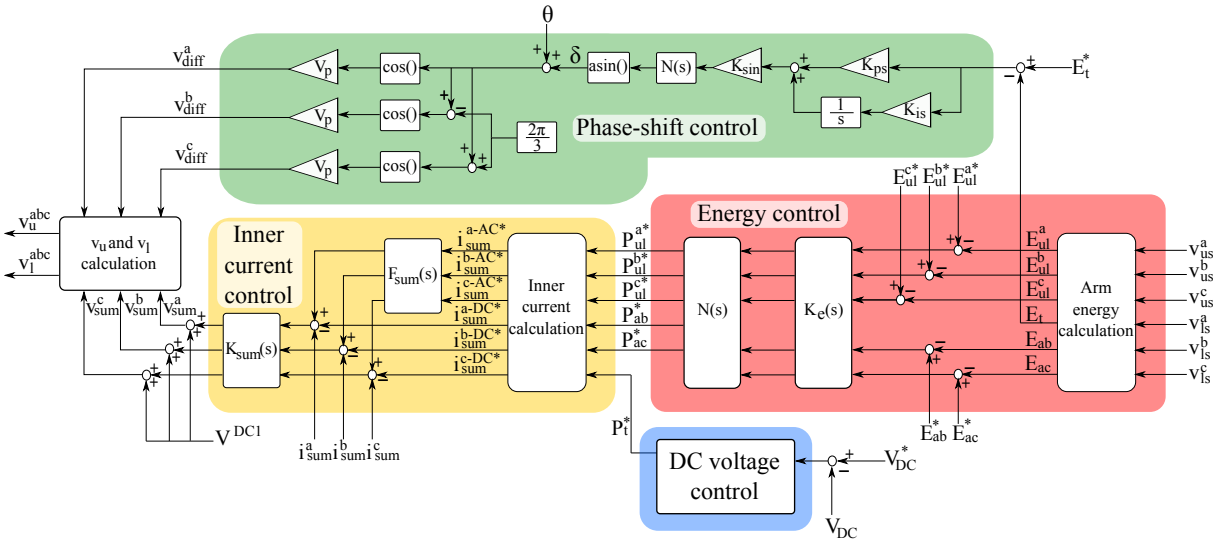

Figure 5.5: Front-to-Front Modular Multilevel Converter master control with voltage regulation

5.3 DC Modular Multilevel Converter

This type of converter is developed based on the classic AC/DC MMC converter. A general schematic of the converter is shown in Figure 5.6.

It can convert a DC voltage V^{DC1} into another voltage V^{DC2}, which is generally lower in magnitude. To achieve this conversion the DC-MMC has N submodules (SM) in each arm. These sub-modules have capacitors connected in series. These capacitors can be controlled individually to be inserted or to be bypassed, so each arm can behave as a controllable voltage source. This is used to achieve the desired exchange of power and to maintain the internal energy balance. The DC power transferred between DC grids causes a deviation of the energy stored in the upper and lower arms, charging one arm and discharging the other, depending on the power flow direction. This can be solved introducing an AC circulating current to exchange active power between the upper and lower arms.

This converter can be represented by the following equations:

$$V^{DC1} - V^{DC2} - v_u^j = R_a i_u^j + L_a \frac{di_u^j}{dt} + R_s i_s^j + L_s \frac{di_s^j}{dt} \tag{5.8}$$

$$V^{DC2} - v_l^j = R_a i_l^j + L_a \frac{di_l^j}{dt} - R_s i_s^j - L_s \frac{di_s^j}{dt} \tag{5.9}$$

5.3.1 DC Modular Multilevel Converter: Modeling

The model that has been chosen to represent the converter is the same as the one used in Section 4.3 as this converter have the same aspects as an AC/DC MMC. This model is able to represent with accuracy this DC/DC converter with the same limitations as the ones explained before.

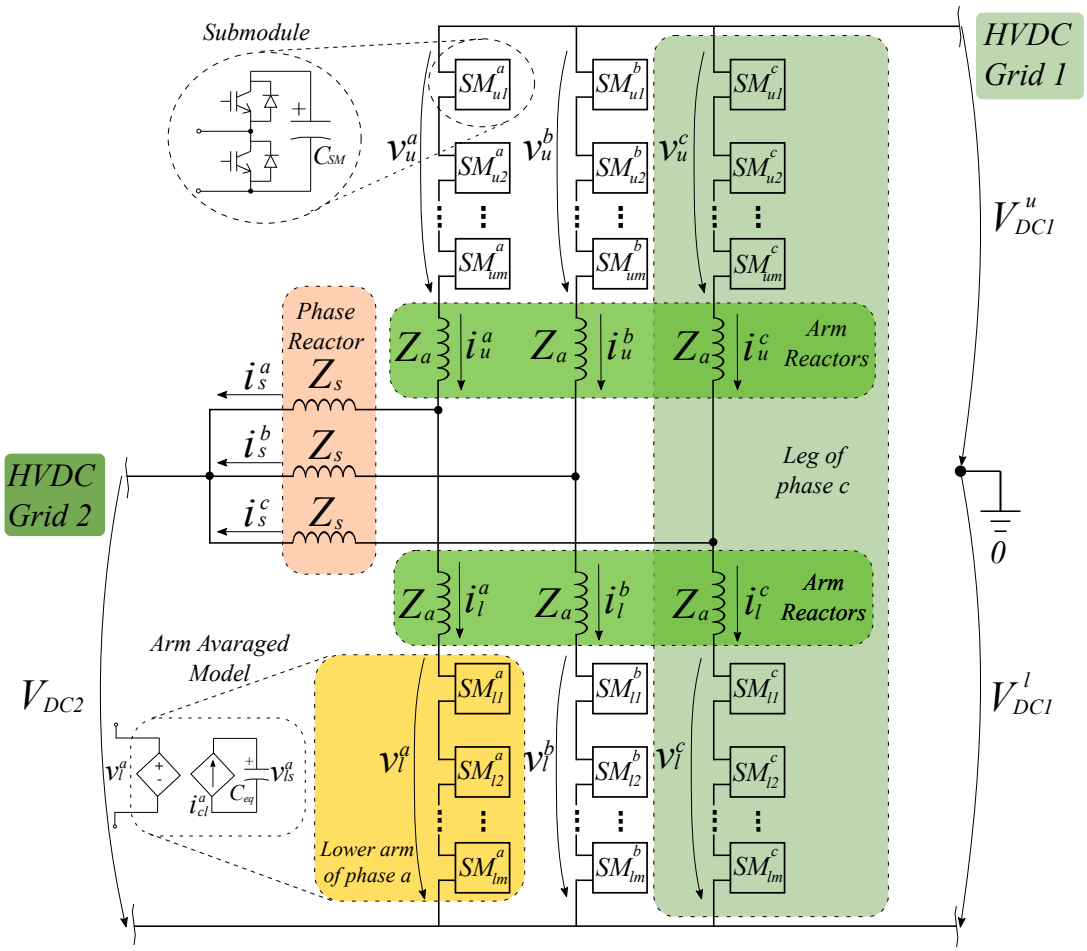

Figure 5.6: DC/DC Modular Multilevel Converter scheme

5.3.2 DC Modular Multilevel Converter: Control

In order to control this converter a decoupled model is used. To achieve this decoupled system new variables are introduced as 5.10, where $j = a,\ b,\ c$:

$$\begin{cases} v^j_{diff} & = \frac{1}{2}(-v^j_u + v^j_l) \\ v^j_{sum} & = v^j_u + v^j_l \\ i^j_{sum} & = \frac{1}{2}(i^j_u + i^j_l) \\ R & = R_s + \frac{R_a}{2} \\ L & = L_s + \frac{L_a}{2} \end{cases} \quad \text{and} \quad \begin{cases} v^j_u & = -v^j_{diff} + \frac{1}{2}v^j_{sum} \\ v^j_l & = v^j_{diff} + \frac{1}{2}v^j_{sum} \\ i^j_u & = \frac{1}{2}i^j_s + i^j_{sum} \\ i^j_l & = -\frac{1}{2}i^j_s + i^j_{sum} \end{cases} \tag{5.10}$$

Finally, the following system (5.11, 5.12) is obtained summing and subtracting Equations 5.8, 5.9 and using the variables previously defined in 5.10.

$$v^j_{diff} - V^{DC2} + \frac{V^{DC1}}{2} = Ri^j_s + L\frac{di^j_s}{dt} \tag{5.11}$$

$$v^j_{sum} - V^{DC1} = -2R_a i^j_{sum} - 2L_a\frac{di^j_{sum}}{dt} \tag{5.12}$$

Where the different voltages and currents can be expressed as:

$$\begin{cases} v^j_{diff} = v^{j-DC}_{diff} + v^{j-AC}_{diff} = V^{DC}_{diff} + V^{AC}_{diff}\cos(\omega t + \phi^j_{diff}) \\ i^j_s \ \ = i^{j-DC}_s + i^{j-AC}_s = I^{DC}_s + I^{AC}_s\cos(\omega t + \phi^j_s) \\ v^j_{sum} = v^{j-DC}_{sum} + v^{j-AC}_{sum} = V^{DC}_{sum} + V^{AC}_{sum}\cos(\omega t + \phi^j_{vsum}) \\ i^j_{sum} = i^{j-DC}_{sum} + i^{j-AC}_{sum} = I^{DC}_{sum} + I^{AC}_{sum}\cos(\omega t + \phi^j_{isum}) \end{cases} \tag{5.13}$$

The angle ϕ^a_{diff} is set to zero in order to fix a reference for the other voltages and currents as the AC system inside the converter is completely generated by control actions.

The first system is used to regulate the power flow, while the second one is used to ensure the energy balance inside the converter. Both systems are also used to minimize the power losses. A general scheme of the control structure is shown in Figure 5.7, having this control strategy five main objectives:

1. Control the desired power flow
2. Total energy balance
3. Energy balance between different legs
4. Energy balance between upper and lower arms
5. Power losses minimization

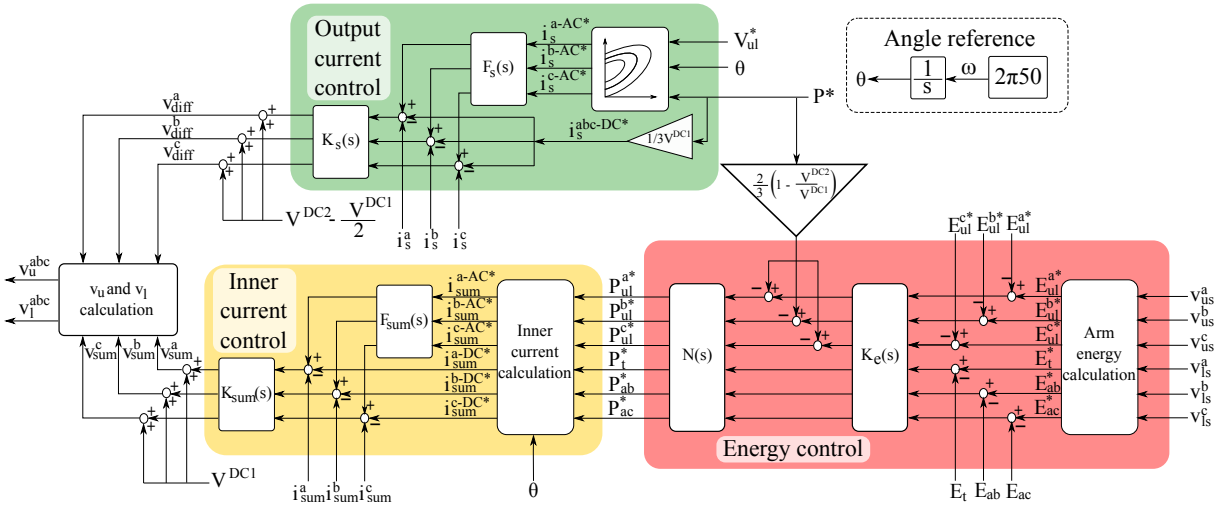

Figure 5.7: DC Modular Multilevel Converter control structure

Steady State analysis

Before introducing all controls is important to understand how this converter works in steady state. As referred before, the power flow between the two DC grids generates an energy unbalance between upper and lower arms. This is caused by a DC power flow between the upper and lower arms that can be calculated as follows:

$$P_u^{j-DC} - P_l^{j-DC} = \frac{2P}{3}(1 - \frac{V^{DC2}}{V^{DC1}}) \tag{5.14}$$

This DC power flow can be added as a feedforward to the upper and lower arms energy control.

This power flow can be compensated by control actions introducing another AC power flow in the opposite direction, which can be calculated as:

$$\begin{aligned} P_{ul}^{j-AC} &= \left(\frac{1}{4}V_{sum}^{AC}I_s^{AC} - V_{diff}^{AC}I_{sum}^{j-AC}\right)\sin(\phi_{vsum}^j - \phi_{diff}^j) \\ &= I_{sum}^{AC}I_s^{AC}(Z_s - \frac{1}{4}Z_{sum})\sin(\phi_{vsum}^j - \phi_{diff}^j) \end{aligned} \tag{5.15}$$

As is derived from Equation 5.15 the angle difference $\phi_{vsum}^j - \phi_{diff}^j$ defines the power flow direction as:

$$\begin{cases} P > 0 : P_{ul}^{j-DC} = P_{ul}^{j-AC} > 0 \ \& \ \phi_{vsum}^j - \phi_{diff}^j \in (\pi, 2\pi) \\ P < 0 : P_{ul}^{j-DC} = P_{ul}^{j-AC} < 0 \ \& \ \phi_{vsum}^j - \phi_{diff}^j \in (0, \pi) \end{cases} \tag{5.16}$$

Having for positive power an angle difference $\phi_{vsum}^j - \phi_{diff}^j$ between π and 2π and for a negative power an angle difference between 0 and π. It is also derived from Equation 5.15 that both AC systems (5.11 and 5.12) are necessary to generate the AC power flow needed for the converter

stability as the voltages and currents of these systems are crossed between them. V_{sum}^{AC} is multiplying I_s^{AC} and V_{diff}^{AC} is multiplying I_{sum}^{AC}.

I_s Current Control

The DC part of I_s is used to ensure the desired exchange of power between DC grids, while the AC part is used to achieve the desired AC voltage amplitude in the upper and lower arms and to minimize the reactive power flowing inside the converter in order to minimize the power losses.

The PI used to control this current has been designed using the IMC method as has been done before with other PI. The parameters for this controller are the following ones:

$$K_{s-DCMMC}(s) = K_{p,s-DCMMC} + \frac{K_{i,s-DCMMC}}{s} \tag{5.17}$$

$$\begin{cases} K_{p,s-DCMMC} = \frac{L}{\tau_s} \\ K_{i,s-DCMMC} = \frac{R}{\tau_s} \end{cases} \tag{5.18}$$

An AC reference pre-filter is calculated to compensate the deviation applied by the closed loop controller being able to track correctly the AC part of this current reference. This pre-filter can be designed as the one presented in Subsection 4.4.4.

To calculate the reference for this controller the following equation can be used:

$$4Z_s^2\left(\frac{Z_s}{Z_{sum}}-\frac{1}{4}\right)^2 I_s^{AC*4} - 4V_{ul}^{AC2}\left(\frac{Z_s}{Z_{sum}}-\frac{1}{4}\right)^2 I_s^{AC*2} + \frac{4P^{*2}}{9}\left(1-\frac{V^{DC2}}{V^{DC1}}\right)^2 = 0 \tag{5.19}$$

Equation 5.19 shows that more than one I_s^{AC} are possible for a given active power P and desired V_{ul}^{AC} (amplitude of the upper and lower arms) as is also shown in Figure 5.8a. In order to minimize the total current through each arm and, as a consequence lower power losses, high I_s^{AC} is preferred. Setting a high I_s^{AC} corresponds to a low I_{sum}^{AC}, minimizing the sum of both currents, as can be conclude from Figure 5.8b. V_{ul}^{AC} is chosen as the maximum possible, because this sets a lower current for a given P_{ul}^{DC}.

Then, the AC current references are expressed as:

$$I_s^{j-AC*} = I_s^{j-AC*}\cos(\theta + \phi_{is}^j) \tag{5.20}$$

Where the angle ϕ_{is} is approximately 90 degrees, as the system 5.11 is mainly inductive.

The DC reference part can be calculated as:

$$I_s^{j-DC} = \frac{P^*}{3V^{DC2}} \tag{5.21}$$

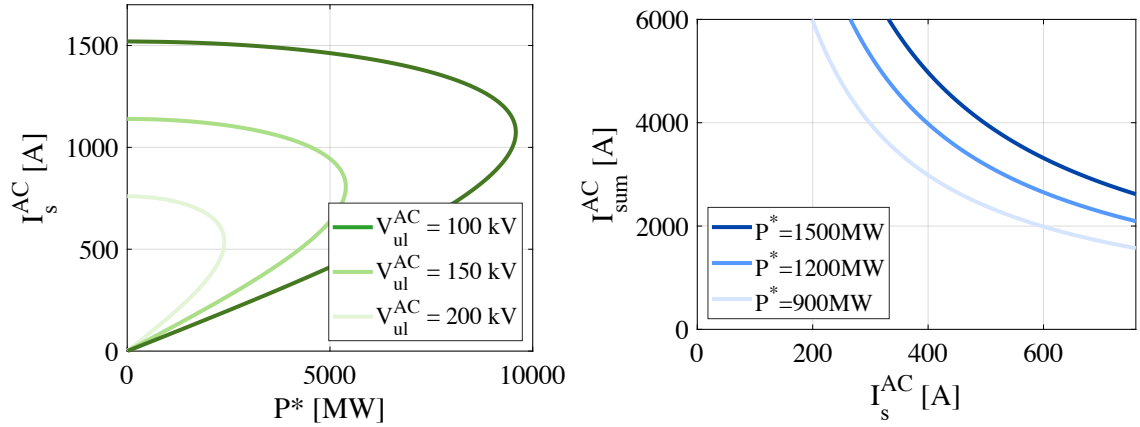

(a) Relation between I_s^{AC} and P^* for different V_{ul}^{AC}

(b) Relation between I_s^{AC} and I_{sum}^{AC} for different P^*

Figure 5.8: Converter operation points

DC voltage control

The DC voltage control is set instead the I_s^{DC} reference calculation. It is only possible to control the power flow or the DC voltage in the DC link, so controlling the DC voltage disables the DC power control. The DC voltage can be regulated with a PI, having as input the voltage error and as output the power to inject to the DC grid necessary to control the DC voltage. This control scheme is sketched in Figure 5.9. The parameters chosen for this PI are the following ones:

$$PI_{VDC,DCMMC} = K_{p,VDC-DCMMC} + \frac{K_{i,VDC-DCMMC}}{s} \tag{5.22}$$

$$\begin{cases} K_{p,VDC-DCMMC} = 4.2 \cdot 10^{-3} \\ K_{i,VDC-DCMMC} = 1.254 \end{cases} \tag{5.23}$$

Energy control

The energy control is set before the inner current control. This control gives the different power references necessary to calculate all the inner converter currents. There are six different controllers in order to regulate the following energies:

1. Total energy
2. Energy difference between legs a and b
3. Energy difference between legs a and c
4. Energy difference between upper and lower arms of phase a
5. Energy difference between upper and lower arms of phase b
6. Energy difference between upper and lower arms of phase c

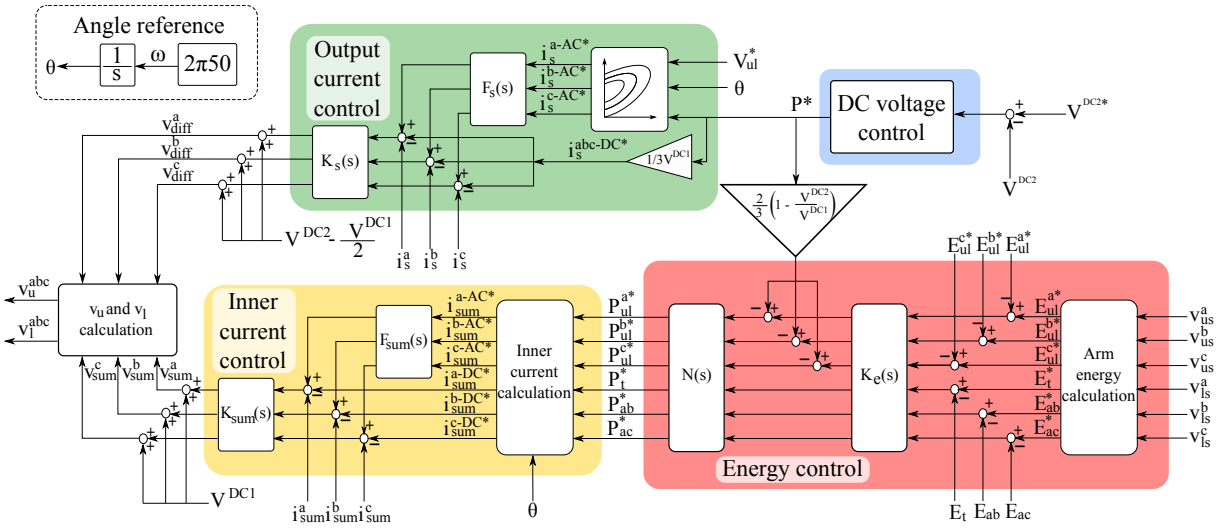

Figure 5.9: DC Modular Multilevel Converter control structure with DC voltage regulation

As it is done previously in the classic MMC AC/DC (Subsection 4.4.3) to ensure the converter stability, the energy difference between legs and between upper and lower arms are regulated to zero. The total energy of the converter is regulated to a constant value, which in this case is set as:

$$E_t^* = 3\frac{1}{2}\frac{C_{module}^u}{N_{arm}^u}(V_{module}^u)^2 + 3\frac{1}{2}\frac{C_{module}^l}{N_{arm}^l}(V_{module}^l)^2 \tag{5.24}$$

where V_{module}^u and V_{module}^l are the nominal voltage of the upper and lower arms sub-module, C_{module}^u and C_{module}^l are the capacitance in the upper and lower arms and N_{arm}^u and N_{arm}^l are the number of sub-modules in the upper and lower arms.

The control design followed for this converter is the same explained in Subsection 4.4.3 for the MMC AC/DC. The parameters obtained are the following ones:

$$PI_{e,DCMMC} = K_{e,p-DCMMC} + \frac{K_{e,i-DCMMC}}{s} \tag{5.25}$$

$$\begin{cases} K_{e,p-DCMMC} = 100 \\ K_{e,i-DCMMC} = 200 \end{cases} \tag{5.26}$$

Inner current control

As in the MMC AC/DC converter the total energy and the energy difference between legs can be compensated using the DC part of the I_{sum} current (I_{sum}^{DC}), while the energy difference between the upper and lower arms can be compensated with the AC part of the I_{sum} current (I_{sum}^{AC}).

The reference for I_{sum}^{AC} is obtained from the following equation:

$$I_{sum}^{j-AC*} = \frac{P_{ul}^{j-AC}}{I_s^{AC*}} \frac{1}{Z_s - \frac{1}{4}Z_{sum}} \tag{5.27}$$

where Z_s is the impedance of the system 5.11 and Z_{sum} is the impedance of the system 5.12.

Then, the AC inner current references are expressed as:

$$i_{sum}^{j-AC*} = I_{sum}^{j-AC*} \cos(\theta + \phi_{isum}^{j}) \tag{5.28}$$

The angle ϕ_{isum} is fixed to 90º as this sets the reactive power flowing inside the converter near zero, since the angle differences $\phi_{vsum}^{j} - \phi_{isum}^{j}$ and $\phi_{diff}^{j} - \phi_{s}^{j}$ are approximately 90º. This is reflected in Equation 5.29, when power losses are neglected.

$$Q_{ul}^{j} = -(\frac{1}{4}V_{sum}^{AC} I_s^{AC} + V_{diff}^{AC} I_{sum}^{AC}) \cos(\phi_{vsum}^{j} - \phi_{diff}^{j}) \tag{5.29}$$

The minimization of the reactive power flowing inside the converter combined with the application of the maximum voltage amplitude for the upper and lower arms is the way chosen to reduce the power losses generated by this converter.

It is important to highlight that choosing this angles set the amplitudes of the upper and lower arm voltages at the same level as can be concluded from Equation 5.30.

$$\begin{cases} V_u^{AC\,2} = V_{diff}^{AC\,2} + \frac{1}{2}V_{sum}^{AC\,2} - V_{diff}^{AC} V_{sum}^{AC} \cos(\phi_{vsum}^{j} - \phi_{diff}^{j}) \\ V_l^{AC\,2} = V_{diff}^{AC\,2} + \frac{1}{2}V_{sum}^{AC\,2} + V_{diff}^{AC} V_{sum}^{AC} \cos(\phi_{vsum}^{j} - \phi_{diff}^{j}) \end{cases} \tag{5.30}$$

This define all the converter voltages and currents for positive and negative power flow as shown in Figure 5.10.

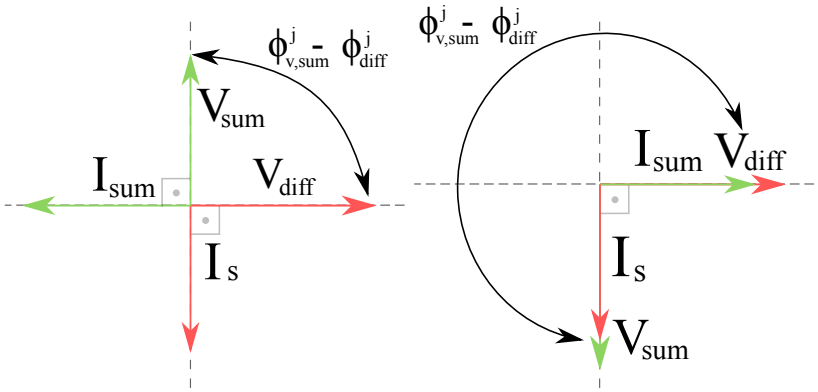

(a) Negative active power (P*<0)

(b) Positive active power (P*>0)

Figure 5.10: Current and voltage angles in terms of active power direction

The reference for I_{sum}^{DC} can be obtained from the following system of equations:

$$\begin{bmatrix} P_t \\ P_{a-b} \\ P_{a-c} \end{bmatrix} = V^{DC1} \begin{bmatrix} 1 & 1 & 1 \\ 1 & -1 & 0 \\ 1 & 0 & -1 \end{bmatrix} \begin{bmatrix} i_{sum}^{a-DC*} \\ i_{sum}^{b-DC*} \\ i_{sum}^{c-DC*} \end{bmatrix} + \left(\frac{V^{DC1}}{2} - V^{DC2} \right) \begin{bmatrix} 1 & 1 & 1 \\ 1 & -1 & 0 \\ 1 & 0 & -1 \end{bmatrix} \begin{bmatrix} i_{s}^{a-DC*} \\ i_{s}^{b-DC*} \\ i_{s}^{c-DC*} \end{bmatrix} \tag{5.31}$$

The current control strategy and design for I_{sum} is the same as Subsection 4.4.4. The PI and the Lead Compensator can be calculated as done in Subsection 4.4.4.

$$K_{sum,DCMMC} = K_{p,sum-DCMMC} + \frac{K_{i,sum-DCMMC}}{s} \tag{5.32}$$

$$\begin{cases} K_{p,sum-DCMMC} = \frac{2L_a}{\tau_{sum}} \\ K_{i,sum-DCMMC} = \frac{2R_a}{\tau_{sum}} \end{cases} \tag{5.33}$$

5.4 Interconnecting different HVDC grids configurations

As presented in Section 2.2, there are different grounding schemes configurations for HVDC grids. This Section will discuss the possibility to interconnect these different schemes with the two proposed DC/DC converters.

5.4.1 Asymmetric Monopole - Asymmetric Monopole

Interconnecting two asymmetric monopole LCC or VSC links with a DC/DC converter is straightforward. The only consideration to take into account is that one pole of the DC/DC converter would be grounded and the other one should be the positive pole of the lines to interconnect. Figure 5.11 shows how the system would look like.

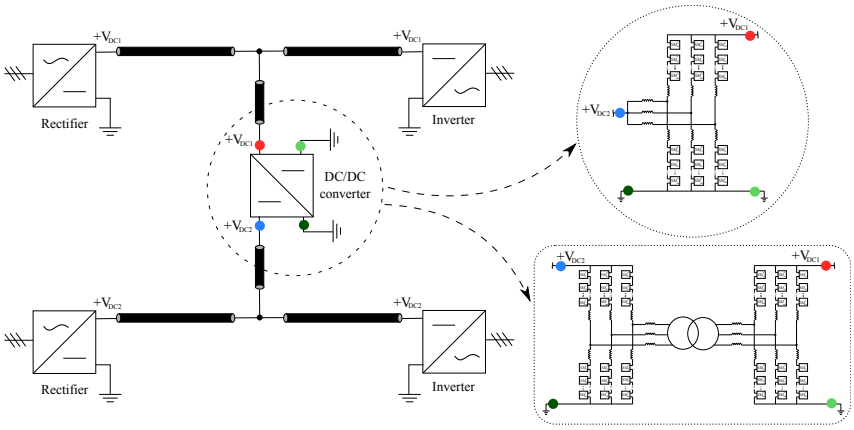

Figure 5.11: Asymmetric Monopole - Asymmetric Monopole interconnection

5.4.2 Symmetric Monopole - Symmetric Monopole

Linking two symmetric monopole systems with the F2F MMC converter does not present any problems and can be achieved without taking any special considerations. Figure 5.12 shows two symmetric monopole point-to-point schemes interconnected with a Front-to-Front converter.

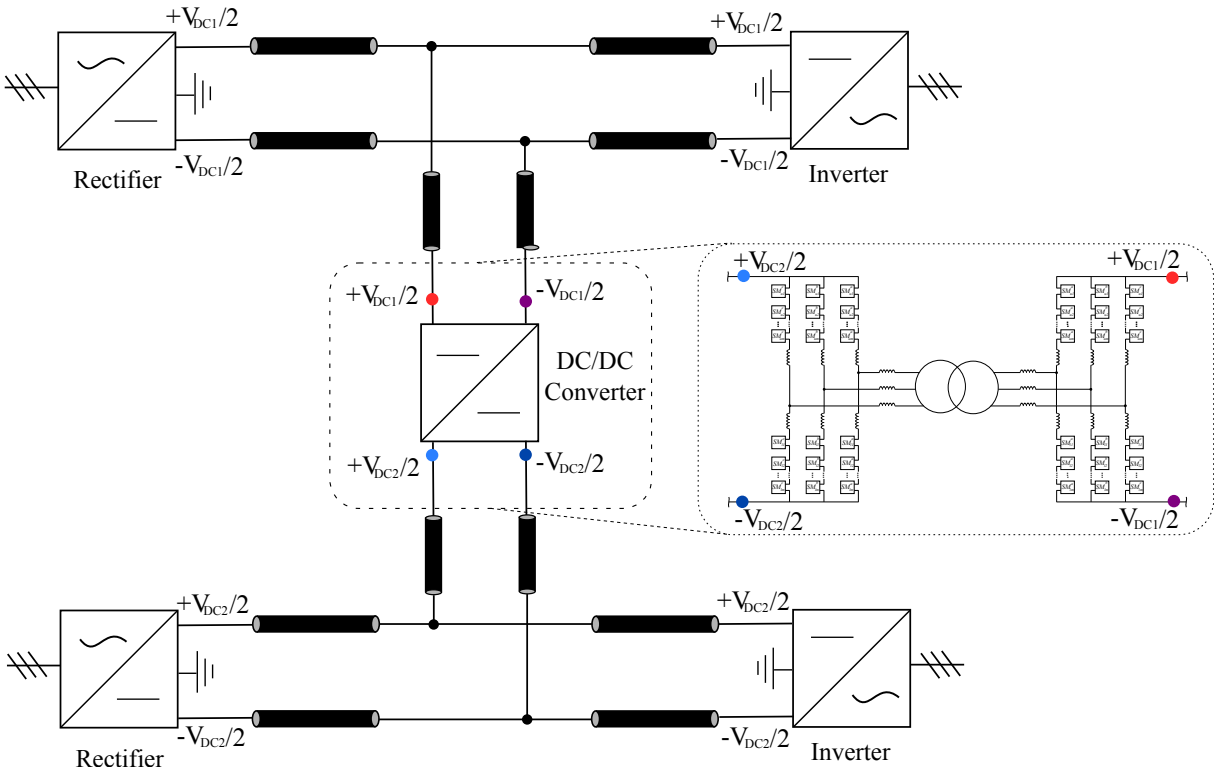

Figure 5.12: Symmetric Monopole - Symmetric Monopole interconnection with a F2F

In the case of the DC-MMC it is not possible to connect this converter between these lines, as one of the poles of the converter will be shared with the two HVDC links and the nominal voltages of such lines could be different. It is important to highlight that when these HVDC links are constructed, these are designed to withstand a specific voltage and if this converter is placed between these lines this voltage would be modified. Is then necessary to present the bipolar configuration of this converter which allows the interconnection of this kind of HVDC links. This is sketched in Figure 5.13. This configuration consists of two DC-MMC connected in series. Both converter can be controlled separately and its control can be the same as the one presented in Section 5.3.2. The only consideration is that converter 2 has negative voltage references. Figure 5.14 shows the converter placed between these point-to-point lines.

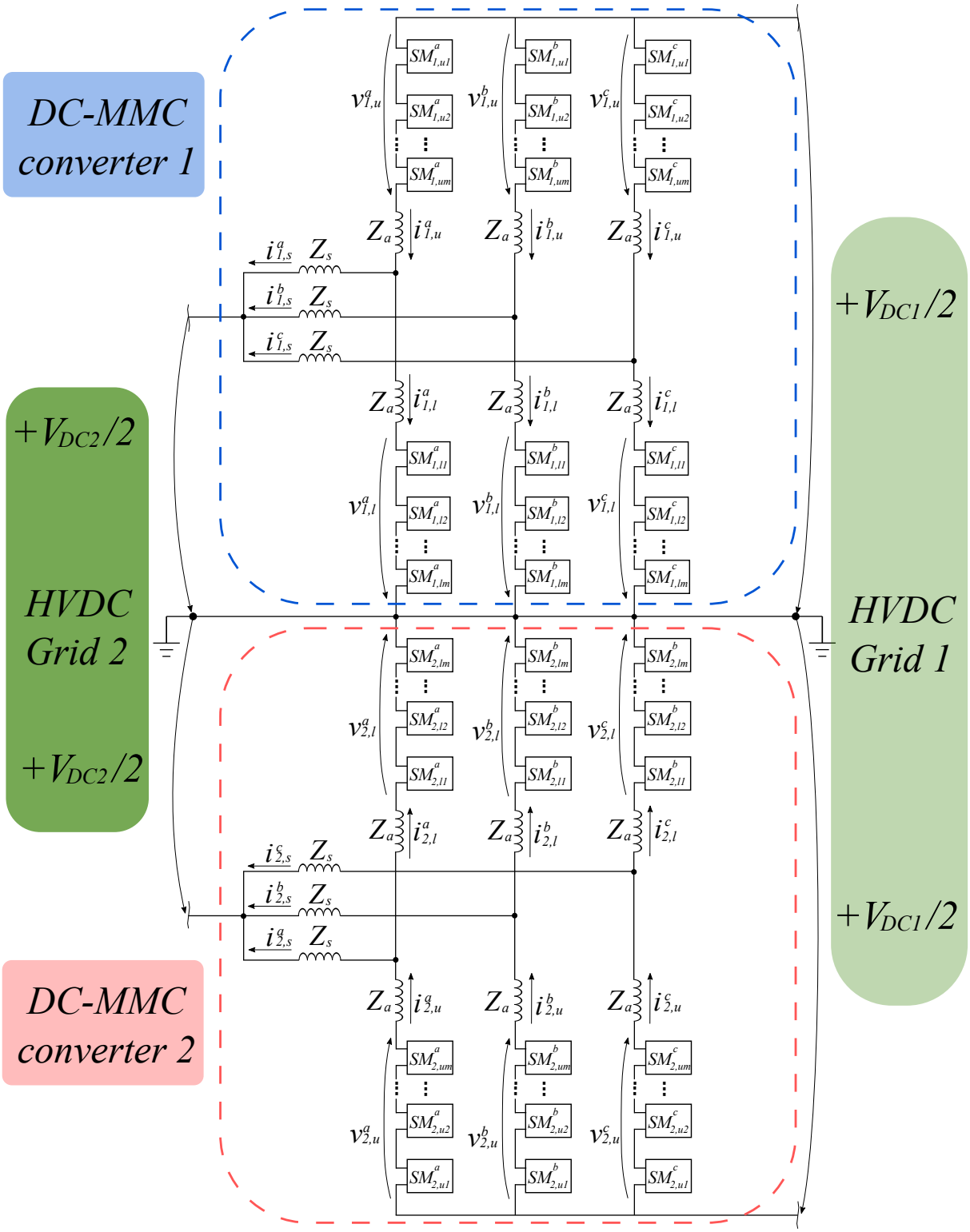

Figure 5.13: DC-MMC bipolar configuration scheme

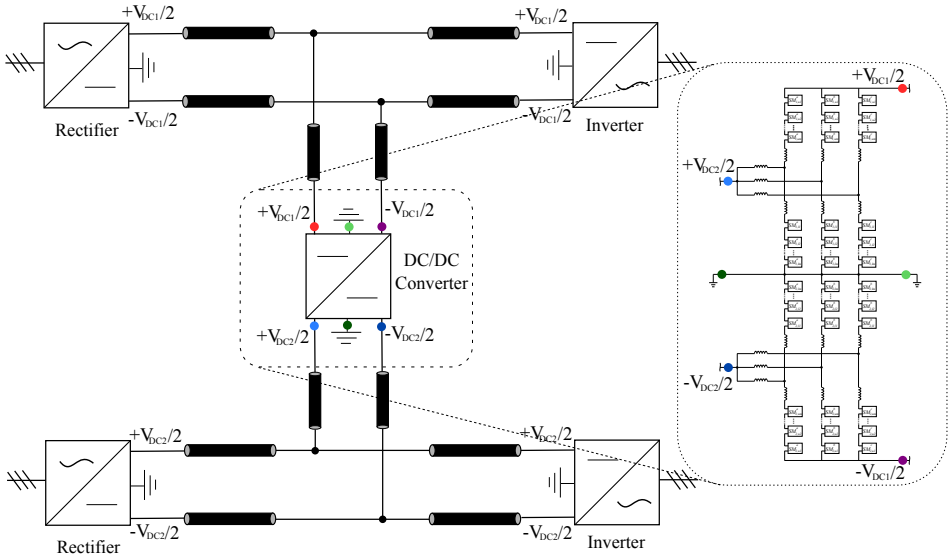

Figure 5.14: Symmetric Monopole - Symmetric Monopole interconnection with a bipolar DC-MMC

5.4.3 Bipolar - Bipolar

Connect two bipolar point-to-point schemes with the F2F MMC converter is done in a similar way than in the previous configuration. For the DC-MMC it is another time necessary to use the bipolar configuration presented in the previous case. Figure 5.15 shows this system with the two different DC/DC converters.

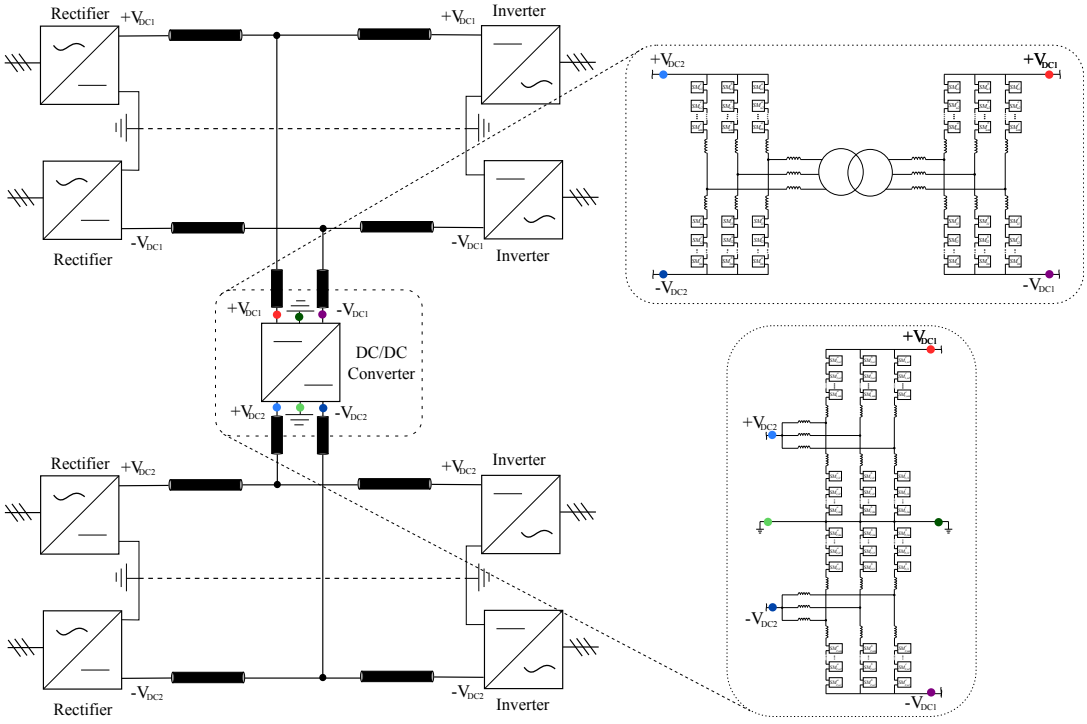

Figure 5.15: Bipolar - Bipolar interconnection

5.4.4 Asymmetric Monopole - Symmetric Monopole

The current case is the first one interconnecting two different grounding schemes. As the F2F converter is isolated it does not present any complication. On the contrary, the DC-MMC converter it is not suitable to be interconnected between these two configurations. The bipolar configuration is another time needed to interconnect these two grounding schemes. Figure 5.16 shows this configuration.

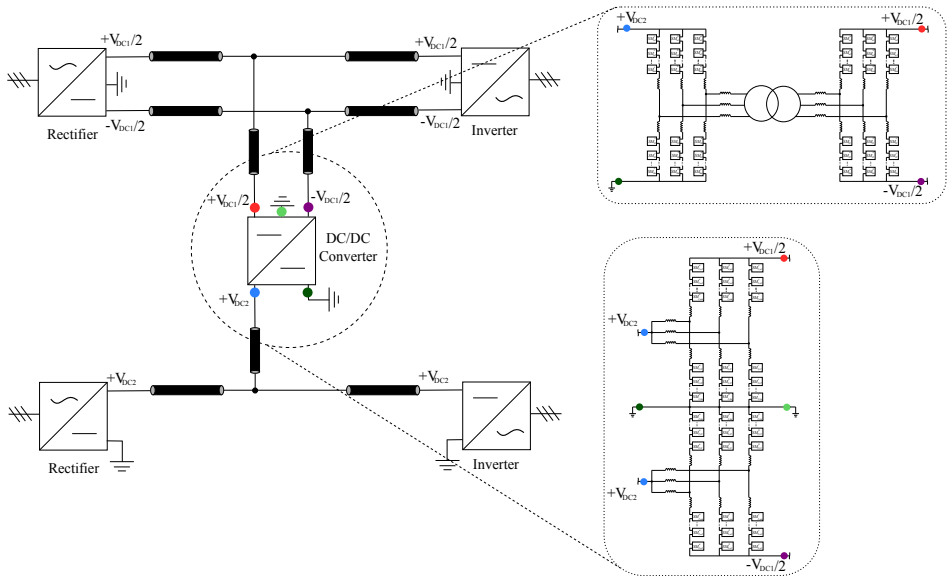

Figure 5.16: Asymmetric Monopole - Symmetric Monopole interconnection

5.4.5 Asymmetric Monopole - Bipolar

The interconnection between these grounding schemes can be solved as it is done in the linking between two symmetric monopole schemes. This scheme is shown in Figure 5.17.

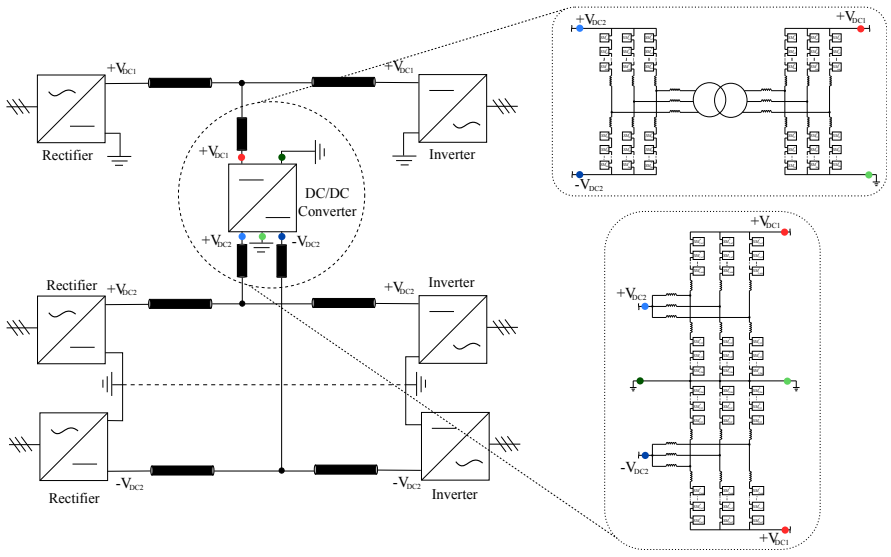

Figure 5.17: Asymmetric Monopole - Bipolar interconnection

5.4.6 Symmetric Monopole - Bipolar

This last case presents the same issues as the interconnection of an asymmetric monopole with a symmetric monopole and the same solutions are possible. This grounding scheme configuration with both DC/DC converters is shown in Figure 5.18.

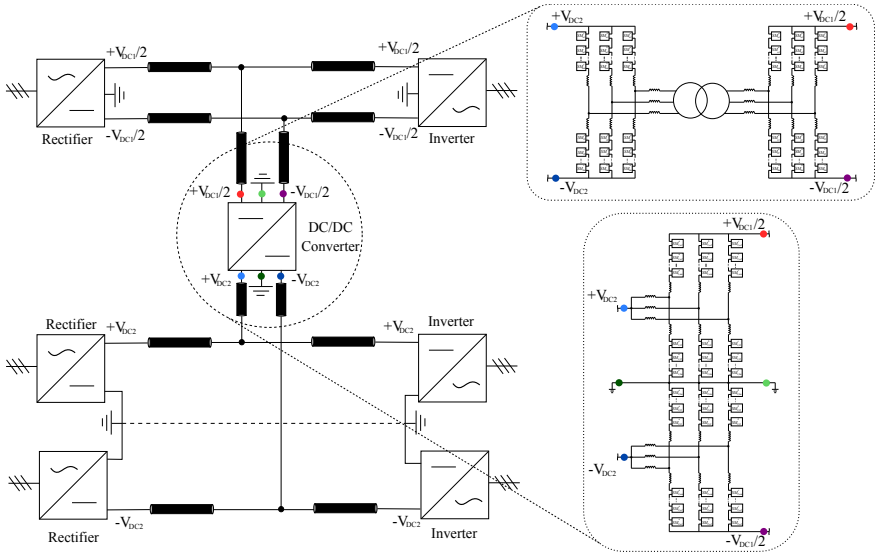

Figure 5.18: Symmetric Monopole - Bipolar interconnection

5.5 Interconnecting different HVDC grids technologies

As presented before, both HVDC technologies presents pros and cons, being probable for the future HVDC grid to include both technologies. It is necessary to study the viability of these systems interconnection.

The main difference between an LCC and a VSC system is its behavior during a power reversal. In a VSC system the DC voltage polarity remains the same and is the current direction that is changed. On the other hand, in an LCC system the current direction remains unchanged and is the voltage polarity that changes [17]. A DC/DC converter interconnecting this different technologies should be able to maintain the DC voltage polarity on one side of the converter, while in the other side, there is a change in the DC voltage polarity [18].

In the case of the F2F converter, the converter should provide full-bridge sub-modules in the LCC side, as is then possible to withstand negative voltages. The VSC side can be left with half-bridge sub-modules.

Similarly to the F2F, the DC-MMC converter also needs full-bridge sub-modules to provide the possibility of power reversal in the LCC link. In this case, these full-bridge sub-modules should be placed in the upper or lower arms, depending on where the LCC link is connected. If the LCC link is placed in the bounds of the upper and lower arms these sub-modules have to be placed in the upper arms. If the LCC link is placed between the phase inductors and the lower arm, the full-bridge sub-modules have to be placed in the lower arms.

Chapter 6

Multi-terminal HVDC grid validation

6.1 Introduction to the case study

The aim of this Section is to validate the proposed models and controls presented in the previous Sections in a multi-terminal HVDC grid. The configuration of this system is a link between the two point-to-point schemes presented in Section 3.5 and 4.5. Both DC/DC converters studied in this thesis, the Front-to-Front MMC converter and the DC-MMC converter, are placed connecting these two HVDC systems in the middle of each line. Figure 6.1 shows the studied system and Table 6.1 present its main parameters.

The grid is composed by 5 converters where each one can have different roles. As presented during this Thesis, these converters can control the power flow or the DC voltage in the DC grid. In the case of the AC/DC MMC converter it can also control the reactive power flowing to the AC grid. Is then possible to propose 8 different scenarios, 4 for each DC/DC converter. These are listed bellow:

- Case 1. DC/DC converter controlling power flow in the LCC link: In this scenario, one LCC converter is controlling power, and the other one is regulating the DC voltage. In the VSC link one MMC converter is controlling active and reactive power flow, and the second one is controlling the DC voltage and the reactive power.

- Case 2. DC/DC converter controlling the DC voltage in the LCC link: In this case as the DC converter is controlling the DC voltage in the LLC link, both LCC converters are controlling the power flow. The VSC link presents the same control strategy as Case 1.

- Case 3. DC/DC converter controlling power flow in the VSC link: This is the same situation as Case 1, but with the DC converter controlling power in the VSC side. The control strategy for the LCC and VSC links are the same as Case 1.

- Case 4. DC/DC converter controlling the DC voltage in the VSC link: In this last configuration, both VSC converters are controlling the active and reactive power flow. For the LCC link the control strategy is the same as Case 1.

These different case studies are reflected in Table 6.2. There are more possible configurations such as voltage-power droop control, but this will not be studied in this Thesis.

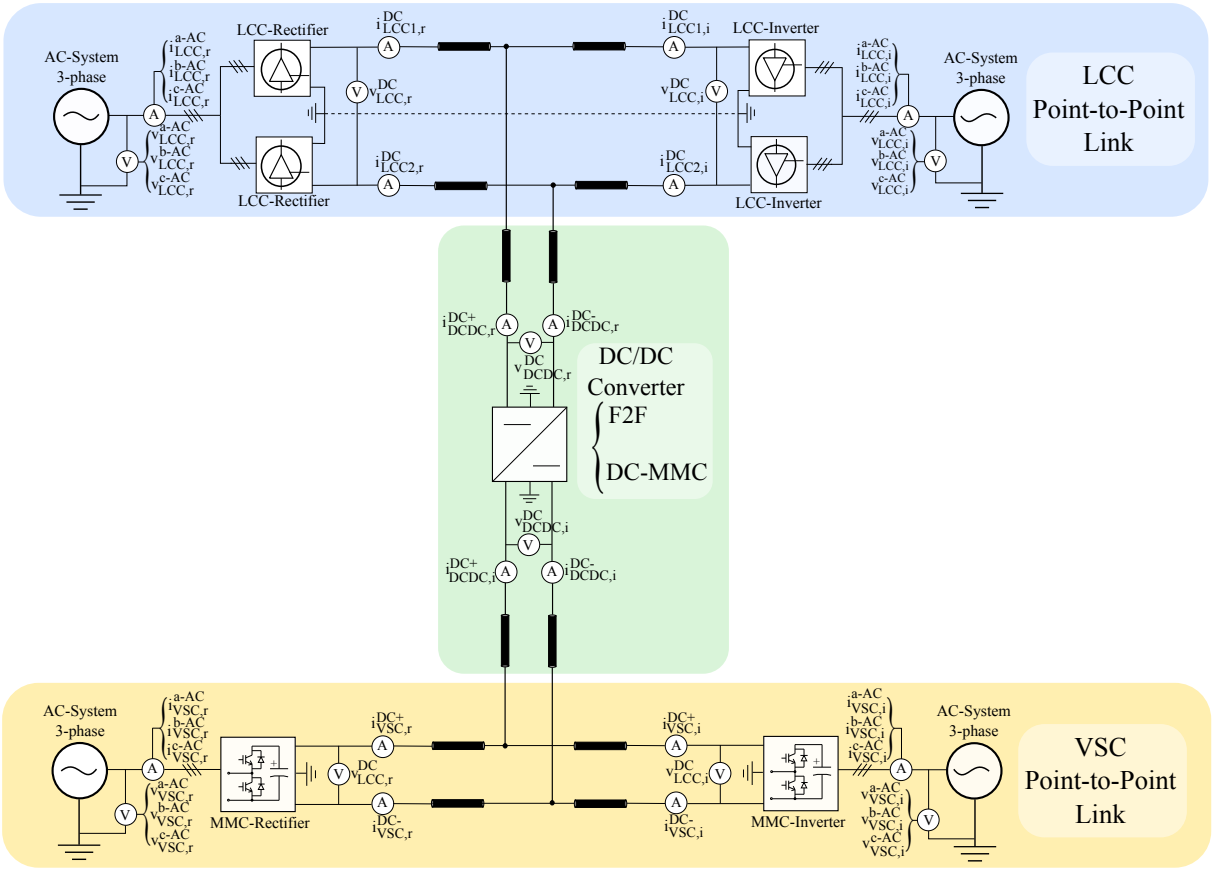

Figure 6.1: Multiterminal HVDC grid scenario

Table 6.1: System parameters for the case study

Magnitudes	Symbol	Value	Units
AC frequency	f_{AC}	50	Hz
LCC-AC Grid Voltage (Line to Line)	V_{LCC}^{AC}	220	kV
VSC-AC Grid Voltage (Line to Line)	V_{VSC}^{AC}	400	kV
LCC-DC Grid voltage	V_{LCC}^{DC}	500	kV
VSC-DC Grid voltage	V_{VSC}^{DC}	400	kV
DC cable capacitance	C_{DC}	0.1908	$\frac{\mu C}{km}$
DC cable inductance	L_{DC}	2.112	$\frac{mH}{km}$
DC cable resistance	R_{DC}	9.5	$\frac{m\Omega}{km}$
LCC line length	d_{LCC}	100	km
VSC line length	d_{VSC}	300	km
DC/DC converter line length	d_{DCDC}	150	km

Table 6.2: Case studies summary

	Converter	Control Mode	Point-to-Point Line
Case 1	LCC-rectifer	P	LCC
	LCC-inverter	V_{DC}	LCC
	VSC-rectifier	P	VSC
	VSC-inverter	V_{DC}	VSC
	DC/DC	P	LCC
Case 2	LCC-rectifer	P	LCC
	LCC-inverter	P	LCC
	VSC-rectifier	P	VSC
	VSC-inverter	V_{DC}	VSC
	DC/DC	V_{DC}	LCC
Case 3	LCC-rectifer	P	LCC
	LCC-inverter	V_{DC}	LCC
	VSC-rectifier	P	VSC
	VSC-inverter	V_{DC}	VSC
	DC/DC	P	VSC
Case 4	LCC-rectifer	P	LCC
	LCC-inverter	V_{DC}	LCC
	VSC-rectifier	P	VSC
	VSC-inverter	P	VSC
	DC/DC	V_{DC}	VSC

6.2 Multiterminal HVDC Front-to-Front MMC converter simulation results

Simulations of the proposed system presented in Figure 6.1 linked with the F2F converter have been carried out in the four different cases previously presented. In each case, the different DC and AC voltages and currents are studied during transient responses on a change in the different possible power set points.

All the results are shown in Appendix C. In the following Subsections only the more relevant results are presented.

6.2.1 Case 1

In the VSC link the power reference is changed following a step in time 2 seconds injecting 300 MW to the AC grid, as is reflected in Figure 6.4b. The voltage of this link is kept constant by the inverter as can be seen in Figure 6.3b. Figures 6.2a, 6.2b and 6.3a show how this change in the VSC link is not reflected in the LCC point-to-point link as the F2F converter acts as a barrier to the changes in the VSC link. The AC current in the VSC line is also changed in the rectifier and inverter side as the power injected by the rectifier comes from the inverter side of the VSC link as can be seen in Figures 6.5a and 6.5b.

At time 3 seconds the F2F converter starts to inject power to the LCC link as showed in Figures 6.4c and 6.4a. This power is absorbed by the inverter LCC converter as the rectifier is controlling the DC power in its side. This change in the F2F power reference is also reflected in the VSC link as this power is injected by the LCC inverter as seen in Figure 6.4b.

A power reference set point change is also simulated in the LCC link in second 4 this produces a change in the DC current of this link as reflected in Figures 6.2a and 6.2b. The voltage is regulated after a transient by the LCC inverter, Figure 6.3a.

The energies of the MMC are kept constant during all this different operations as can be seen in Figures 6.6a, 6.6b for the rectifier and Figures 6.7a, 6.7b for the inverter. The F2F energies are also kept constant by the control as is shown in Figures 6.8c, 6.8d, 6.8a and 6.8b.

A summary of the different operations carried out in this case is shown in Table 6.3

Table 6.3: Operations summary F2F Case 1

Converter	Time [s]	Operation
VSC_r	2	Injects 300 MW to the AC grid
F2F	3	Injects 300 MW to the LCC link
LCC_r	4	Power reference set point change from 400 MW to 500 MW
VSC_r	5	Injects 200 MVar to the AC grid

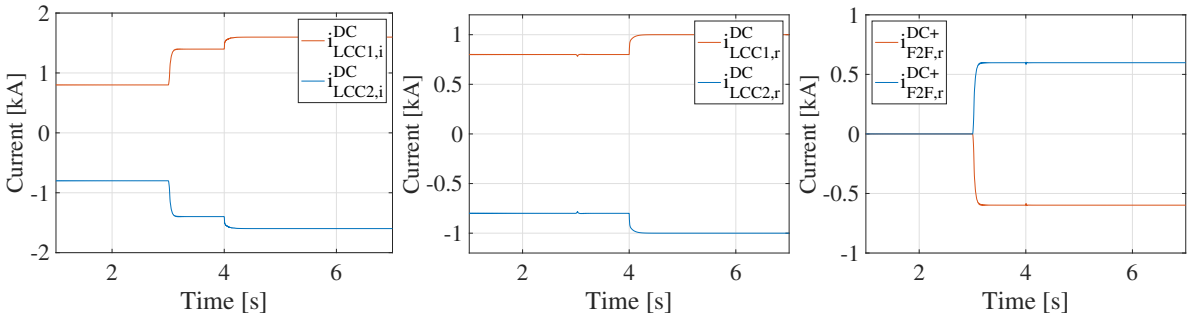

(a) DC current in the inverter side

(b) DC current in the LCC rectifier side

(c) DC current in the DC-MMC converter rectifier side

Figure 6.2: DC current in the LCC link

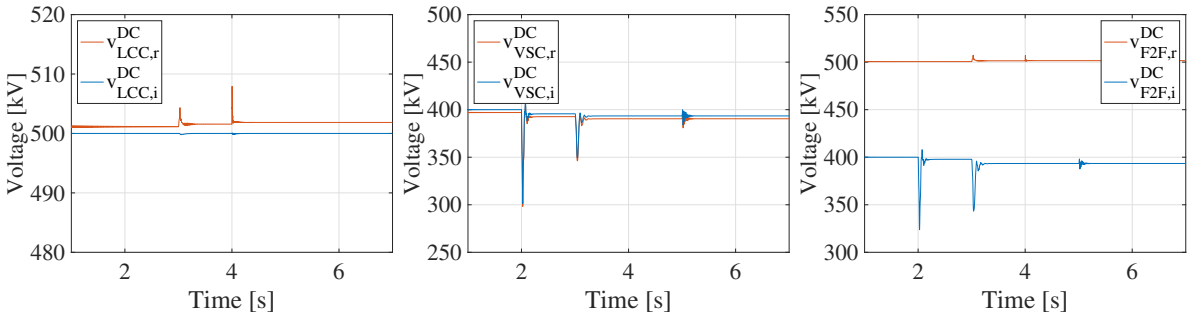

(a) DC voltages in the LCC link

(b) DC voltages in the VSC link

(c) DC voltages in the DC-MMC converter sides

Figure 6.3: DC voltages in the multiterminal HVDC grid

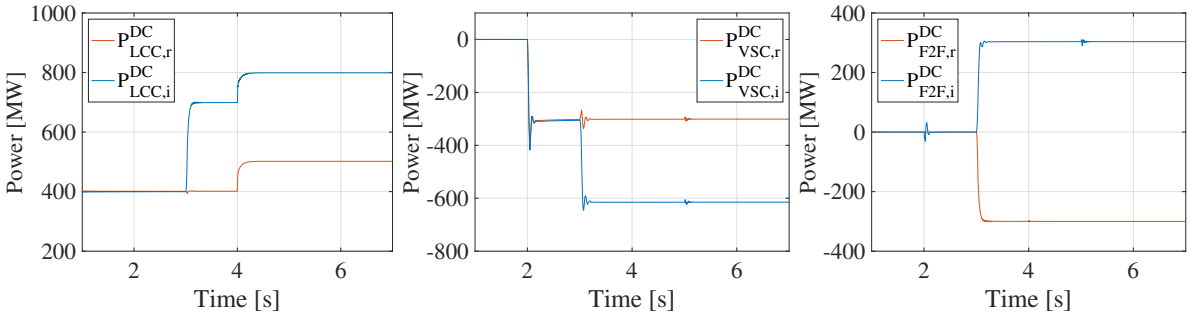

(a) DC power in the LCC link

(b) DC power in the VSC link

(c) DC power in the F2F converter sides

Figure 6.4: DC power flow in the multiterminal HVDC grid

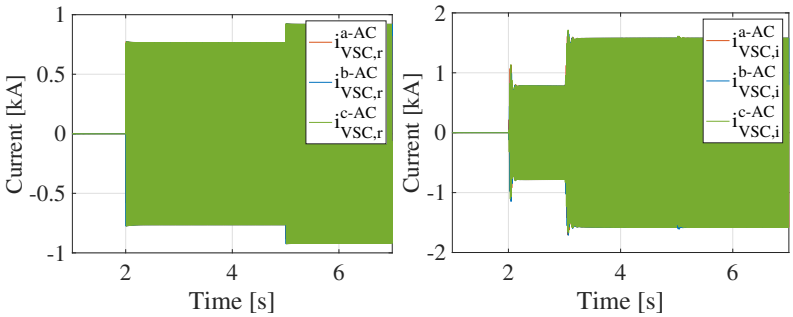

(a) AC current in the VSC rectifier

(b) AC current in the VSC inverter

Figure 6.5: AC currents in the VSC link

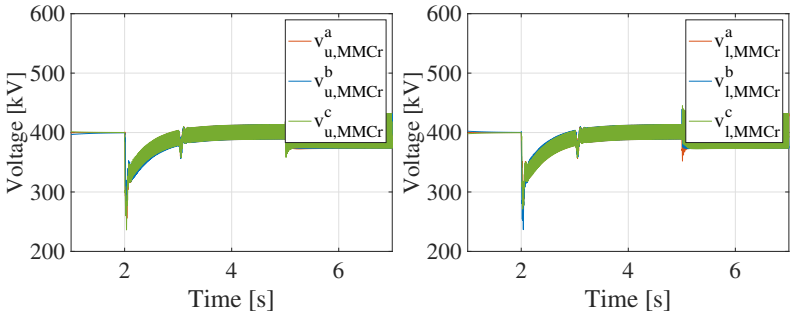

(a) MMC upper arms rectifier energies

(b) MMC lower arms rectifier energies

Figure 6.6: MMC rectifier energies

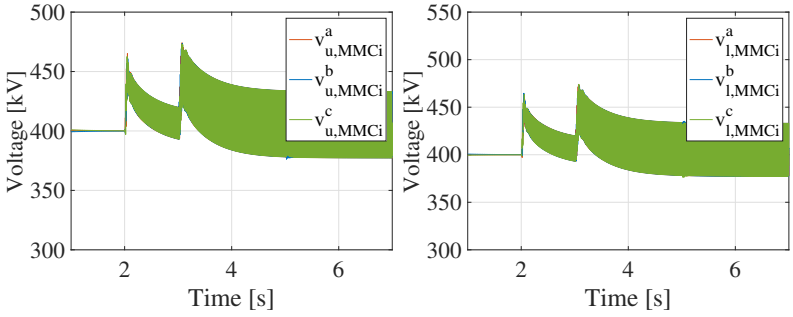

(a) MMC upper arms inverter energies

(b) MMC lower arms inverter energies

Figure 6.7: MMC inverter energies

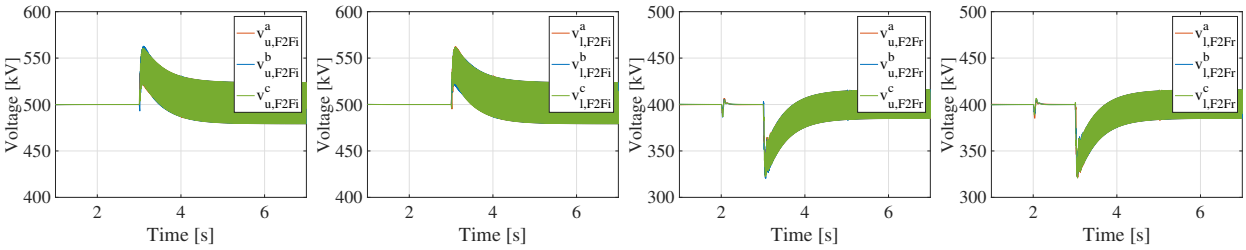

(a) MMC upper arms F2F inverter energies

(b) MMC lower arms F2F inverter energies

(c) MMC upper arms F2F rectifier energies

(d) MMC lower arms F2F rectifier energies

Figure 6.8: MMC Front-to-Front energies

6.2.2 Case 2

In the VSC link the power reference is changed following a step in time 4 seconds injecting 300 MW to the AC grid, as is reflected in Figure 6.11b. The voltage of this link is kept constant by the inverter as can be seen in Figure 6.10b. Figures 6.9a, 6.2b and 6.10a shows how this change in the VSC link is not reflected in the LCC point-to-point link similarly to the previous case. The AC current in the VSC line is also changed in the rectifier and inverter side as the power injected by the rectifier comes from the inverter side of the VSC link as can be seen in Figures 6.14a and 6.14b.

At time 6 seconds both LCC converters change its current reference. The rectifier starts to inject 500 MW to the HVDC grid, while the inverter changes from injecting 400 MW to the AC line to inject 200 MW. This modification effects the VSC line as the MMC inverter extracts less power from the grid. This variation in the whole grid is reflected in Figures 6.11a, 6.11b, 6.12b, 6.12a, 6.13b and 6.13a.

Finally, at time 9 seconds the MMC rectifier injects reactive power the the AC grid as shown in Figure 6.13a. This change becomes into a small perturbation in the VSC line.

The energies of the MMC are kept constant during all this different operations as can be seen in Figures 6.15a, 6.15b for the rectifier and Figures 6.16a, 6.16b for the inverter.

The F2F energies are also kept constant by the control as is shown in Figures 6.17c, 6.17d, 6.17a and 6.17b.

A summary of the different operations carried out in this case is shown in Table 6.4

Table 6.4: Operations summary F2F Case 2

Converter	Time [s]	Operation
VSC_r	4	Injects 300 MW to the AC grid
LCC_r	6	Power reference set point change from 400 MW to 500 MW
LCC_i	6	Power reference set point change from 400 MW to 200 MW
VSC_r	9	Injects 200 MVar to the AC grid

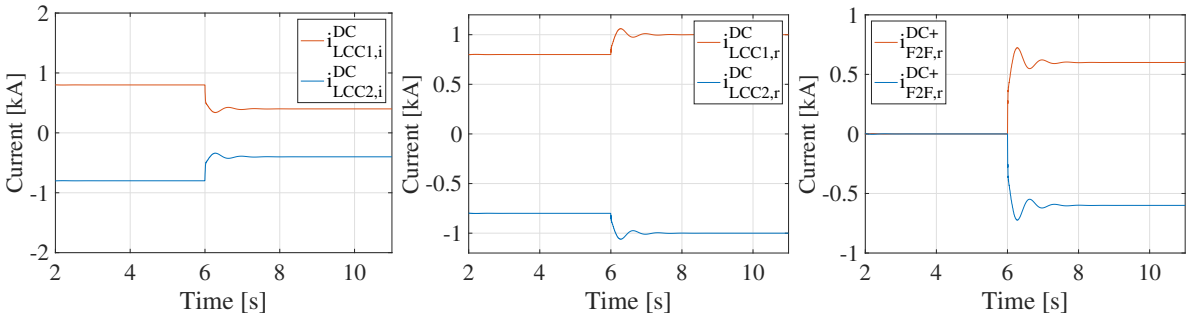

(a) DC current in the inverter side

(b) DC current in the LCC rectifier side

(c) DC current in the DC-MMC converter rectifier side

Figure 6.9: DC current in the LCC link

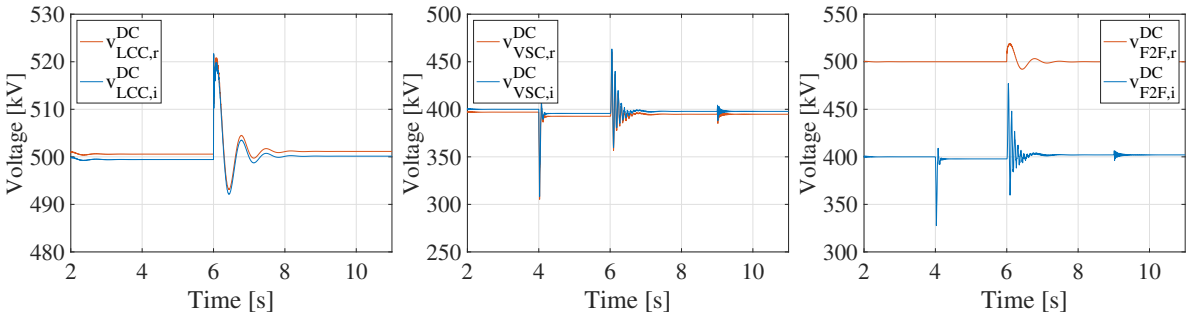

(a) DC voltages in the LCC link

(b) DC voltages in the VSC link

(c) DC voltages in the DC-MMC converter sides

Figure 6.10: DC voltages in the multiterminal HVDC grid

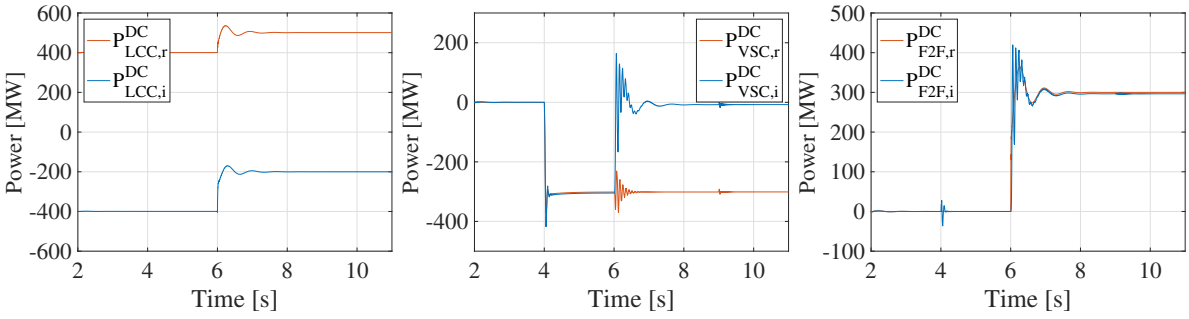

(a) DC power in the LCC link

(b) DC power in the VSC link

(c) DC power in the F2F converter sides

Figure 6.11: DC power flow in the multiterminal HVDC grid

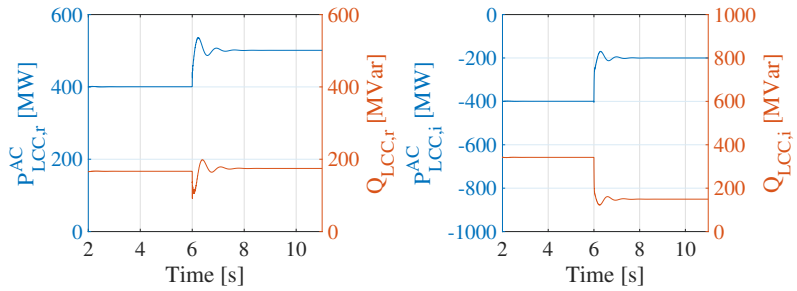

(a) Active and reactive power in the LCC rectifier

(b) AC and reactive power in the LCC inverter

Figure 6.12: Active and reactive power flowing to the HVAC LCC link

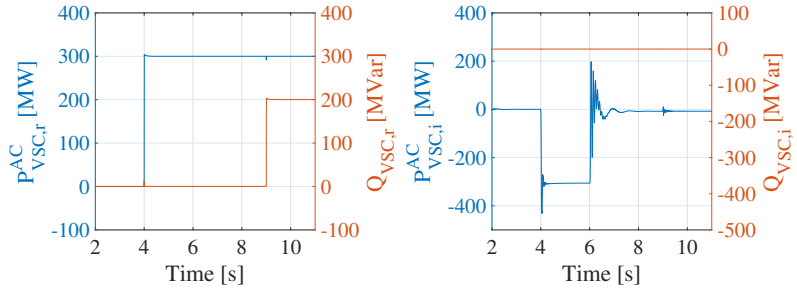

(a) Active and reactive power in the VSC rectifier

(b) AC and reactive power in the VSC inverter

Figure 6.13: Active and reactive power flowing to the HVAC VSC link

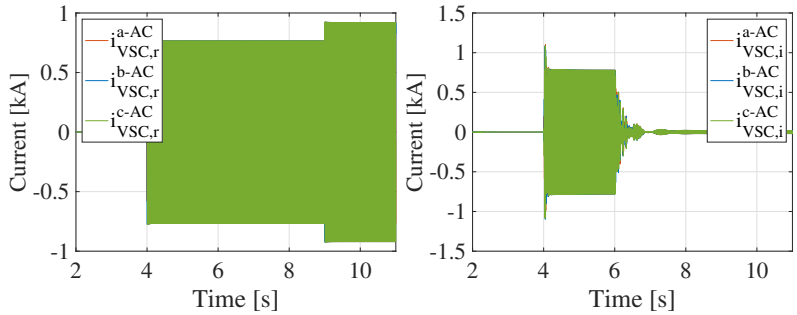

(a) AC current in the VSC rectifier

(b) AC current in the VSC inverter

Figure 6.14: AC currents in the VSC link

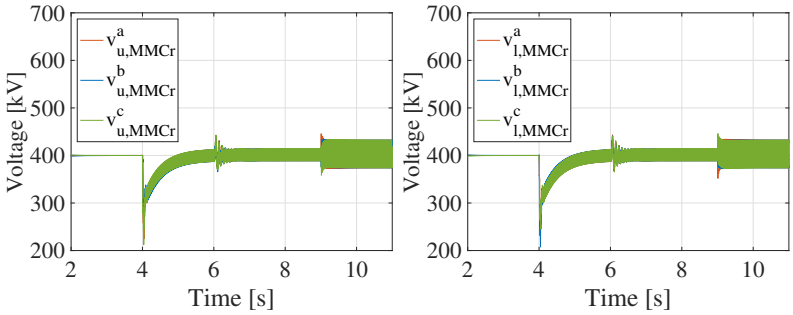

(a) MMC upper arms rectifier energies

(b) MMC lower arms rectifier energies

Figure 6.15: MMC rectifier energies

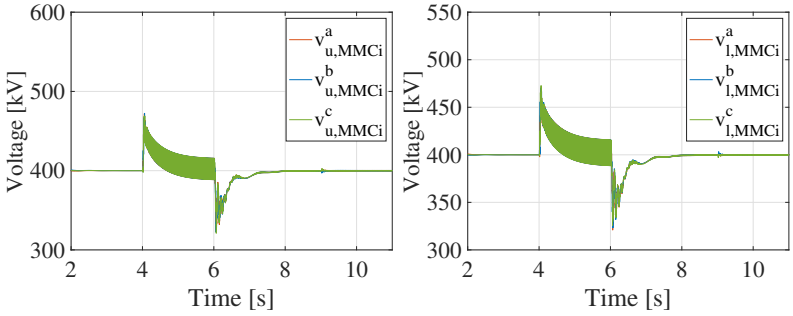

(a) MMC upper arms inverter energies

(b) MMC lower arms inverter energies

Figure 6.16: MMC inverter energies

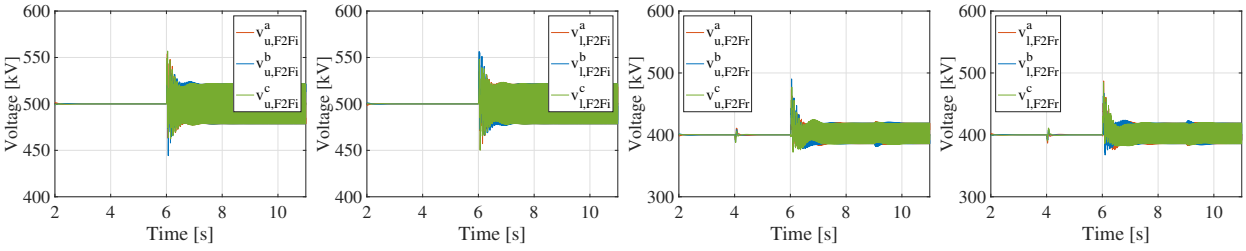

(a) MMC upper arms F2F inverter energies

(b) MMC lower arms F2F inverter energies

(c) MMC upper arms F2F rectifier energies

(d) MMC lower arms F2F rectifier energies

Figure 6.17: MMC Front-to-Front energies

6.2.3 Case 3

In the VSC link the power reference is changed following a step in time 2 seconds injecting 300 MW to the AC grid, as is reflected in Figure 6.18b. The AC current in the VSC line is also changed in the rectifier and inverter side as the power injected by the rectifier comes from the inverter side of the VSC link as can be seen in Figures 6.21a and 6.21b. The F2F converter is

regulating the power flowing to the VSC link and it has its reference to zero so all this power flows to the VSC inverter.

At time 3 seconds the F2F converter starts to inject 300 MW to the VSC link. As a consequence the LCC inverter absorbs less power varying it from 400 MW to 100 MW. Finally this power flows to the VSC rectifier, letting the inverter without power consumption. The DC power flow is shown in Figures 6.18a, 6.18b and 6.18c.

Finally, at time 5 seconds the MMC rectifier injects reactive power to the AC grid as shown in Figure 6.20a. This change becomes into a small perturbation in the VSC line, as can be seen in numerous figures such as Figure 6.10b.

The energies of the MMC are kept constant during all this different operations as can be seen in Figures 6.22a, 6.22b for the rectifier and Figures 6.23a, 6.23b for the inverter. The F2F energies are also kept constant by the control as is shown in Figures 6.24c, 6.24d, 6.24a and 6.24b.

A summary of the different operations carried out in this case is shown in Table 6.5

Table 6.5: Operations summary F2F Case 3

Converter	Time	Operation
VSC_r	2	Injects 300 MW to the AC grid
F2F	3	Injects 300 MW to the VSC line
LCC_r	4	Power reference set point change from 400 MW to 500MW
VSC_r	5	Injects 200 MVar to the AC grid

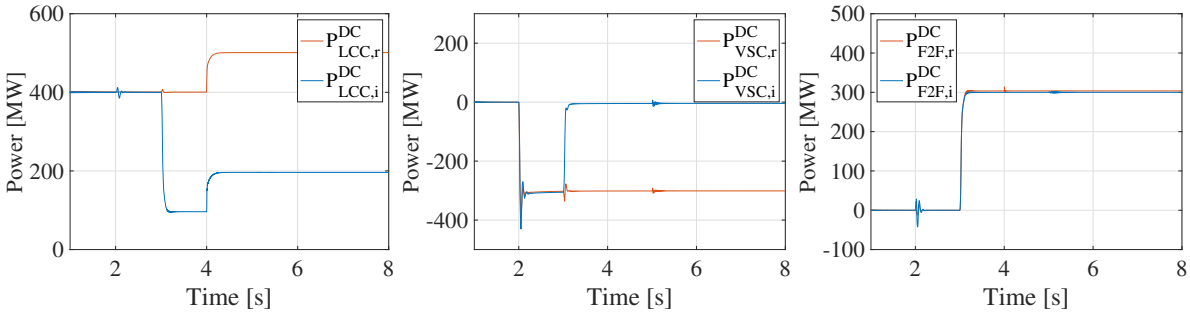

(a) DC power in the LCC link

(b) DC power in the VSC link

(c) DC power in the F2F converter sides

Figure 6.18: DC power flow in the multiterminal HVDC grid

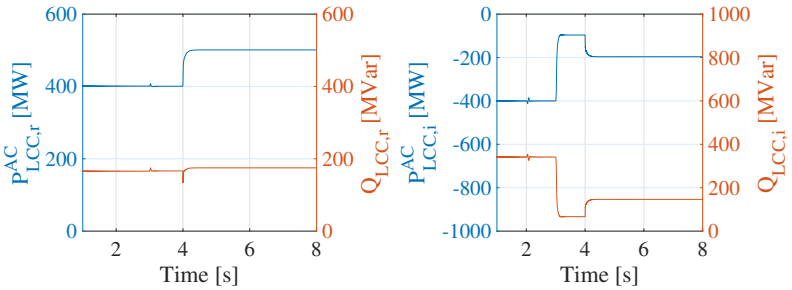

(a) Active and reactive power in the LCC rectifier

(b) AC and reactive power in the LCC inverter

Figure 6.19: Active and reactive power flowing to the HVAC LCC link

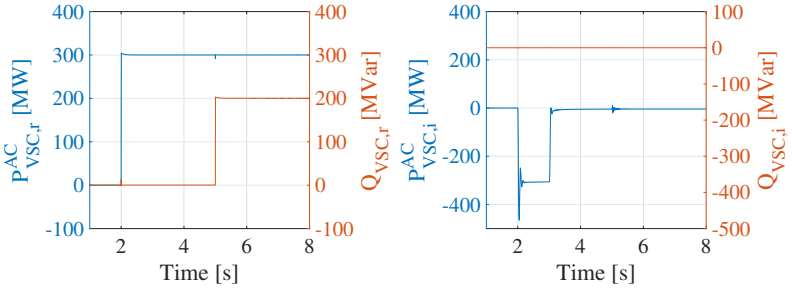

(a) Active and reactive power in the VSC rectifier

(b) AC and reactive power in the VSC inverter

Figure 6.20: Active and reactive power flowing to the HVAC VSC link

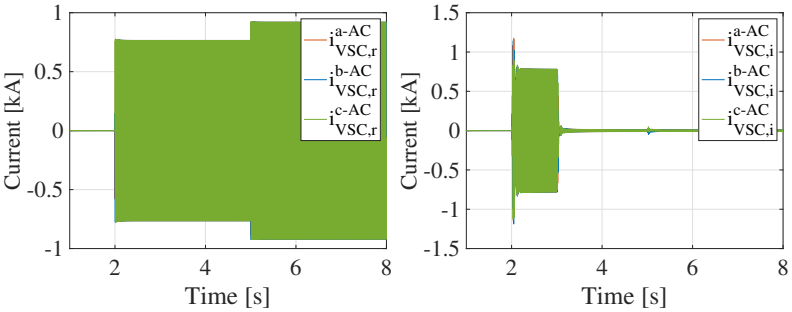

(a) AC current in the VSC rectifier

(b) AC current in the VSC inverter

Figure 6.21: AC currents in the VSC link

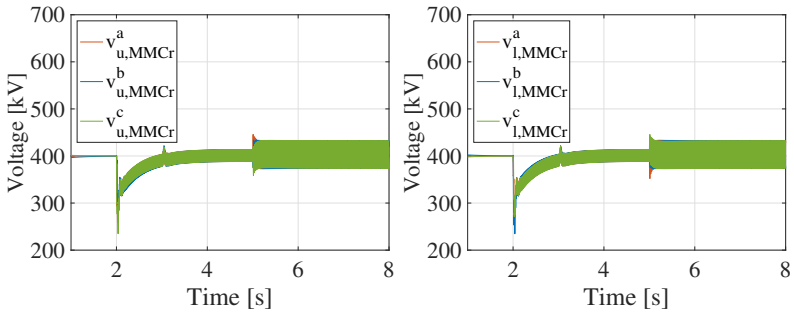

(a) MMC upper arms rectifier energies

(b) MMC lower arms rectifier energies

Figure 6.22: MMC rectifier energies

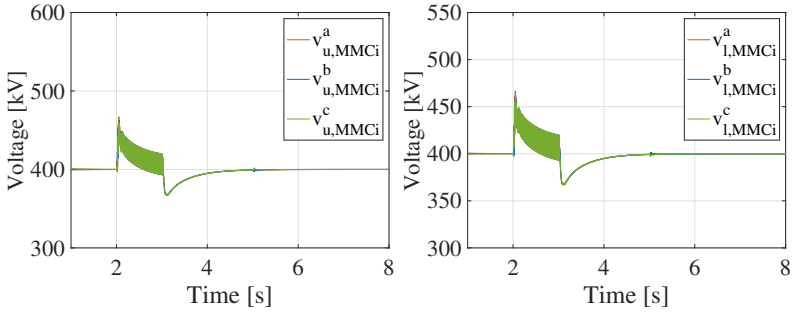

(a) MMC upper arms inverter energies

(b) MMC lower arms inverter energies

Figure 6.23: MMC inverter energies

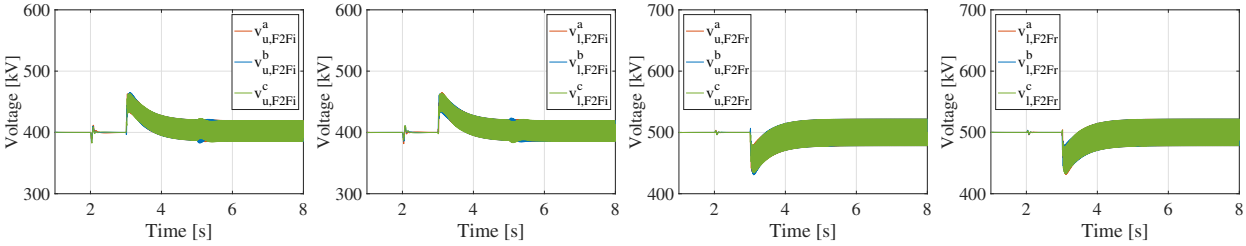

(a) MMC upper arms F2F inverter energies

(b) MMC lower arms F2F inverter energies

(c) MMC upper arms F2F rectifier energies

(d) MMC lower arms F2F rectifier energies

Figure 6.24: MMC Front-to-Front energies

6.2.4 Case 4

In the LCC link the power reference is changed following a step in time 4 seconds injecting 500 MW to the HVDC grid, as is reflected in Figure 6.26a. The voltage of this link is kept constant by the inverter as can be seen in Figure 6.25a. This power is all absorbed by the LCC inverter because both VSC converters are controlling the power and have its references fixed to zero, as shown in Figures 6.28a, 6.28b and 6.26b.

At time 5 seconds the MMC inverter injects 200 MVar to the AC grid as shown in Figure 6.28b. At time 6 seconds the VSC rectifier injects 300 MW to the AC grid. This change the power

absorbed by the LCC inverter as shown in Figure 6.27b. Finally, at time 10 seconds the MMC inverter injects active power the the AC grid as shown in Figure 6.28b.

The energies of the MMC are kept constant during all this different operations as can be seen in Figures 6.29a, 6.29b for the rectifier and Figures 6.30a, 6.30b for the inverter. The F2F energies are also kept constant by the control as is shown in Figures 6.31c, 6.31d, 6.31a and 6.31b.

A summary of the different operations carried out in this case is shown in Table 6.6

Table 6.6: Operations summary F2F Case 4

Converter	Time [s]	Operation
LCC_r	4	Power reference set point change from 400 MW to 500 MW
VSC_i	5	Injects 200 MVar to the AC grid
VSC_r	6	Injects 300 MW to the AC grid
VSC_r	8	Injects 200 Mvar to the AC grid
VSC_i	10	Injetcs 100 MW to the AC grid

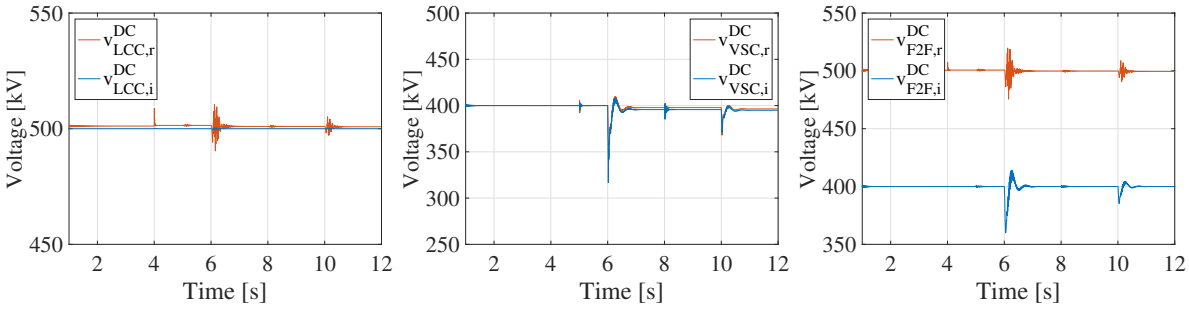

(a) DC voltages in the LCC link

(b) DC voltages in the VSC link

(c) DC voltages in the DC-MMC converter sides

Figure 6.25: DC voltages in the multiterminal HVDC grid

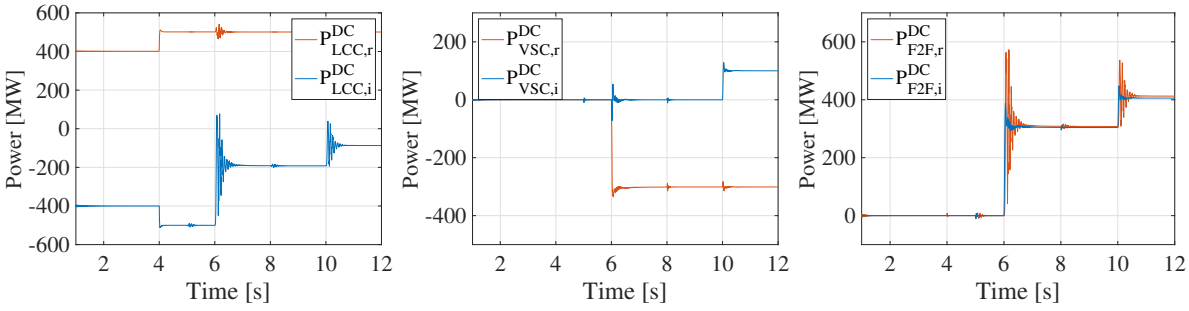

(a) DC power in the LCC link

(b) DC power in the VSC link

(c) DC power in the F2F converter sides

Figure 6.26: DC power flow in the multiterminal HVDC grid

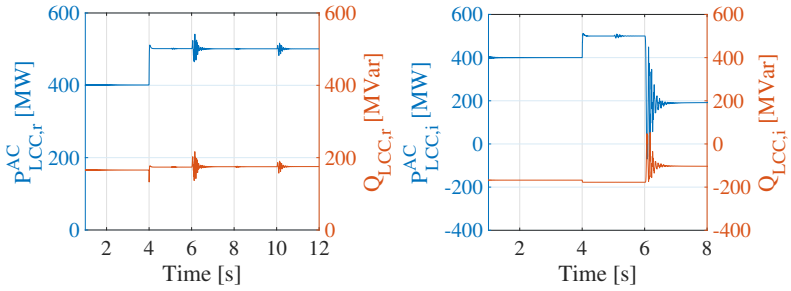

(a) Active and reactive power in the LCC rectifier

(b) AC and reactive power in the LCC inverter

Figure 6.27: Active and reactive power flowing to the HVAC LCC link

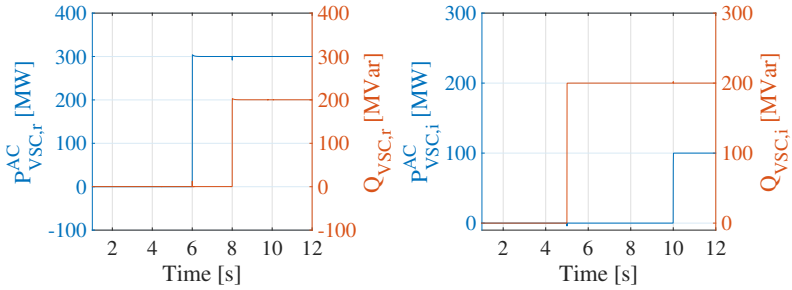

(a) Active and reactive power in the VSC rectifier

(b) AC and reactive power in the VSC inverter

Figure 6.28: Active and reactive power flowing to the HVAC VSC link

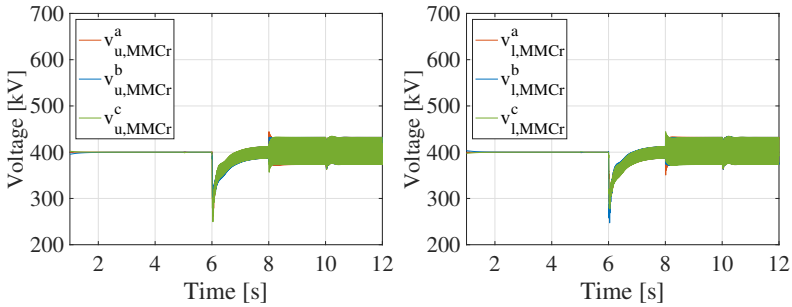

(a) MMC upper arms rectifier energies

(b) MMC lower arms rectifier energies

Figure 6.29: MMC rectifier energies

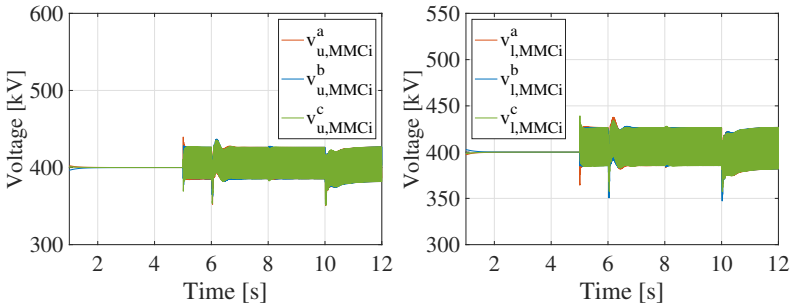

(a) MMC upper arms inverter energies

(b) MMC lower arms inverter energies

Figure 6.30: MMC inverter energies

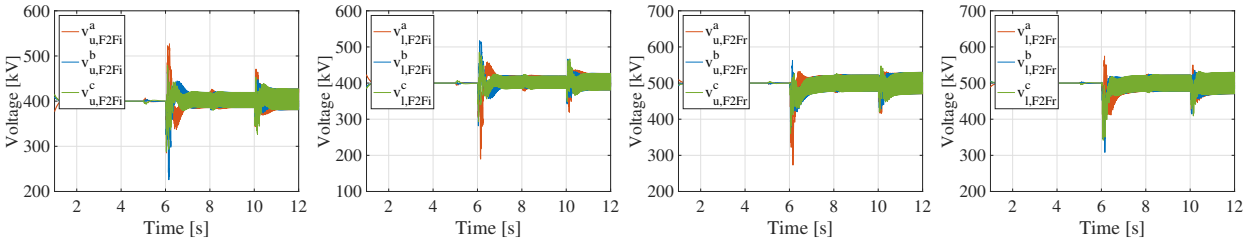

(a) MMC upper arms F2F inverter energies

(b) MMC lower arms F2F inverter energies

(c) MMC upper arms F2F rectifier energies

(d) MMC lower arms F2F rectifier energies

Figure 6.31: MMC Front-to-Front energies

6.3 Multiterminal HVDC DC-MMC converter simulation results

As it is done previously with the F2F converter different simulations of the proposed system presented in Figure 6.1 linked with the DC-MMC converter have been carried out in the four different cases presented in the Introduction of this Chapter 6.1. In each case, the different DC and AC voltages and currents are studied during transient responses on a change in the different possible power set points.

All the results are shown in Appendix C. In the following Subsections only the more relevant results are presented.

6.3.1 Case 1

In the LCC link the power reference is changed following a step in time 5 seconds as reflected in Figure 6.34a. The voltage of this link is kept constant by the voltage regulation of the rectifier as can be seen in Figure 6.33a. This change in the DC power reference causes a change in the active and reactive power consumed by the LCC inverter and rectifier as is shown in Figures 6.35a and 6.35b, this change is also reflected in the firing angle of both converters Figure C.64.

A power reference set point change is also simulated in the VSC link in second 7 this produces a change in the DC current of this links as reflected in Figures 6.32b and 6.32a. The voltage is regulated after a transient by the MMC inverter, Figure 6.33b. In second 11 the MMC rectifier

injects 200 MVar to the AC grid as can be seen in Figure 6.36a. The energies of the MMC are kept constant during all this different operations as can be seen in Figures 6.38a,6.38b for the rectifier and Figures 6.39a, 6.39b for the inverter.

The DC-MMC converter change its power reference in second 9 as can be seen in Figure 6.34c injecting 300 MW to the LCC link. Its energies are kept constant by the control as is shown in Figure 6.40a, 6.40b, 6.40c and 6.40d. This power is absorbed by the LCC rectifier as can be seen in Figure 6.35b. The DC voltages in the DC-MMC sides are regulated by the LCC inverter and MMC inverter as can be seen in Figure 6.33c

A summary of the different operations carried out in this case is shown in Table 6.7

Table 6.7: Operations summary DC-MMC Case 1

Converter	Time [s]	Operation
LCC_r	5	Power reference set point change from 400 MW to 500 MW
VSC_r	7	Injects 300 MW to the AC grid
DC-MMC	9	Injects 300 MW to the LCC link
VSC_r	11	Injects 200 Mvar to the AC grid

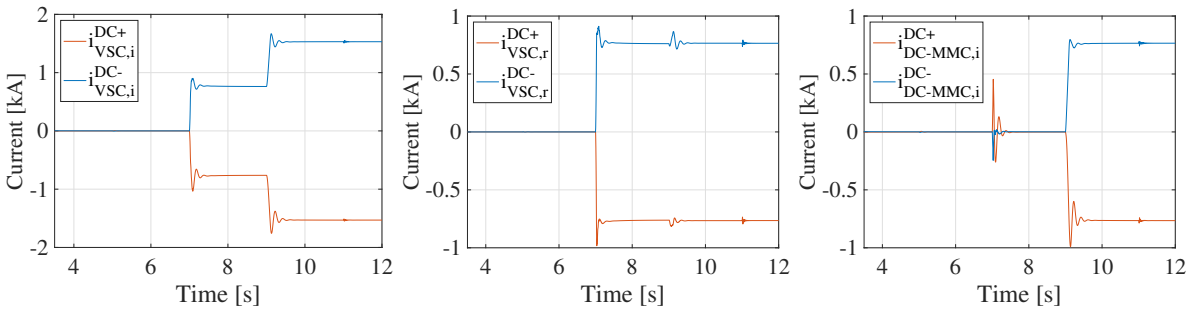

(a) DC current in the inverter side

(b) DC current in the LCC rectifier side

(c) DC current in the DC-MMC converter inverter side

Figure 6.32: DC current in the VSC link

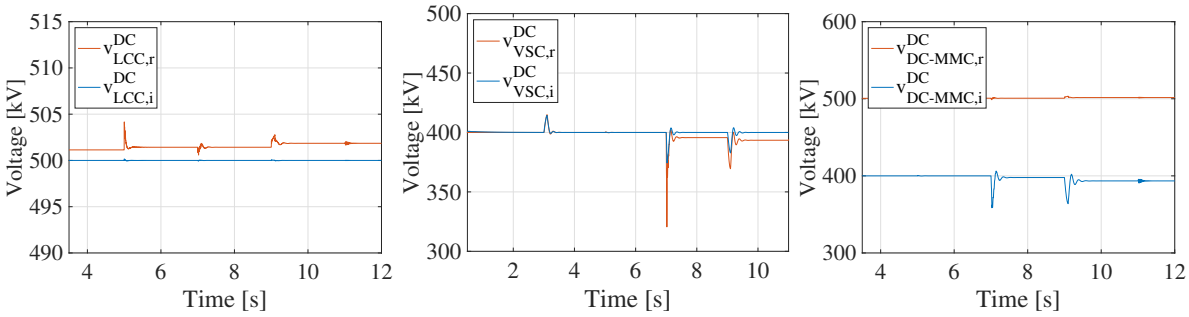

(a) DC voltages in the LCC link

(b) DC voltages in the VSC link

(c) DC voltages in the DC-MMC converter sides

Figure 6.33: DC voltages in the multiterminal HVDC grid

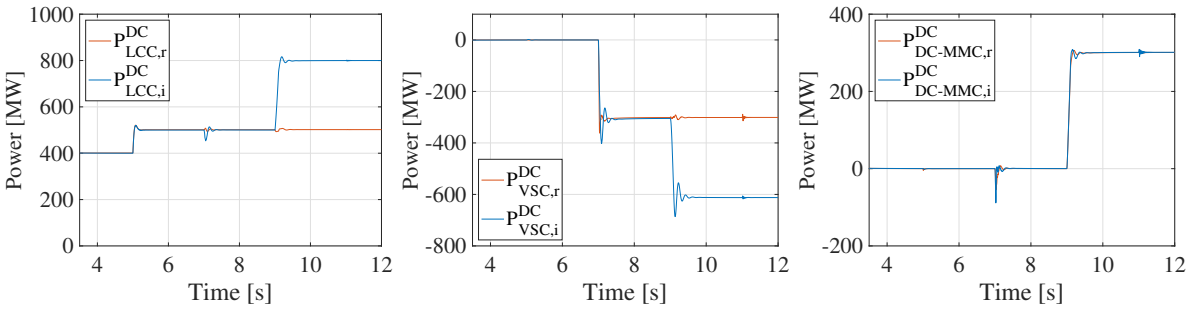

(a) DC power in the LCC link

(b) DC power in the VSC link

(c) DC power in the DC-MMC converter sides

Figure 6.34: DC power flow in the multiterminal HVDC grid

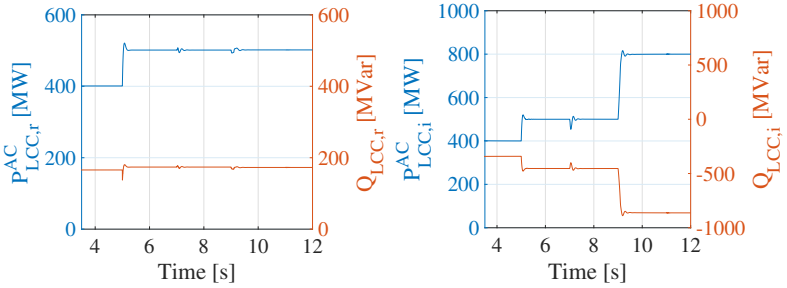

(a) Active and reactive power in the LCC rectifier

(b) AC and reactive power in the LCC inverter

Figure 6.35: Active and reactive power flowing to the HVAC LCC link

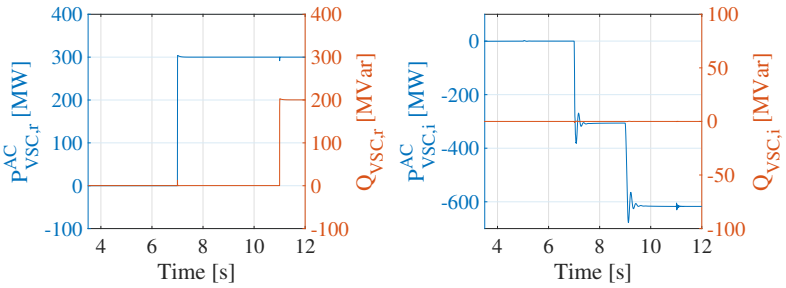

(a) Active and reactive power in the VSC rectifier

(b) AC and reactive power in the VSC inverter

Figure 6.36: Active and reactive power flowing to the HVAC VSC link

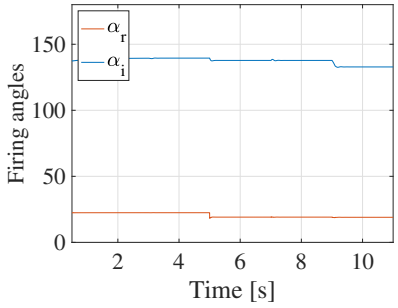

Figure 6.37: LCC converters firing angles

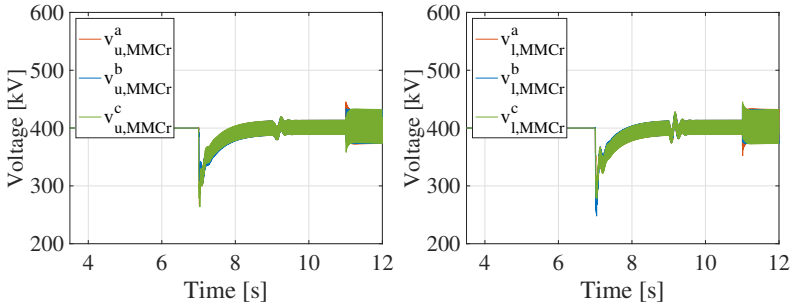

(a) MMC upper arms rectifier energies

(b) MMC lower arms rectifier energies

Figure 6.38: MMC rectifier energies

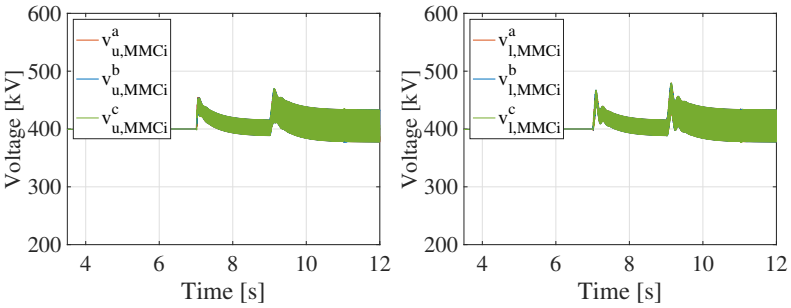

(a) MMC upper arms inverter energies

(b) MMC lower arms inverter energies

Figure 6.39: MMC inverter energies

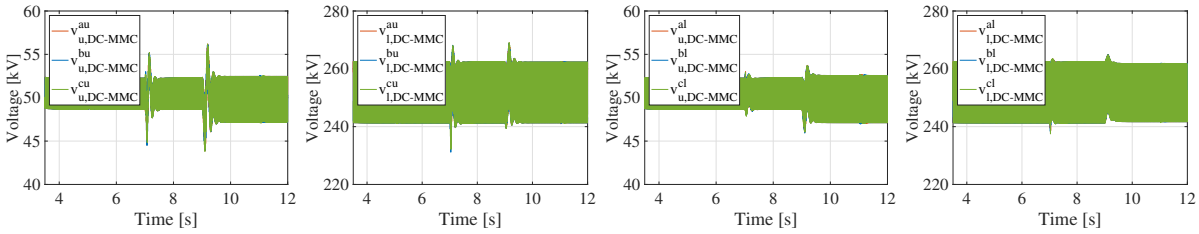

(a) Upper DC-MMC upper arms inverter energies

(b) Upper DC-MMC lower arms inverter energies

(c) Lower DC-MMC upper arms inverter energies

(d) Lower DC-MMC lower arms inverter energies

Figure 6.40: DC-MMC energies

6.3.2 Case 2

In the LCC link the power reference is changed following a step in time 3 seconds as reflected in Figure 6.43a. This power is absorbed by the DC-MMC converter as the other LCC converter is also controlling the power reference and its fixed to 500 MW. This also effects to the VSC inverter as can be seen in Figure 6.43b as this power flows to the VSC link.

The voltage of the LCC link is kept constant by the voltage regulation of the DC-MMC converter as can be seen in Figure 6.42a. This change in the DC power reference causes a change in the active and reactive power consumed by the LCC rectifier as is shown in Figure 6.44a, while the inverter is parameters are kept constant as seen in Figure 6.44b. This change is also reflected in the firing angle of the rectifier converter Figure 6.46.

A power reference set point change is also simulated in the VSC link in second 5 this produces a change in the DC current of this links as reflected in Figures 6.41b and 6.41a. The voltage is regulated after a transient by the MMC inverter, Figure 6.42b. In second 7 the MMC rectifier injects 200 MVar to the AC grid as can be seen in Figure 6.45a.

The energies of the MMC are kept constant during all this different operations as can be seen in Figures 6.47a, 6.47b for the rectifier and Figures 6.48a, 6.48b for the inverter. The DC-MMC converter energies are kept constant by the control as is shown in Figure 6.49a, 6.49b, 6.49c and 6.49d.

A summary of the different operations carried out in this case is shown in Table 6.8

Table 6.8: Operations summary DC-MMC Case 2

Converter	Time [s]	Operation
LCC_r	3	Power reference set point change from 400 MW to 500 MW
VSC_r	5	Injects 300 MW to the AC grid
VSC_r	7	Injects 200 Mvar to the AC grid

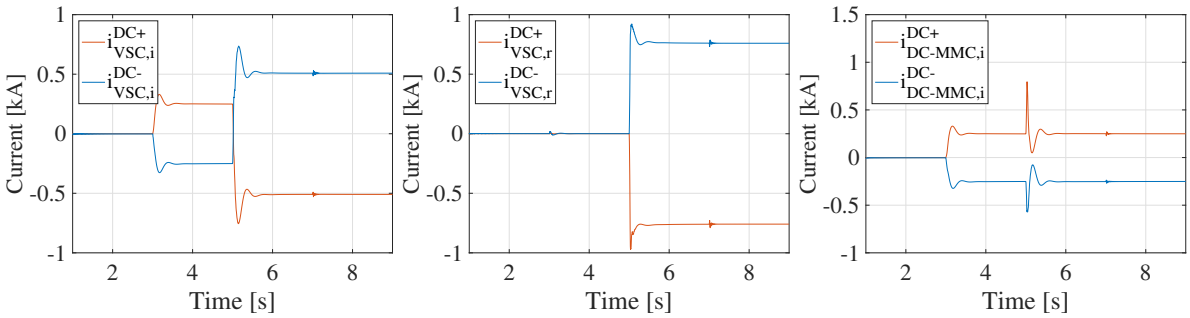

(a) DC current in the inverter side

(b) DC current in the LCC rectifier side

(c) DC current in the DC-MMC converter inverter side

Figure 6.41: DC current in the VSC link

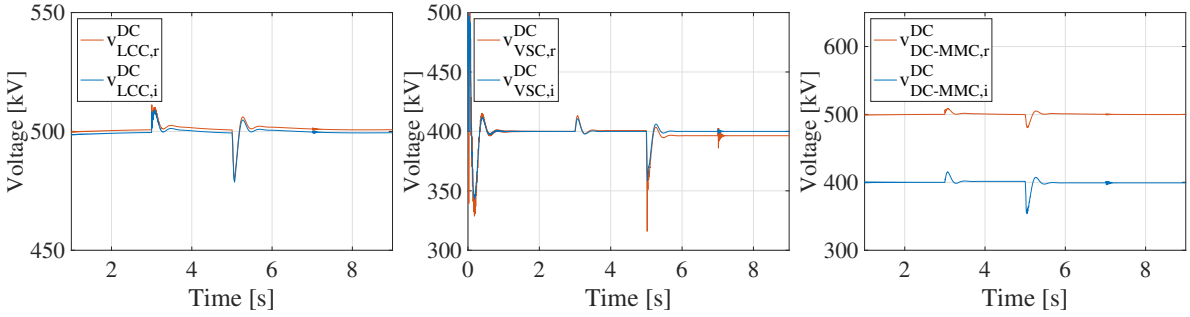

(a) DC voltages in the LCC link

(b) DC voltages in the VSC link

(c) DC voltages in the DC-MMC converter sides

Figure 6.42: DC voltages in the multiterminal HVDC grid

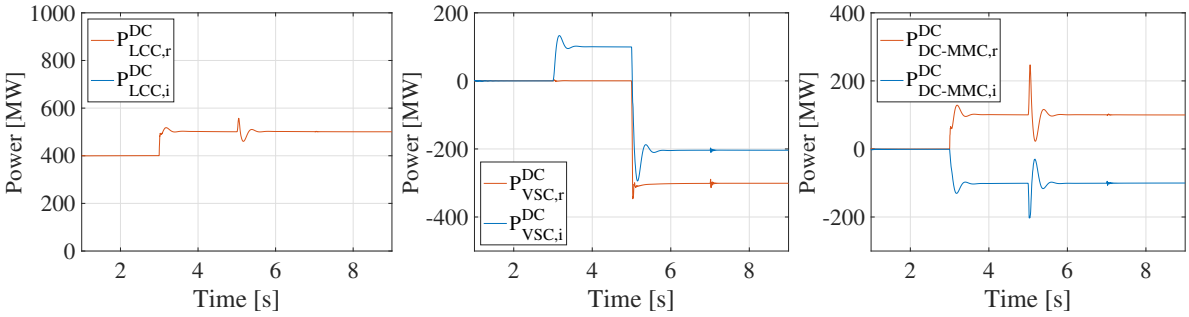

(a) DC power in the LCC link

(b) DC power in the VSC link

(c) DC power in the DC-MMC converter sides

Figure 6.43: DC power flow in the multiterminal HVDC grid

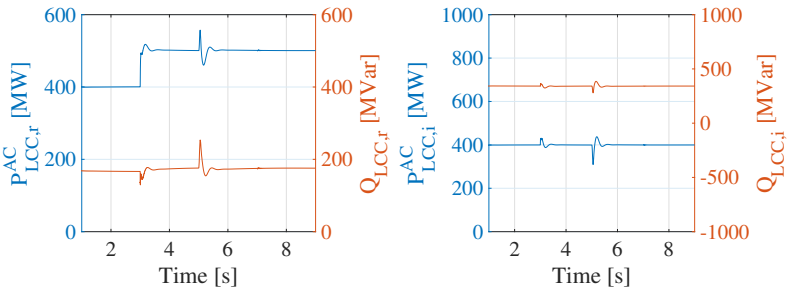

(a) Active and reactive power in the LCC rectifier

(b) AC and reactive power in the LCC inverter

Figure 6.44: Active and reactive power flowing to the HVAC LCC link

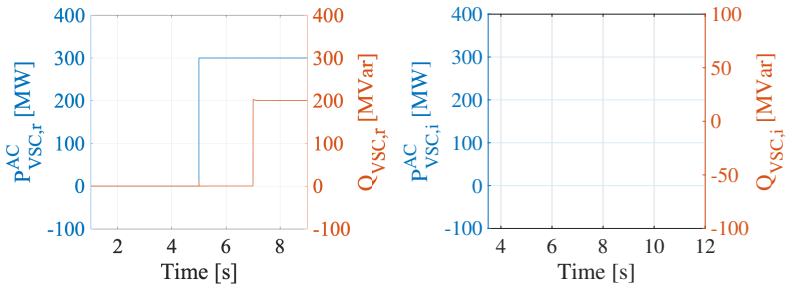

(a) Active and reactive power in the VSC rectifier

(b) AC and reactive power in the VSC inverter

Figure 6.45: Active and reactive power flowing to the HVAC VSC link

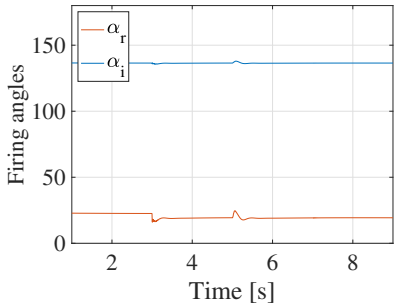

Figure 6.46: LCC converters firing angles

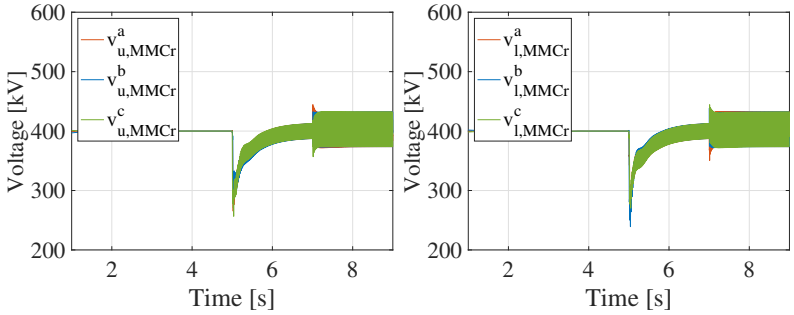

(a) MMC upper arms rectifier energies

(b) MMC lower arms rectifier energies

Figure 6.47: MMC rectifier energies

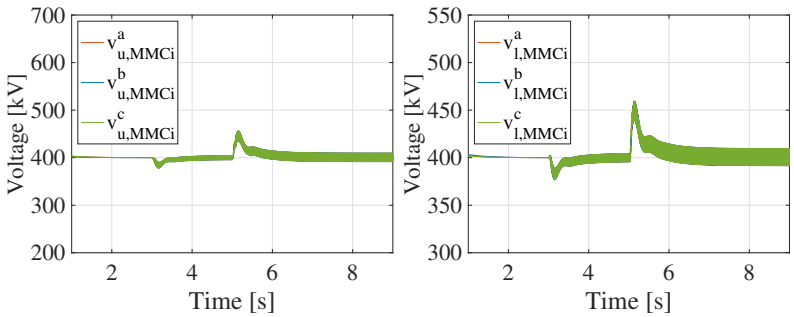

(a) MMC upper arms inverter energies

(b) MMC lower arms inverter energies

Figure 6.48: MMC inverter energies

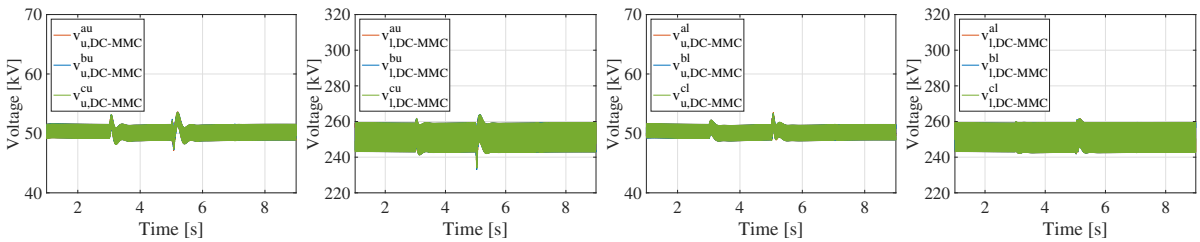

(a) Upper DC-MMC upper arms inverter energies

(b) Upper DC-MMC lower arms inverter energies

(c) Lower DC-MMC upper arms inverter energies

(d) Lower DC-MMC lower arms inverter energies

Figure 6.49: DC-MMC energies

6.3.3 Case 3

In the LCC link the power reference is changed following a step in time 3 seconds as reflected in Figure 6.52a. This power is absorbed by the LCC inverter as the DC-MMC converter is controlling the power in the VSC link, not letting this power to flow to this link. The voltage of the LCC link is kept constant by the LCC inverter converter as can be seen in Figure 6.51a. This change in the DC power reference causes a change in the active and reactive power consumed by the LCC rectifier and inverter as is shown in Figure 6.53a and 6.53b. This change is also reflected in the firing angle of the rectifier and inverter converter Figure 6.55.

A power reference set point change is also simulated in the VSC link in second 5, producing a change in the DC current of this links as reflected in Figures 6.50b and 6.50a. The voltage is regulated after a transient by the MMC inverter.

At second 7, the DC-MMC converter starts to inject power from the LCC to the VSC link. As a consequence, the LCC inverter reduces its power consume from 500 MW to 350 MW.

Finally, the VSC rectifier injects 200 MVar to the AC grid, as can be seen in Figure 6.54a.

The energies of the MMC are kept constant during all this different operations as can be seen in Figures 6.56a, 6.56b for the rectifier and Figures 6.57a, 6.57b for the inverter. The DC-MMC converter energies are kept constant by the control as is shown in Figure 6.58a, 6.58b, 6.58c and 6.58d.

A summary of the different operations carried out in this case is shown in Table 6.9

Table 6.9: Operations summary DC-MMC Case 3

Converter	Time [s]	Operation
LCC_r	3	Power reference set point change from 400 MW to 500 MW
VSC_r	5	Injects 300 MW to the AC grid
DC-MMC	7	Injects 150 MW to the VSC link
VSC_r	9	Injetcs 200 MVar to the AC grid

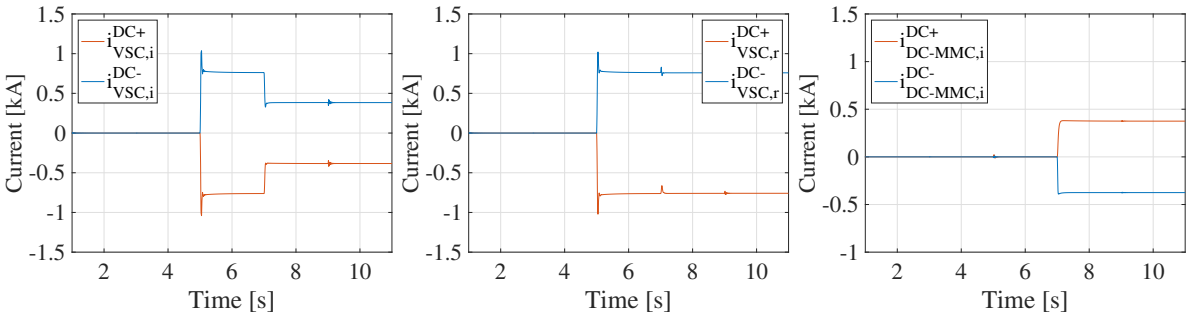

(a) DC current in the inverter side

(b) DC current in the LCC rectifier side

(c) DC current in the DC-MMC converter inverter side

Figure 6.50: DC current in the VSC link

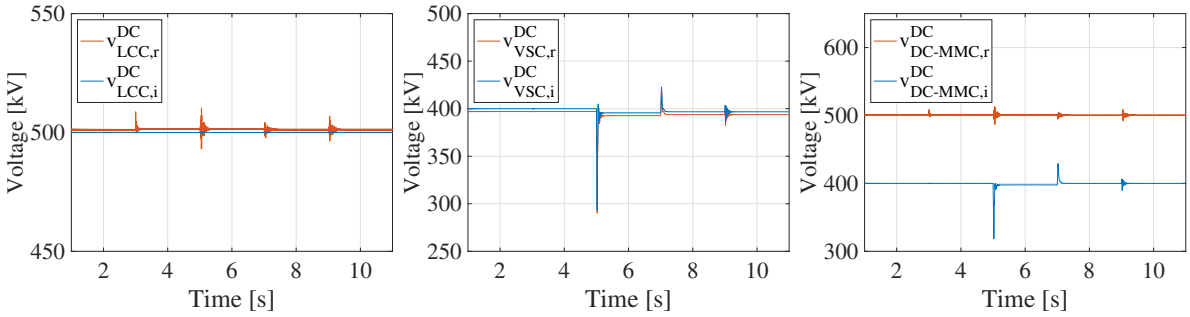

(a) DC voltages in the LCC link

(b) DC voltages in the VSC link

(c) DC voltages in the DC-MMC converter sides

Figure 6.51: DC voltages in the multiterminal HVDC grid

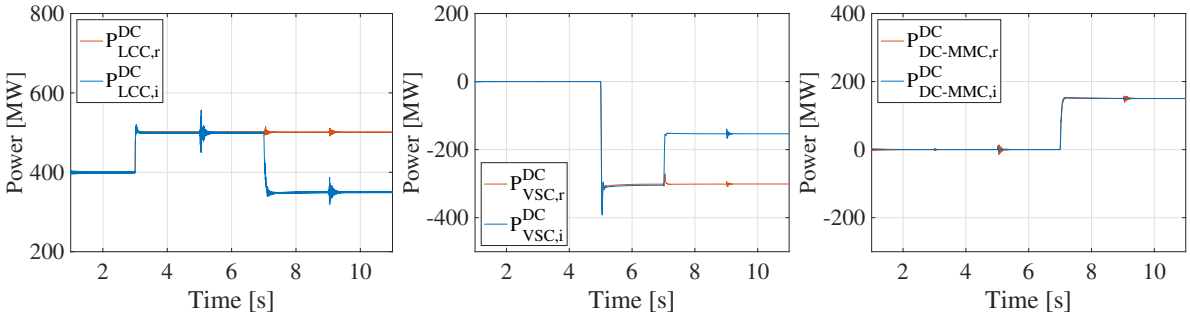

(a) DC power in the LCC link

(b) DC power in the VSC link

(c) DC power in the DC-MMC converter sides

Figure 6.52: DC power flow in the multiterminal HVDC grid

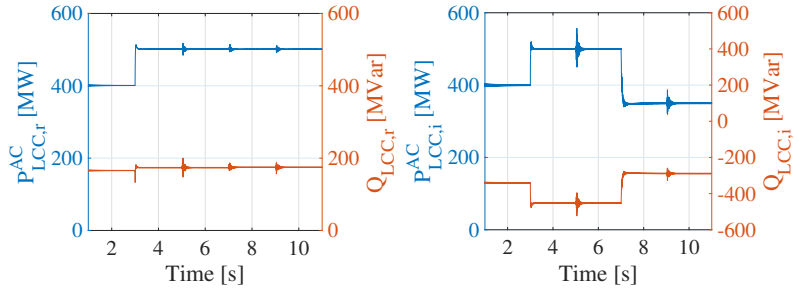

(a) Active and reactive power in the LCC rectifier

(b) AC and reactive power in the LCC inverter

Figure 6.53: Active and reactive power flowing to the HVAC LCC link

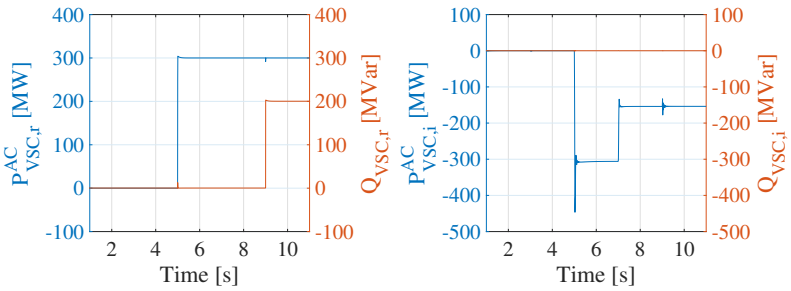

(a) Active and reactive power in the VSC rectifier

(b) AC and reactive power in the VSC inverter

Figure 6.54: Active and reactive power flowing to the HVAC VSC link

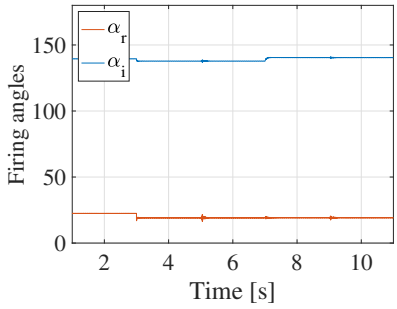

Figure 6.55: LCC converters firing angles

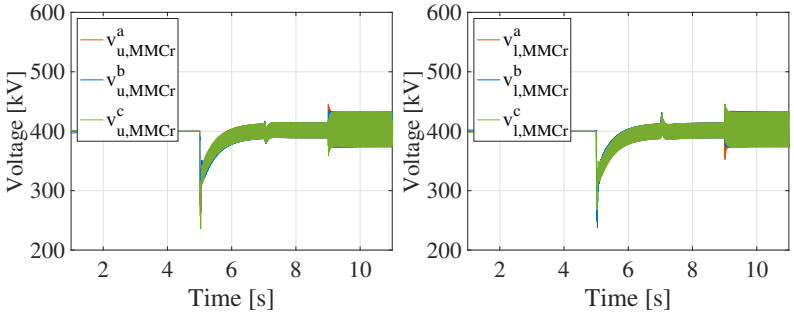

(a) MMC upper arms rectifier energies

(b) MMC lower arms rectifier energies

Figure 6.56: MMC rectifier energies

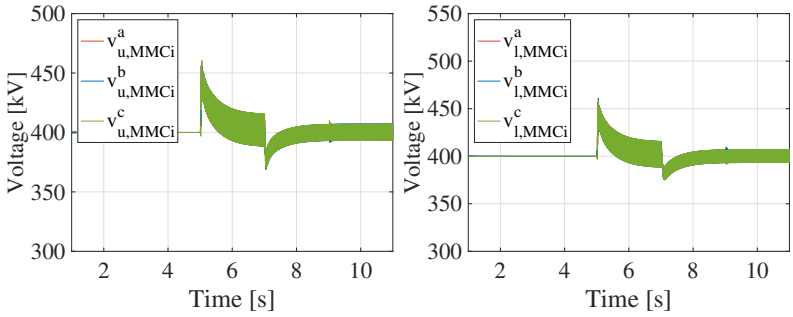

(a) MMC upper arms inverter energies

(b) MMC lower arms inverter energies

Figure 6.57: MMC inverter energies

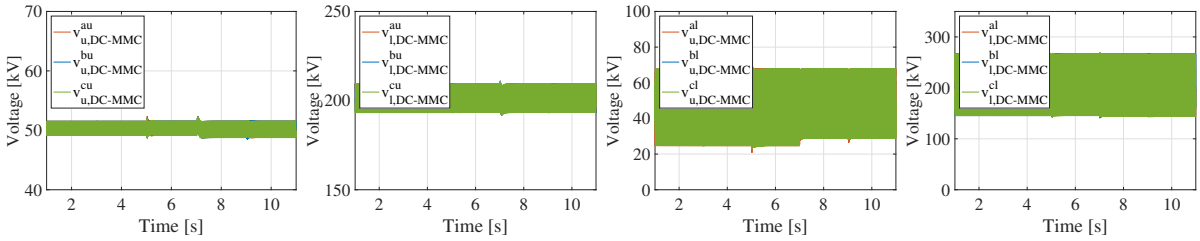

(a) Upper DC-MMC upper arms inverter energies

(b) Upper DC-MMC lower arms inverter energies

(c) Lower DC-MMC upper arms inverter energies

(d) Lower DC-MMC lower arms inverter energies

Figure 6.58: DC-MMC energies

6.3.4 Case 4

In the LCC link the power reference is changed following a step in time 5 seconds as reflected in Figure 6.61a. This power is absorbed by the LCC inverter as the DC-MMC converter is controlling the voltage in the VSC link and the MMC converters in the VSC link are both controlling power. The voltage of the LCC link is kept constant by the voltage regulation of the LCC inverter converter as can be seen in Figure 6.60a. This change in the DC power reference causes a change in the active and reactive power consumed by the LCC rectifier and inverter as is shown in Figure 6.62a and 6.62b. This change is also reflected in the firing angle of the rectifier and inverter converter Figure 6.63.

A power reference set point change is also simulated in the VSC link in second 7 this produces a change in the DC current of this links as reflected in Figures 6.59b and 6.59a. The power consumed by the MMC inverter is not affected as this converter is also regulating the power flow. As can be seen in Figure 6.59a the current flowing to this converter is always kept to zero. The voltage is regulated after a transient by the DC-MMC converter.

The energies of the MMC are kept constant during all this different operations as can be seen in Figures 6.64a, 6.64b for the rectifier and Figures 6.65a, 6.65b for the inverter. The DC-MMC converter energies are kept constant by the control as is shown in Figure 6.66a, 6.66b, 6.66c and 6.66d.

A summary of the different operations carried out in this case is shown in Table 6.10

Table 6.10: Operations summary DC-MMC Case 4

Converter	Time [s]	Operation
LCC_r	5	Power reference set point change from 400 MW to 500 MW
VSC_r	7	Injects 300 MW to the AC grid

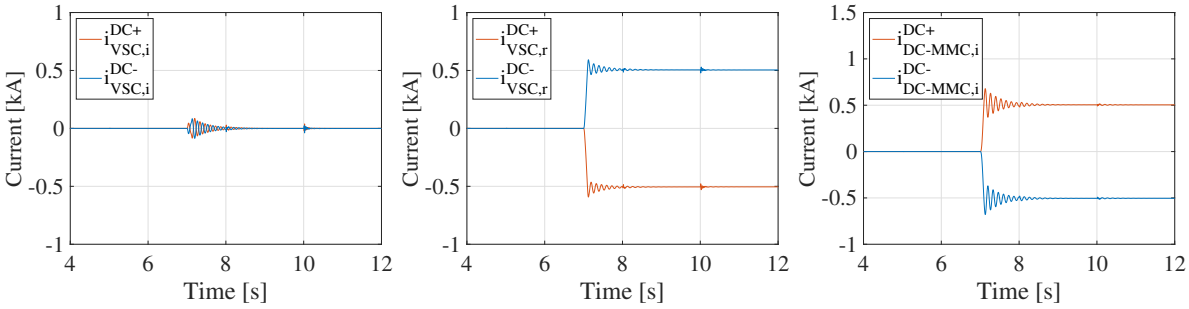

(a) DC current in the inverter side

(b) DC current in the LCC rectifier side

(c) DC current in the DC-MMC converter inverter side

Figure 6.59: DC current in the VSC link

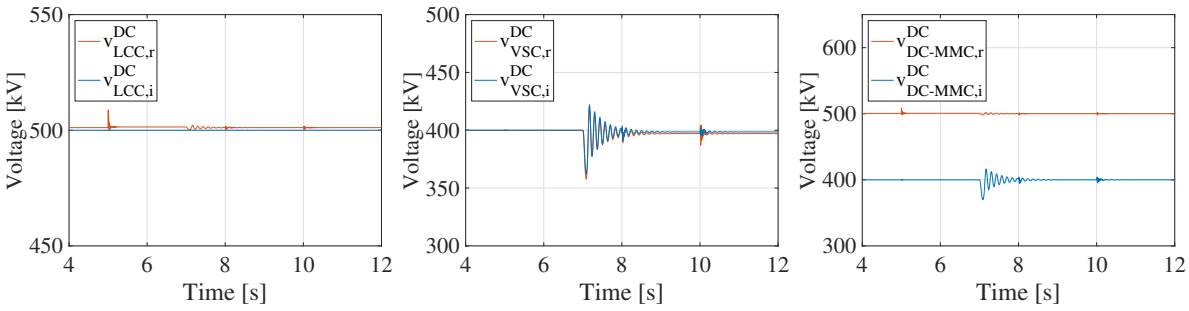

(a) DC voltages in the LCC link

(b) DC voltages in the VSC link

(c) DC voltages in the DC-MMC converter sides

Figure 6.60: DC voltages in the multiterminal HVDC grid

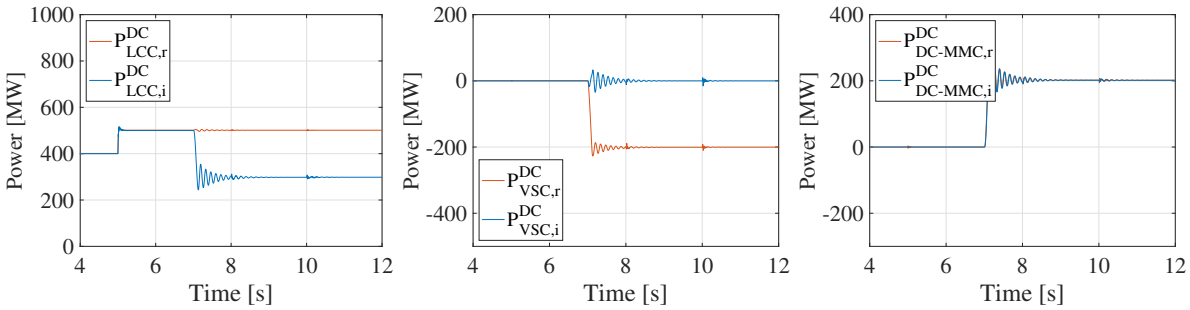

(a) DC power in the LCC link

(b) DC power in the VSC link

(c) DC power in the DC-MMC converter sides

Figure 6.61: DC power flow in the multiterminal HVDC grid

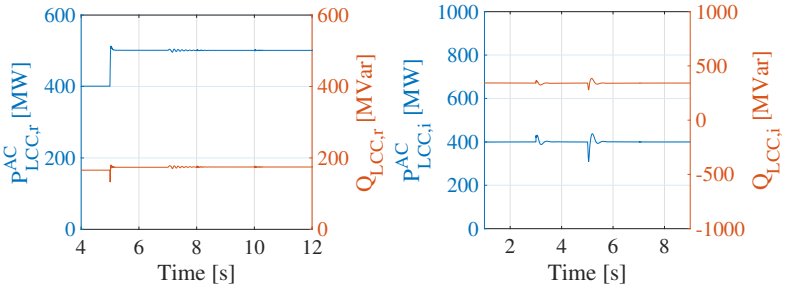

(a) Active and reactive power in the LCC rectifier

(b) AC and reactive power in the LCC inverter

Figure 6.62: Active and reactive power flowing to the HVAC LCC link

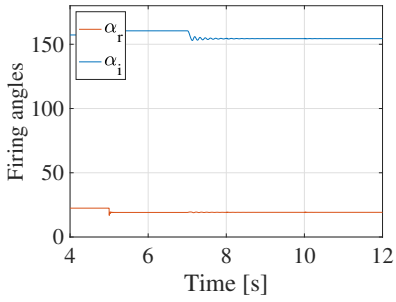

Figure 6.63: LCC converters firing angles

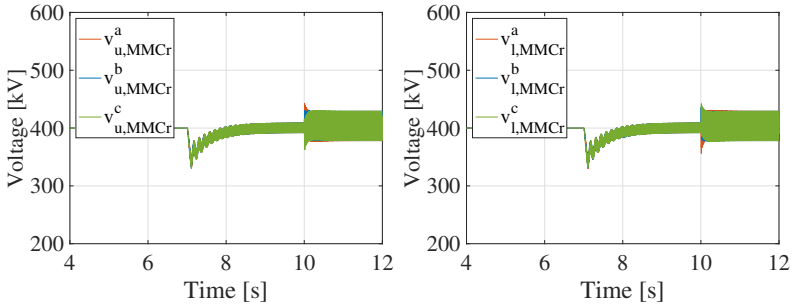

(a) MMC upper arms rectifier energies

(b) MMC lower arms rectifier energies

Figure 6.64: MMC rectifier energies

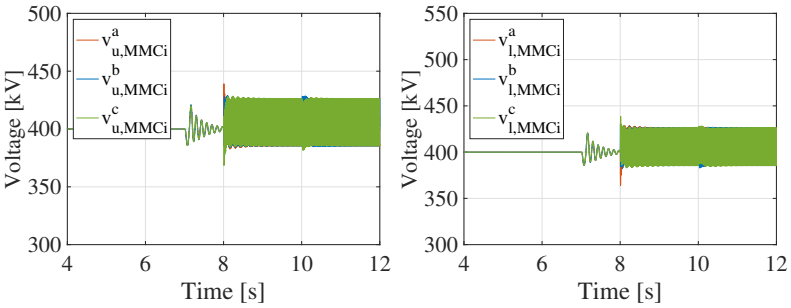

(a) MMC upper arms inverter energies

(b) MMC lower arms inverter energies

Figure 6.65: MMC inverter energies

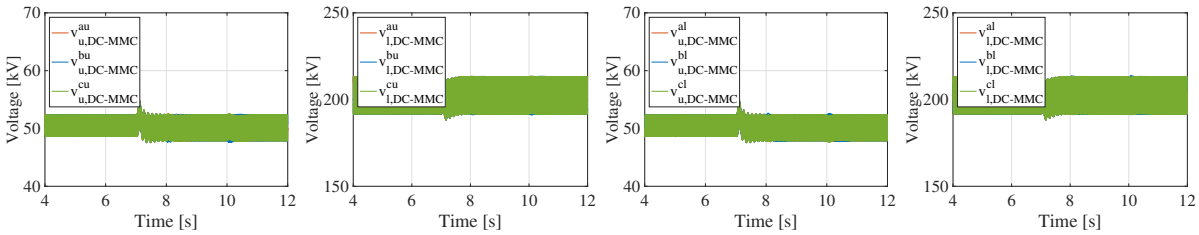

(a) Upper DC-MMC upper arms inverter energies

(b) Upper DC-MMC lower arms inverter energies

(c) Lower DC-MMC upper arms inverter energies

(d) Lower DC-MMC lower arms inverter energies

Figure 6.66: DC-MMC energies

6.4 Results Summary

After the study of the different cases, the controls proposed have been validated for the studied multi-terminal grid. The controls presented for the LCC converters, MMC converters and the DC/DC converters present a good performance in all the different scenarios. Both DC/DC converters have been able to control properly the power flow and the DC voltage in both lines.

The main difference in the behaviour of the DC/DC converters can be found when the F2F converter is controlling the power flow. In this case, when there is a power reference change in the LCC link or in the VSC link, this is not reflected in the other grid. When the DC-MMC converter is placed instead, some perturbations appear in the other link. This small transient could be smoothed changing the control parameters, but this study will not be carried out in this thesis.

The main drawback of the DC-MMC converter is its difficult placement between grids with different grounding schemes, being necessary to use its bipolar configuration. On the other hand, when it is not necessary to use this configuration it provides the same features as the F2F converter with less sub-modules, making it a more compact converter.

One of the main advantages of the DC-MMC converter is that it has more degrees of freedom compared with the F2F converter, at least with the proposed control in this thesis. This facilitates the power losses optimization.

Chapter 7

Environmental Impact

This Section exposes the environmental impact derived form HVDC systems. The typical effects of high voltage transmission systems are listed below:

- Magnetic field: The magnetic field depends on the current and the distance from the conductor. This magnetic flux grew up with the current and decrease with the distance. In [19] it is said that for a 450 kV installation the flux density is about 25 μT, where the natural earth flux density is 40 μT. On the other hand, in [20] it is said that in a range of less than 20 m from the cable the flux density can be superior to the natural earth field in similar installation.
- Electric field: The electric field can change with the weather, seasonal variation and relative humidity. If compared with AC transmission systems, DC has less electric field thanks to the lack of steady-state displacement current [19].
- Corona: This is the principal cause of radiated noise. It also leads to small ozone pollution near the line. This HVDC lines produces 10 ppb (part per billion) if it is compared with the natural concentration [19].
- Visual impact: Compared with a classic HVAC overhead system, a HVDC transmission system causes less visual impact as these lines are more compact.
- CO_2 emissions: HVDC is mostly chosen for its lower power losses compared with an HVAC system. The reduction of the power losses transmission has a significant effect on the reduction of CO_2 emissions.
- Integration of renewable energy: The advantage of the HVDC technology on introducing renewable energy in the existing grid has been already proven. For example, VSC based HVDC has been proven to be a feasible technology to incorporate offshore wind power plants to the grid.

Chapter 8

Budget

8.1 Labour costs

Labour costs are divided respectively in research hours, development hours and writing hours. Considering the author hourly salary during the development of this thesis.

Concept	**Hourly rate[€/h]**	**Hours** (h)	**Cost**(€)
Research	5.8	200	1160
Simulation and development	5.8	300	1740
Writing	5.8	100	580
Subtotal		600	3480
VAT(21%)			730.8
Total			4210.8

Table 8.1: Labour costs

8.2 Developement tools and office material

This cost item includes the necessary tools to develop this project. The cost of IEEE articles or other literature material is not included, as the university provides free access to those contents.

Concept	**Unit cost[€/ut]**	**Units**	**Cost**(€)
Personal computer (MacBook Pro)	1505.59	1	1505.59
Matlab®2019 (Academic use)	500	1	500
Subtotal			2005.59
VAT(21%)			421.17
Total			2426.76

Table 8.2: Development costs

8.3 Total cost

Considering the previous items, total cost can be seen in table 8.3. A plus of 494.17 €should be added as this is the cost of the university tuition tax to enroll in this master thesis.

Item	**Cost[€]**
Labour	4210.8
Development	2426.76
Total (VAT included)	**6637.56**

Table 8.3: Total cost

Conclusions

This Master thesis presented the modelling, control and simulation of a multi-terminal hybrid VSC-LCC HVDC grid. The goals set at the beginning of this thesis have been accomplished. The contributions of this thesis are listed below:

1. The principles of LCC-HVDC and VSC-HVDC technologies have been properly understood.
2. A point-to-point line model of both HVDC technologies have been constructed in Matlab Simulink. This also includes the control schemes for both technologies. Being able to control the DC voltage or the power flow.
3. The principles of DC/DC converters have been presented.
4. The modelling and control for a Front-to-Front MMC converter and for a DC-MMC converter have been proposed. These control schemes include DC voltage regulation and power flow control.
5. A multi-terminal HVDC grid including both point-to-point lines, one of LCC technology and the other one of VSC technology, linked by a DC/DC converter has been modeled in Matlab Simulink. Including four different configurations for each DC/DC converter.

Upon completion on this thesis, several tasks can be considered in order to extend the understanding of multi-terminal HVDC grids. These future works are the following ones:

1. The model of both LCC and VSC HVDC AC systems can include more dynamics such as the AC grid filters.
2. The converters models could include the modulation dynamics.
3. The black-start of the multi-terminal grid can be analyzed.
4. Different AC and DC faults can be simulated in order to study the grid response.
5. The interaction of the different converters controls can be studied.

Bibliography

[1] Dirk Van Hertem, Oriol Gomis-Bellmunt, and Jun Liang, editors. *HVDC Grids For Offshore and Supergrid of the Future*. Wiley. 17, 19, 20, 21

[2] Dragan Jovcic and Khaled Ahmed. *High Voltage Direct Current Transmission*. Wiley, Aberdeen, 2015. 19, 24, 25, 26, 31

[3] Olof Heyman, Lars Weimers, and Mie-lotte Bohl. HVDC – A key solution in future transmission systems. pages 1–16. 19

[4] Willem Leterme, Student Member, Pieter Tielens, Student Member, Steven De Boeck, Student Member, Dirk Van Hertem, and Senior Member. Overview of Grounding and Configuration Options for Meshed HVDC Grids. *IEEE Transactions on Power Delivery*, 29(6):2467–2475, 2014. 20

[5] IEEE Transmission Committee and Distribution. HVDC Projects Listing. Technical Report March, IEEE Transmission and Distribution Comittee, 2012. 23

[6] Stig Nilsson Willis Long. HVDC Transmission: Yesterday and Today. *IEEE power & energy magazine*, pages 22–31, 2007. 31

[7] Roberto Rudervall, J Charpentier, and Raghuveer Sharma. High Voltage Direct Current (HVDC) Transmission Systems Technology Review Paper. (Energy Week 2000):1–17, 1999. 31

[8] Mike Barnes and Theodor Heath. UK's HVDC Links. *VSC-HVDC Newsletter*, 7(05):1–13, 2019. 31

[9] Eduardo Prieto-Araujo, Adrià Junyent-Ferré, Carlos Collados-Rodríguez, Gerard Clariana-Colet, and Oriol Gomis-Bellmunt. Control design of Modular Multilevel Converters in normal and AC fault conditions for HVDC grids. *Electric Power Systems Research*, 2017. 32, 37, 38, 39

[10] Kamran Sharifabadi, Lennart Harnefors, Hans Peter Nee, Staffan Norrga, and Remus Teodorescu. *Design, Control, and Application of Modular Multilevel Converters for HVDC Transmission Systems*. Wiley, 2016. 32

[11] Green Energy and Technology. *Modeling and Control of Suistainable Power Systems*. Springer, 2012. 34, 103, 105

[12] L. Harnefors and H.-P. Nee. Model-based current control of AC machines using the internal model control method. *IEEE Transactions on Industry Applications*, 34(1):133–141, 1998. 36

[13] Enric Sánchez-sánchez, Student Member, and Eduardo Prieto-araujo. Analysis of MMC Energy-Based Control Structures for VSC-HVDC Links. *IEEE Journal of Emerging and Selected Topics in Power Electronics*, 6(3):1065–1076, 2018. 37, 47

[14] J D Páez, D Frey, J Maneiro, S Bacha, Senior Member, and P Dworakowski. Overview of DC-DC Converters dedicated to HVDC Grids. 8977(c), 2018. 43

[15] Stephan Kenzelmann, Alfred Rufer, Drazen Dujic, Senior Member, Francisco Canales, and Yales Rˆ. Isolated DC / DC Structure Based on Modular Multilevel Converter. 30(1):89–98, 2015. 44

[16] Stephan Kenzelmann. *Modular DC/DC Converter for DC Distribution and Collection Networks PAR*. PhD thesis, École Polytechnique Fédérale de Lausanne, 2012. 46

[17] Xia Chen, Haishun Sun, Jinyu Wen, Wei-jen Lee, Xufeng Yuan, Naihu Li, and Liangzhong Yao. Integrating Wind Farm to the Grid Using Hybrid Multiterminal HVDC Technology. 47(2):965–972, 2011. 61

[18] C D Barker, C C Davidson, D R Trainer, and R S Whitehouse. Requirements of DC-DC Converters to facilitate large DC Grids United Kingdom. (Lcc), 2012. 61

[19] Kala Meah, Student Member, Sadrul Ula, and Senior Member. Comparative Evaluation of HVDC and HVAC Transmission Systems. pages 1–5, 2007. 95

[20] Eugeniusz Andrulewicz, Dorota Napierska, and Zbigniew Otremba. The environmental effects of the installation and functioning of the submarine SwePol Link HVDC transmission line : a case study of the Polish Marine Area of the Baltic Sea. 49:337–345, 2003. 95

[21] Stephan Kenzelmann, Alfred Rufer, Michail Vasiladiotis, Drazen Dujic, École Polytéchnique, and Fédérale De Lausanne. A Versatile DC-DC Converter for Energy Collection and Distribution using the Modular Multilevel Converter Keywords. *Proceedings of the 2011 14th European Conference on Power Electronics and Applications*, (Mv):1–10.

[22] Ned Mohan, Tore M Undeland, and William P Robbins. *Power electronics*. 3 edition, 2003.

[23] R. H. Park. Two Reaction Theory of Synchronous Machines Generalized Method of Analysis-Part I. *A.I.E.E.*, pages 716–727, 1929. 103

[24] International Renewable and Energy Agency. *Renewable-Powered Future: Solutions to integrate*.